Modeling of the Flow Dynamics through Incompressible Porous Media in Solid-Liquid Filtration

by

Siying Zhang

Bachelor of Engineering, Tianjin University, 2014

Master of Science in Chemical Engineering, University of Pittsburgh, 2015

Submitted to the Graduate Faculty of

Swanson School of Engineering in partial fulfillment

of the requirements for the degree of

Doctor of Philosophy

University of Pittsburgh

2019

UNIVERSITY OF PITTSBURGH

SWANSON SCHOOL OF ENGINEERING

This dissertation was presented

by

Siying Zhang

It was defended on

July 17, 2019

and approved by

Robert M. Enick, Ph.D., Professor, Department of Chemical and Petroleum Engineering

Andrew P. Bunger, Ph.D., Associate Professor, Department of Chemical and Petroleum
Engineering

Carla A. Ng, Ph.D., Assistant Professor, Department Civil and Environmental Engineering

Dissertation Director: Joseph J. McCarthy, Ph.D., Professor, Department of Chemical and
Petroleum Engineering

Modeling of the Flow Dynamics through Incompressible Porous Media in Solid-Liquid Filtration

Siying Zhang, PhD

University of Pittsburgh, 2019

Solid-liquid filtration is a long-standing engineering practice and has been widely used in the chemical, process and mineral industries. Current models are semi-empirical in nature; thus, they require significant experimental and/or computational resources in order to determine the empirical quantities. In contrast, this dissertation provides a model to predict the dynamic behavior for both the liquid and solid phase of a filtration process without the requirement of empirical parameters. Instead, the model relies solely on the to-be-captured particle size distribution of contaminants as well as the pore size distribution of the filtration media. The new algorithm is capable of describing filtration based on both "steric" capture of contaminants as well as capture within dead-end pores in the material.

This dissertation shows the performance of the model in modeling beds comprised of high void fraction materials (diatomaceous earth) that is used for the removal of multi-modal mixtures of contaminant. By formally accounting for the complex pore size distribution, the predict flow dynamics that are much closer to experimental results than the predictions of the traditional Kozeny-Carmen (K-C) model and show that this approach is viable for both statically formed and evolving (dynamic) beds. In an effort to understand the relationship between flow dynamics and pore size distribution more fully, a dynamic filter cake model is proposed that continuously modifies the pore size distribution as contaminants (polydispere spheres) are deposited. This dissertation also describes a simulation model capable of describing the capture of spherical

particles within dead-end pores. A 3D discrete element method-lattice Boltzmann method (DEM-LBM) coupling approach is applied to investigate the particle capture under conditions of different particle size and pore structures. Both the pressure drop and the fluid density are examined to indicate this capture performance. The predicted flow dynamics of this new model match the dynamic experimental results remarkably well, setting the stage for a priori prediction of filtration times, flow-rates, particle capture, and pressure requirements from simple measurements of the size distribution of both the filter media pores as well as the contaminant particles/droplets.

Table of Contents

List of Tables

List of Figures

xiv

xv

Preface

I would like to thank my advisor, Dr. Joseph J. McCarthy for his guidance and support during my project. All the technical knowledge and research skills I learnt from him enrich me to be a better graduate student. The rigorous scientific approach and innovative thinking I gained while working with him would benefit me for a lifetime.

I would also like to thank all the members of my PhD dissertation committee, I would also like to thank my friends and colleagues who study and work with me in Pittsburgh, especially, Dr. Melissa Lash, Shichao Jiao for their help in study particle development; Megan Cala, Dr. Siying Liu, Ramon Lopez for their help in simulations; Michael McMahon and Nicole Salamacha for their help with my filtration experiments. I am also grateful to Cliff Kowall and Roger Parsons from the Lubrizol Corporation for their support.

Finally, I would like to dedicate this work to my parents, Lan Zhang and Shufang Sun, for their support and sacrifice. I would like to thank my cousins and grandparents for encourage and assist me every time I feel bad during my life. I also acknowledge my friends, Yu Zhang, Yan Zhang and Xue Wang with their valuable suggestions and guidance. I would like to express my special thanks to my fiancé Jingran Su for his support in my journey.

1.0 Introduction

Filtration is the process of separation that involves the flow of a solid-liquid (or liquid-liquid) mixture through a fixed bed that is filled with a porous material(Kavoosi 2014). Application for a filtration separation process have been developed in a wide range of industries. The most commonly used filtration process include cake filtration, depth filtration and cross-flow filtration(Yim and Kwon 1997). Filtration in the separation of solid-liquid mixtures has been studied for 90 years. However, the lack of a generalized set of laws for filtration has increased the difficulty of incorporating equations from one model into another(Tien 2006). Thus, economic optimization of a filtration process, which can help industries reach their least cost design with respect to the filtration velocity, the operating time and the filter medium consumption, has long been identified but there are no algorithms reach these requirements(Dharmappa et al. 1992).

The conventional cake filtration theory originates from Ruth's pioneering work(Ruth 1946), who introduced electric analogy and proposed a two-resistance theory. The development of conventional filtration theory consists two steps: (1)combining the mass balance equation for the liquid phase by considering both porosity(Tiller 1953) and pressure drop(Tiller 1953) during the filtration process and (2) assuming only point contacts(Willis et al. 1991) exist between particles. With some empirical quantities related to pressure and porosity, the governing equations can be numerically solved(Carman 1956). Flow through a packed bed is commonly modeled using the so-called Kozeny-Carman (K-C) model (Carman 1956, Wyllie and Gardner 1958), in order to predict the pressure drop during a cake filtration process. However, works of literature show that the K-C model does not fit when the cake has high porosity, non-spherical particles, or systems of particles that are multi-disperse(Mauran, Rigaud, and Coudevylle 2001). Two issues that make the

1

prediction of the K-C model limited to strict filtration are (1) the empirical quantity used in the K-C model to represent the tortuosity of a packed bed and (2) the lack of validated description of the complex structure of a filter medium. Thus, analysis for the theoretical quantity to replace the empirical quantity is discussed in this dissertation. A novel method to describe the structure of filter mediums is also introduced.

Depth filtration always uses the same separating agent with cake filtration. However, the roles played by the filter medium are different(Kuhn and Briesen 2016). The main problems for the prediction of depth filtration are the retention of particles through a filter medium, resulting in the change of the structure of the filter medium(Chi and Payatakes 1979). Current approach affords only limited insight about the depth filtration with empirical quantities(Herzig, Leclerc, and Goff 1970a). Despite the inherent complexities of the depth filtration, the problem can be studied based on fundamental analysis. The flow behavior of a depth filtration is also related to the pore size distribution of the filter medium and the pressure drop in the fluid phase(Wong and Mettananda 2010). Thus, the depth/dynamic filtration model can be derived from the cake/static filtration model by adding in the analysis of the dynamic change of the pore size distribution during the particle retention.

The dissertation is organized as follows. Chapter 2.0 introduces the basic filtration knowledge and the difference between surface/depth filtration. The simulation methods that are used to mimic the filtration process, DEM and LBM, are also discussed. Chapter 3.0 verifies the traditional K-C model with polydisperse glass beads as the filter medium. The limitations are discussed based on the comparison between empirical and predicted flow rates. Then a modified K-C model is proposed, which fits the experimental results better. Chapter 4.0 introduces a new model called the PSD model that can predict the filtration process with a highly porous medium.

The model has been verified with both steric and dynamic filtration experiments. Chapter 5.0 analysis the ability of intrinsic pores in the filter medium capture relatively small contaminants, haze induced particles. The change of concentration of the contaminants is tested. Two mechanisms are proposed and tested with surface modification and DEM/LBM simulation. Under the analysis of the capture mechanism, a model, capture model, is proposed to mimic the capture ability of the intrinsic pores in a filtration process. Chapter 6.0 describes a semi-empirical deep bed filtration model to predict the migration of micro- and semi microparticles in porous media. Chapter 7.0 organizes the filtration models together and discusses the possibility of these new models work with the prediction of a real industrial filtration process.

2.0 Background

Filtration is a process that separates one phase of material from another phase. Types of filtration can be classified by different types of filters (i.e., cake filtration, frame filtration and candle filters). This dissertation is focused on fluid flow through a porous filter medium, which is widely applied in groundwater flow, oil transport in porous rock, the permeation of ink in paper, and other engineering applications(Tien 2006). It is a technique that creates a cake – a layer that is composed of solids – on the filter that is then used to separate (additional) solid(s) from the liquid(Kavoosi 2014), as shown in Figure 1. A porous cake and its interconnect voids are a heterogeneous system. The void space allows fluid to pass through. In constant pressure filtration, external pressure is added across the filter. In constant flow filtration, a positive displacement pump is used to push the liquid through at a constant flow rate(Rushton, Ward, and Holdich 2008). A non-constant filtration is a pressure filter fed by a pump.

Studies on cake filtration have been reported for over ninety years. They changed from simple restricted results to more exact and relaxed results. The conventional theory was developed during the beginning of the last century by Ruth, Grace, Tiller, and Shirato(Tien 2006). That is the mainstay in design calculations, scale-up, and data interpretation of cake filtration systems(Mauran, Rigaud, and Coudevylle 2001). This theory is based on assumptions that the particle velocity is negligible, and the fluid flow follows Darcy's law(Whitaker 1986). This indicates that the flow rate of fluid in the filtration process is directly proportional to the ultimate pressure drop and inversely proportional to the flow resistance between the cake and the medium(Flickinger 2013).

Filtration is always composed of multi-sized particles in industry applications. The Kozeny-Carman model and other theories cannot be directly applied to the multi-disperse system. In order to verify the change for a multi-disperse system, the studies during the last decade have been focused on drag forces because the drag forces between fluid and particles are very important in filtration(Rong, Dong, and Yu 2014). Koch proposed new relations based on numerical data from simulations(Koch and Hill 2001). Van der Hoef determined the drag forces of particles in bi-sized spheres in 2005(van der Hoef, Beetstra, and Kuipers 2005). Yin and Sundaresan generated a fluid-particle drag forces equation for binary and ternary systems(Yin and Sundaresan 2009). Because these works were based on very loosely packed beds, the equations may not work well in dense systems. Based on previous works, Rong organized the relationship between fluid and particles more accurately and reasonably(Rong, Dong, and Yu 2014). However, Rong and coworkers assumed that the particles remained stationary when the fluid flowed through them and used very low pressure during the experiment and simulation.
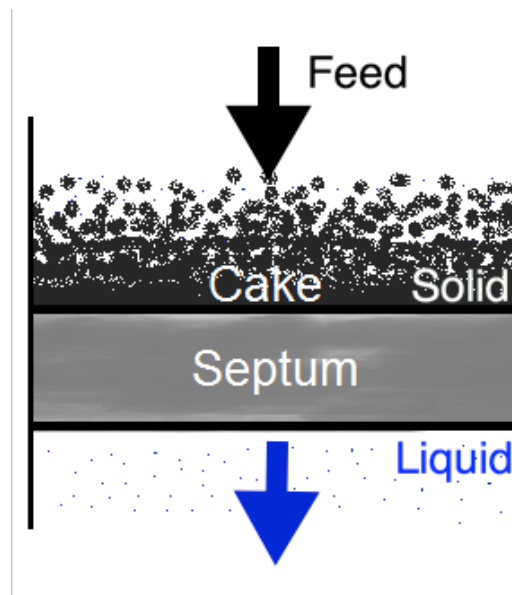
2.1 Surface and Depth Filtration

From a first-principles mechanistic standpoint, depth and surface filtration (see Figure 2 and Figure 3) has been investigated extensively as the key components of cake filtration. Iwasaki first formulated a mathematical model describing the differences between depth and surface filtration(Iwasaki 1937). Later, Hermia provided a blocking model to describe the flux decline during the stage of depth/surface filtration(Hermia 1982). This model includes several stages/mechanisms of blocking, including "standard" (some particles accumulate inside the filter medium); "intermediate" (some particles accumulate inside the filter medium, others accumulate on the top of the medium leading to an increase in medium thickness); and "complete" (particles seal off the pores since the particle sizes are larger than the pore size). Based on the blocking model, Bowen generated a set of equations to describe the steps of the membrane blocking (Bowen, Calvo, and Hernandez 1995). Based on the blocking mechanisms of pores(Chudacek and Fane 1984), we can classify the filtration into surface filtration (boundary layer resistance)(Sampath, Shukla, and Rathore 2014) and depth filtration (pore blocking) (Johnson and Johnson 1987). Researchers have been studied the behavior of depth/surface filtration based on this model with experimental data (Sampath, Shukla, and Rathore 2014). Thus, the current depth/surface filtration models are extremely depended on the experimental results.

Figure 1 Solid liquid separation filtration process.

2.1.1 Surface Filtration

In general, during surface filtration, the filter medium acts as a screen so that particles of the suspension to be treated are retained solely on the surface of the medium(Zularisam, Ismail,

and Salim 2006), resulting in the formation of an increasing large filter cake, as shown in Figure 2. The pores in this model are assumed to become less accessible as the particles deposit on the surface. Thus, the cake thickness grows leading to a decrease in the filtrate volumetric flow (Chudacek and Fane 1984, Bowen, Calvo, and Hernandez 1995). Mathematically, this model can be described via

$$\frac{d^2t}{dm^2} = k\left(\frac{dt}{dm}\right)^0 = k \qquad (2\text{-}1)$$
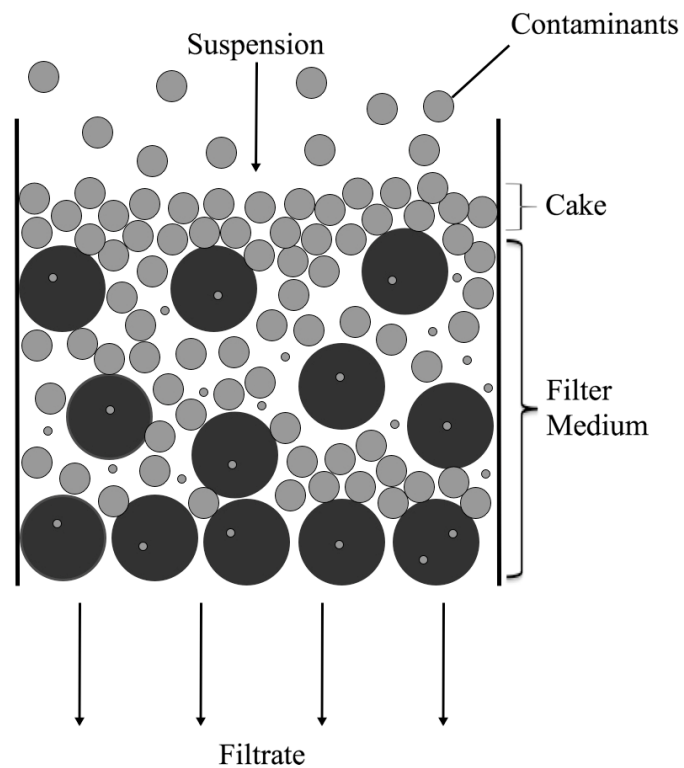
Figure 2 Surface filtration process.

2.1.2 Depth Filtration

During depth filtration, separation is effected through particle deposition throughout the entire depth of the medium as shown in Figure 3. In other words, the individual entities constituting the medium act as particle collectors(Tobiason and O'melia 1988). In this process, particles go through the pores and deposit on the pore walls when the particle size is smaller than the pore size of the filter medium. Thus the pore volume is decreased as a result of deposition: (Chudacek and Fane 1984).

$$\frac{d^2 t}{dm^2} = k \left(\frac{dt}{dm}\right)^{1.5}$$

(2-2)
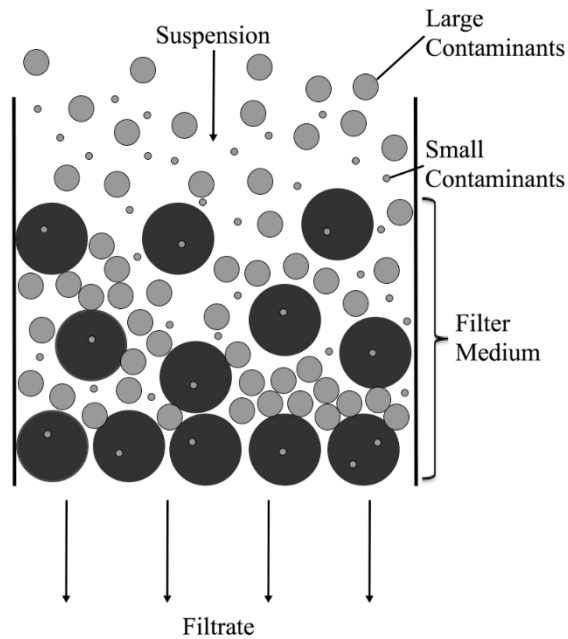
Figure 3 Depth filtration process.

2.2 Filter Aids

Filter aids are widely used in the solid-liquid filtration. These systems often contain impurities that differ widely in their properties or gelatinous particles, which tend to block the filter medium(Halbfoster 1980). Thus, the use of filter aids assures increased filtration times and lower energy expenditure due to higher filter-cake permeability. This approach is used in a variety of areas, such as chemistry and biotechnology (Flickinger 2013), water filtration(Flickinger 2013), and filtration of beverages. Unfortunately, the selection and dosage of filter aids in industrial practice are mostly based on experience. It is, however, doubtful that the optimal point of operation is always found because the process at hand is rather complicated and comprises many free variables, such as filter-aid material, size distribution, and concentration(Sulpizio 1999). For many decades, the role of the right type and amount of filter aid for successful filtration is emphasized (Sutherland and Hidi 1966, Heertjes and Zuideveld 1978). Some of these researchers present simple models that analysis the cake resistance with the concentration of contaminants. They assume that separation only directly takes place at the surface of the cake(Carman 1938). However, the influence of the depth filtration has been estimated experimentally. Due to computational limitations, these conventional models were simplified to consider filtration process with constant impurity concentrations and a constant porosity of filter aids even though a time-varying porosity of filter aids have been shown experimentally(Höflinger 2000). Thus, a novel theoretical model that describes both surface and depth filtration process is presented in this dissertation with the consideration of all process variables and parameters.

Diatomaceous earth (DE) is a highly porous filter aid that provides the opportunity to combine high porosity with important properties such as high strength and a high thermal and chemical stability(Scheffler and Colombo 2006). This combination is very important for industrial

applications such as filters for gases and molten metals, removal of heavy metal ions (Cr, Ni etc) from sewage water, catalytic supports, and chromatography columns(Green and Colombo 2003). DE has intrinsic pores that smaller than 1.5µm (Al-Ghouti et al. 2003). Even though these pores are too small to let suspension go through, they still have the ability to capture relatively "smaller" particles, haze induced nano-particles(Parfitt 1976). To predict the actual flow behavior and cake structure during the filtration process, the model should not only consider the flow behavior but also consider the capture ability of intrinsic pores.

2.3 Simulations

Due to the limitations such as high costs and small scale in the experimental filtration test, numerical analysis becomes a primary investigative tool. In general, the numerical models may be categorized into continuum method and discrete method. Most continuum methods are formulated within the framework of poroelastic theory (Biot 1941, Hong, Mum, and Lim 2001). Distinct element method (DEM) is the most often used discrete method(Hong, Mum, and Lim 2001).

2.3.1 Discrete Element Method

The discrete element method (DEM), which was pioneered by Cundall in 1971, is a numerical method that is used to compute the physic properties of an extensive number of particles(Parfitt 1976). DEM is widely used in simple models of particle interactions because it models materials as an assemblage of discrete particles(Dong et al. 2009b, Eichholz et al. 2012). It calculates the interaction forces between these particles based on Newton's law(Thornton and

Sokoloff 1998). Then it determines how the motion of each particle would change based on the calculated forces(Zhu et al. 2007).

DEM is a method to solve Newton's laws of motion for each discrete elements allowing for all degrees of freedom to describe the physic properties of each particle individually in the system depending on time t(Eichholz et al. 2012):

$$m_i \frac{d\vec{v_i}}{dt} = \vec{F_i} \qquad (2\text{-}3)$$

$$I_i \frac{d\vec{\omega_i}}{dt} = \vec{T_i} \qquad (2\text{-}4)$$

where v_i is the transitional velocity of particle i, mi is the mass of particle i, ω_i is the rotational velocity of particle i, I_i is the moment of inertial of particle i. The force $(F_i)^-$ is the force that acting on the particle i as shown:

$$\vec{F_i} = \sum \left(\vec{F}_{vdWm,ij} + \vec{F}_{n,ij} + \vec{F}_{t,ij} \right) + \vec{F}_{g,b} \qquad (2\text{-}5)$$

$\vec{T_i}$, the rotation phenomena are not considered. $F_{g,b}$ is the gravity and buoyancy forces that calculated by:

$$\vec{F}_{g,b} = \frac{\pi}{6} d^3 \Delta\rho_{sl}\vec{g}$$
(2-6)

where $\Delta\rho_{sl}$ is the difference of density between particle and the liquid phase, g is the gravitational acceleration, d is the particle diameter. Particle and particle contacts can be treated as a hard-sphere approximation or a soft-sphere approach(Dong et al. 2009a). In this dissertation only the hard-sphere approach is included.

The contact forces during collisions are shown in Figure 4. The normal contact force:

$$\vec{F}_{n,ij}\vec{n}_{ij} = k_n\lambda^{1.5} - \eta_{n,ij}\vec{v}_{rel,n,ij}$$
(2-7)

where k_n is the spring constant in normal direction calculated with:

$$k_n = \frac{\left|\vec{F}_{max}\right|}{[d(1-\lambda^*)]^{1.5}}$$
(2-8)

where λ^* is a defined penetration(Dong et al. 2009a), η_{nij} is the damping constant in normal direction:

$$\eta_{n,ij} = c_n \sqrt{\frac{9}{2}\left(\frac{m_i m_j}{m_i + m_j}\right)} \sqrt{\lambda} k_n \qquad (2\text{-}9)$$

where c_n is the damping coefficient which is equal to 0.3(CHU et al. 2008). Tangential force in static particles is shown as:

$$\vec{F}_{t,ij} = -k_{t,sta}\Delta x_{t,ij} - \eta_{t,ij}\vec{v}_{rel,t,ij} \qquad (2\text{-}10)$$

where $k_{t,sta}$ is the static spring constant in tangential direction and $\eta_{t,ij}$ is the damping constant in tangential direction:

$$k_{t,sta/dyn} = \frac{\mu_{sta/dyn}}{d(1-\lambda^*)}\left|\vec{F}_{max}\right| \qquad (2\text{-}11)$$

$$\eta_{t,ij} = 2\sqrt{\frac{2}{7}\left(\frac{m_i m_j}{m_i + m_j}\right)} k_{t,dyn} \qquad (2\text{-}12)$$

where $\mu_{sta/dyn}$ is the static or dynamic friction coefficient. Tangential forces are changed with the transcending of the static friction and the moving of particles:

$$\vec{F}_{t,ij} = -\mu_{dyn}|\vec{F}_{n,ij}|\vec{t}_{ij}\Delta x_{t,ij} \tag{2-13}$$
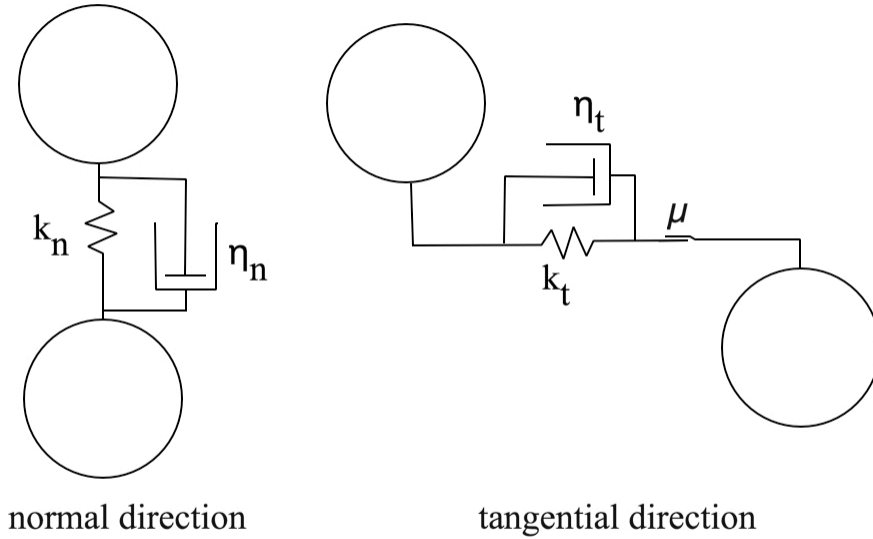
Figure 4 Particle-particle contact models (normal direction: spring and damper; tangential direction: spring, damper and slider) adapted from (Eichholz et al. 2012).

DEM simulation can be run with desired initial conditions, such as the number of particles, particle diameter, and particle size distribution, for multi-disperse systems(Chu and Yu 2008). In DEM, the solid matrix of porous media is modeled by packed particle assembly. The mechanical behaviors of the particle assembly are realized at contacts by appropriate contact and bonding laws. Because DEM can be used to simulate the physical locations of each particle in the model, one method of coupling the DEM and Lattice Boltzmann Method (LBM) techniques is to use the result of a DEM as the initial particle/boundary locations for the LBM (Munjiza, Bangash, and John

2004). LBM has been mathematically verified to represent Navier-Stokes equations in nearly incompressible fluids, its evolution equation is explicit, easy to implement and parallelization (Succi, Benzi, and Higuera 1991, Chen and Doolen 1998).

2.3.2 Lattice Boltzmann Method

The Lattice Boltzmann Method (LBM) is a computational model that is widely used in designing models of the physic properties of fluid flow, such as flow rate(Chen and Doolen 1998). LBM is based on the fact that individual molecules compose the fluid and the total behavior of the fluid can be calculated by summing the behavior of each individual molecule(Mohamad 2011). In LBM, a fluid is assumed to consist of mesoscopic fluid packets that repeatedly propagate and collide on a regular Cartesian lattice representing the flow field. The fundamental idea of LBM is to incorporate the essential physics of the microscopic process in a mesoscopic kinetic model so that the relationship among average properties at macroscale conforms to the Navier-Stokes equations(Succi 2001, Succi, Benzi, and Higuera 1991). Since its appearance (Mcnamara and Zanetti 1988), the lattice Boltzmann method (LBM) has been successfully solving different fluid physical problems, ranging from single-component hydrodynamics (Chen and Doolen 1998, Yu et al. 2003) to multi-phase or multi-component fluid flows (Grunau, Chen, and Egger 1993, Hou et al. 1997), creeping flow to turbulence flow(Luo, Qi, and Wang 2002), pure fluid flow to flow through porous media (Gunstensen and Rothman 1993) and solid particle suspension (Ladd 2015). In the theoretical studies and simulations of LBM, various lattice models have been proposed and examined (Mei, Luo, and Wei 2006): i.e., 3D models include D3Q15, D3Q19 and D3Q27. D3Q19, 3D lattice with 19 discrete velocities, providing best combination of computational stability and accuracy (Mei, Luo, and Wei 2006, Mei et al. 2000) as shown in Figure 5.

15
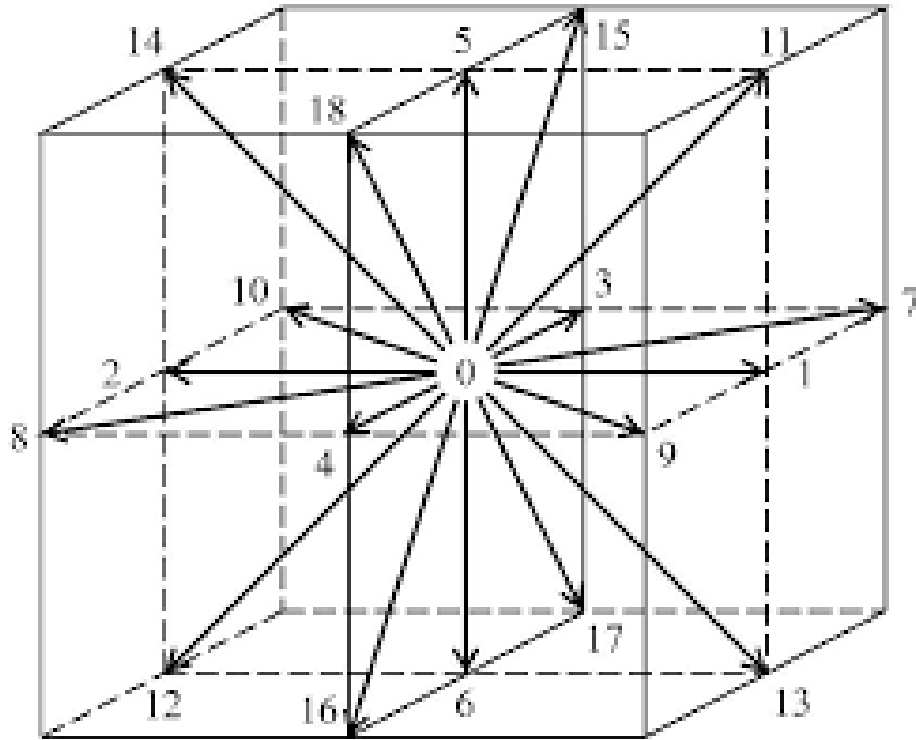
Figure 5 D3Q19 adapted from Luo, 2008 (Rubinstein and Luo 2008).

The LBM models developed by (Qian, D'Humières, and Lallemand 2007) in which the BGK (also called LBGK) collision function is used are implemented in this dissertation. The evolution equation of LBM-BGK model contains two steps in each computational loop: streaming and collision(Qian, D'Humières, and Lallemand 2007):

$$f_\alpha(\boldsymbol{x_i} + \boldsymbol{e}\delta t, t + \delta t) = f_i(\boldsymbol{x}, t) = f_i(\boldsymbol{x}, t) - \frac{1}{\tau}(f_i(\boldsymbol{x}, t) - f_i^{eq}(\boldsymbol{x}, t)) \qquad (2\text{-}14)$$

The left-hand side of (2-14 represents the streaming of fluid particles across the lattice, while the right-hand side describes the collision process via relaxation. The explicit nature of the equation makes LBM very simple to implement; the local nature of the collision operation makes the implementation quite straightforward to parallelize. In the equation, x_i is a physical point in the lattice space; $\mathbf{e}$ is the lattice velocity vector; δt is the timestep; τ is the dimensionless relaxation factor, $\tau = \lambda/\delta t$, λ is the relaxation time; i is the discretized direction; $f_i(x,t)$ is the particle distribution function (PDF); $f_i^{eq}(x,t)$ is the equilibrium distribution function (EDF):

$$f_i^{eq}(x,t) = w_i\rho[1 + 3\frac{\mathbf{e}\cdot\mathbf{u}}{c^2} + \frac{9}{2}\frac{(\mathbf{e}\cdot\mathbf{u})^2}{c^4} - \frac{3}{2}\frac{\mathbf{u}\cdot\mathbf{u}}{c^2}] \qquad (2\text{-}15)$$

where ρ is the density; u is the velocity vector; w_i is a weighting factor. where c is the lattice speed (δx / δt), δx is the lattice node spacing). In three-dimensional, $\mathbf{e}$ is

$$\begin{cases} e_0 = c(0,0,0); \\ e_1 = c(0,1,0); \ e_2 = c(0,-1,0); \\ e_3 = c(0,0,1); \ e_4 = c(0,0,-1); \\ e_5 = c(1,0,0); \ e_6 = c(-1,0,0); \\ e_7 = c(0,1,1); \ e_8 = c(0,-1,-1); \\ e_9 = c(0,1,-1); \ e_{10} = c(0,-1,1); \\ e_{11} = c(1,0,1); \ e_{12} = c(-1,0,-1); \\ e_{13} = c(-1,0,1); \ e_{14} = c(1,0,-1); \\ e_{15} = c(1,1,0); \ e_{16} = c(-1,-1,0); \\ e_{17} = c(-1,1,0); \ e_{18} = c(1,-1,0); \end{cases} \qquad (2\text{-}16)$$

The density ρ and velocity u are related to PDF and EDF as follows:

$$\rho = \sum_i f_i = \sum_i f_i^{eq} \; ; \; \rho\boldsymbol{u} = \sum_i \boldsymbol{e}f_i = \sum_i \boldsymbol{e}f_i^{eq} \tag{2-17}$$

For a node marked as being solid, the bounce-back rule applies to reflect the particles back in their incoming direction at the collision stage. If a periodic boundary condition exists in a particular direction, the last face will be contiguous with the first edge or face to make sure the lattice is closed in that direction (Mei, Luo, and Wei 2006).

The LBM-DEM coupling approach has been used to explore the physics involved in the fluid flow through porous media. Cook(Cundall, Hart, and Shimizu 2004) showed that LBM-DEM simulations were able to reproduce the formation of a sand arch stabilizing the solid matrix. In this dissertation, the DEM is used to simulate packed cakes to verify the changes of cake structure in different particle size distributions. LBM was chosen as the means to calculate the flows of fluid in different particle size systems using the DEM simulated beds.

3.0 Validating Kozeny Carman Model

The content of this chapter is taken from Zhang, Siying, and Joseph J. McCarthy. "Modeling of the pressure drop across polydisperse packed beds in cake filtration." AIChE Journal 65, no. 5 (2019).

3.1 Kozeny Carman Model

The Kozeny-Carman equation can be used in fluid flow through packed beds. It is based on the conventional theory and extended with experiments at constant pressure. For laminar flow in straight tubes, according to the Hagen-Poiseuille (H-P) equation(Schmid and Henningson 1994, Mortensen, Okkels, and Bruus 2005),

$$\Delta p_s = \frac{32 L \bar{V} \mu}{D^2} \tag{3-1}$$

where Δp_s is the pressure loss, L is the length of pipe, μ is the dynamic viscosity, $\bar{V}$ is the average velocity in the channels, and D is the diameter of the tube. In order to determine an effective tube diameter (D_{eq}) that mimics the pores within a cake, the surface area for n monomodal tubes should be equal to the surface-volume ratio times the particle volume:

$$nπD_{eq}L = \frac{A_{cs}L(1-ε)6}{Φ_sD_p}$$

(3-2)

where D_p is the particle diameter, $Φ_s$ is the sphericity, A_{cs} is the cross-sectional area of the bed.

Similarly, the void volume should be equal to the total volume of tubes.

$$A_{cs}Lε = \frac{1}{4}nπD_{eq}^2L$$

(3-3)

Combining (3-2) and (3-3), provides the equation for D_{eq}:

$$D_{eq} = \frac{2}{3}Φ_sD_p\frac{ε}{1-ε}$$

(3-4)

The average volume of channels is proportional to the superficial velocity ($\bar{V}_0$) and inversely proportional to the porosity:

$$\bar{V} = \frac{\bar{V}_0}{ε}$$

(3-5)

where ε is the porosity. Adding a correction factor, λ, into (3-1) represents the fact that channels are tortuous instead of straight and parallel. Combining this modified H-P equation with (3-4), and (3-5) we get

$$\frac{\Delta p}{L} = \frac{72\lambda \bar{V}_0 \mu}{\Phi_s{}^2 D^2} \frac{(1-\varepsilon)^2}{\varepsilon^3} \qquad (3\text{-}6)$$

The correction factor (λ) is typically taken as an empirical number equal to 2.1 so that we obtain(Rong, Dong, and Yu 2014):

$$\frac{\Delta p}{L} = \frac{150 \bar{V}_0 \mu}{\Phi_s{}^2 D^2} \frac{(1-\varepsilon)^2}{\varepsilon^3} \qquad (3\text{-}7)$$

(3-7) indicates that the flow rate is proportional to the ultimate pressure drop and inversely proportional to the fluid viscosity. This equation is similar to Darcy's law; therefore, it does not fit when the cake has high porosity, non-spherical particles, or systems of particles that are multi-disperse(Rushton, Ward, and Holdich 2008).

3.2 Experiments

In order to verify the influence of different multi-disperse systems on the predicted flow rate based on the Kozeny-Carman equation, a Nutsche Filter (a 0.2 Liter stainless steel filter with pressure regulator and down cap, DrM Company)(Reneau Jr 1992), is used at constant operating pressure. Constant pressure filtration is chosen with a cake that is composed of glass beads with regular, smooth surfaces (see Figure 6). The process for each filtration experiment was as follows:

1. Fix filter paper cloth at the bottom of the filter.

2. Pour a known volume and mass of dry glass beads into the filter.

3. Tap the outside chamber several times until the particles have to settle evenly.

4. Pour the fluid into the chamber; make sure the structure of the solid phase is not destroyed.

5. Apply a known pressure into the filter.

6. Allow the fluid flow through the filter continuous into a beaker, which posited on a scale.

7. Calculate the mass of fluid collected every 30 seconds.

8. Run six times for each cake with six different operating pressures.
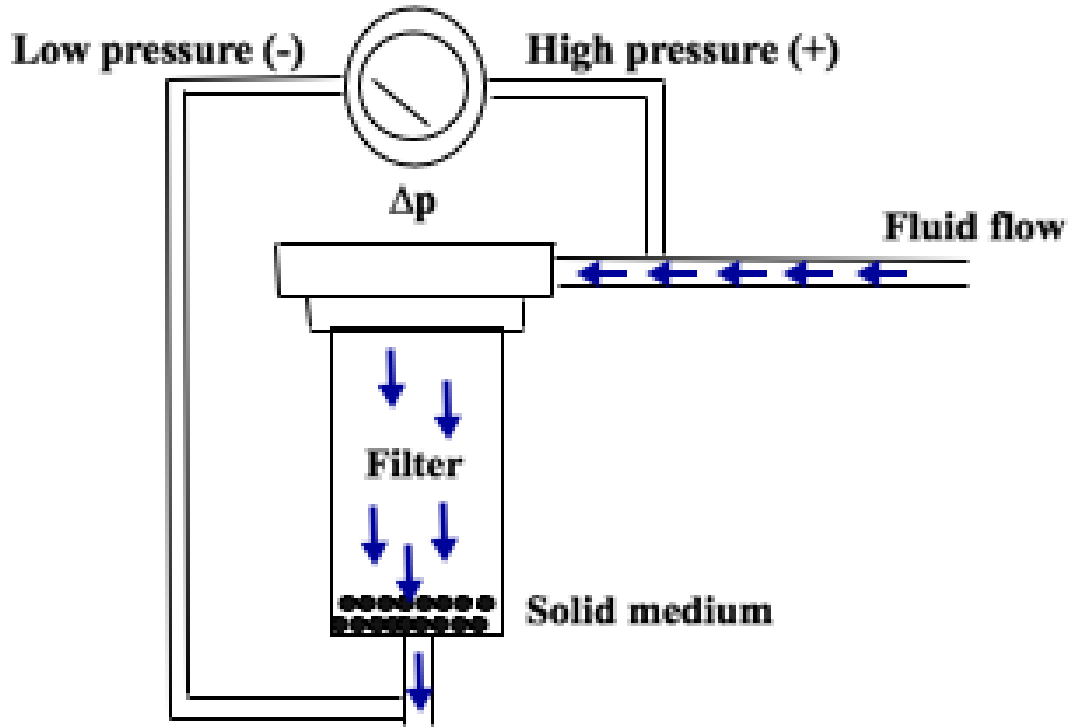
Figure 6 Chart of filtration experiment (Chose a pressure Nutsche filter).

We read the pressure (p) from the pressure gauge during the experiment. The ultimate pressure drop (Δp) is the pressure in the filter minus the atmospheric pressure. The superficial velocity can be calculated by measuring the accumulated mass of filtered fluid as a function of time. The porosity is the fraction of void space in a material. We use the fluid displacement technique, where we combine particles and fluid in a graduated container, in order to determine the porosity. The viscous liquid used for the fluid phase is pure glycerol. We chose different "polydisperse" glass beads with size, from 50 μm to 500 μm. Different grades of particles are used, thus the width of our particle size distributions varies (see Table 1). The criterion used for determining the "wideness" of the particle size distributions is the value of the standard deviation: the narrow size distribution corresponds to a standard deviation of the distribution that is smaller than 10 μm; the wide size distribution means the standard deviation of the distribution is larger

than 10 µm. Experiments are run at six operating pressures (range from 80 kPa to 350 kPa). In

what follows, we attempt to apply the K-C model to polydisperse systems by using the traditional

K-C expression but use an average diameter, the harmonic mean diameter (Zhang et al. 2010):

$$d_{HM} = \frac{n}{\sum_{i=1}^{n} \frac{1}{d_i}}$$

(3-8)

Table 1 Particle size distribution of polydisperse glass beads.

Sample number		1	2	3	1	1
Narrow size distribution (µm)	Mean size µ (µm)	58	69	82.5	98	500
	Standard deviation σ	5	6	7.5	8	0
Wide size distribution (µm)	Mean size µ (µm)	62.5	75	87.5	163.5	195
	Standard deviation σ	12.5	25	12.5	13.5	15

The cake thickness as examined range from $0.5 - 2.5$ cm and other quantities are held

constant. In addition to different grades of "polydisperse" particles, we also examine binary

mixtures in order to specify the more closely consider the particle size distribution. The procedure

for each mixing is similar and is as follows. Before the filtration process, for mixture, a known

volume of small particles and large particles are agitated by hand, while adding a small volume of

water. This creates a roughly homogeneous binary mixture. Then the cake is allowed to dry under

forced air flow. Experiments are run using five different size ratios (see Table 2) and six operating pressures (range from 80 kP a to 350 kP a). Ns/l is the number ratio of the mixture (Number of small particle/ number of large particle) R_l is the particle size of large particle; R_s is the particle size of small particle; $R_{s/l}$ is the size ratio of the mixture (R_s/R_l). The cake thicknesses are nearly 2 cm and other quantities are held constant.

Table 2 Five different size ratio by binary mixing with constant number ratio (N1 =1:1;N1 =3:1;N1 =6:1.).

Rs/l	1	0.84	0.50	0.33	0.20
Rl (µm)	500	98	200	500	500
Rs (µm)	---	82	100	165	100

Constant pressure filtration is used with a cake that is composed of glass beads with regular, smooth surfaces(Andersen 1980). The viscous liquid used for the fluid phase is pure glycerol. We chose different size ranges of glass beads with size from 50 µm to 500 µm. Experiments were run using different particle size distributions and six operating pressures. The cake thicknesses were $0.5 - 2.5$ cm and other factors were kept constant. After that, binary mixing was chosen in order to specify the effects of particle size distribution on the filtration process. The procedure for each filtration experiment is similar to the procedure above. However, before the filtration, a known volume of small particles and large particles were agitated with a mixer by add a little water to create a roughly homogeneous binary mixture and then the cake was allowed to dry under forced air flow. Experiments were run using five different size ratios and six operating pressures. The cake thicknesses were near 2 cm and other factors were kept constant.

3.3 DEM-LBM Simulations

We chose DEM, a numerical method that is used to compute the mechanical response of an extensive number of particles(Cundall and Strack 1979), to simulate the particle packing. DEM is a method to solve for the motion and physical response of a collection of particles through the solution of Newton's laws of motion for each discrete element within the system.

A detailed discussion of implementing this technique may be found in Chapter 2.3. Here, we use this approach to obtain the detailed pore structure of a bed of particles (as follows). A pore in our DEM model is defined as the void space inside a Delaunay cell(Reboul, Vincens, and Cambou 2008). In mathematics, a Voronoi diagram is a partitioning of a space into regions based on distance to points in a specific subset of the space. In this study, the specific subset of space is the set of positions that correspond to the location of the centers of the particles within the packed bed. That set of points is specified beforehand and are closer to a given point of the set to any other points. The Delaunay triangulation (DT), is another fundamental computational geometrical structure(Aurenhammer 1991). For the set of position in Voronoi diagram, a DT of these points ensures that no position is inside the circumcircle associated with each triangle, which is obtained by attaching entire pairs of points belongs to in the set point whose Voronoi regions share a common Voronoi edge (see Figure 7). Thus, a pore volume in this study is defined as the volume of an inscribed sphere of DT. Because the positions of the centers of the particles in the computational cake are known via the DEM, we can determine each void volume based on their positions by exporting the position into MATLAB with the Delaunay triangulation analysis.

Therefore, DEM can be used to obtain the void size distribution and particle packing for beds com- posed of different particle size distributions. LBM was chosen as the means to calculate the flows of fluid in different particle size systems using the DEM simulated beds. LBM is based

on the fact that individual molecules compose the fluid and the total behavior of the fluid can be

calculated by summing the behavior of each individual molecule(Mohamad 2011). Details of this

technique can be found in Chapter 2.3.
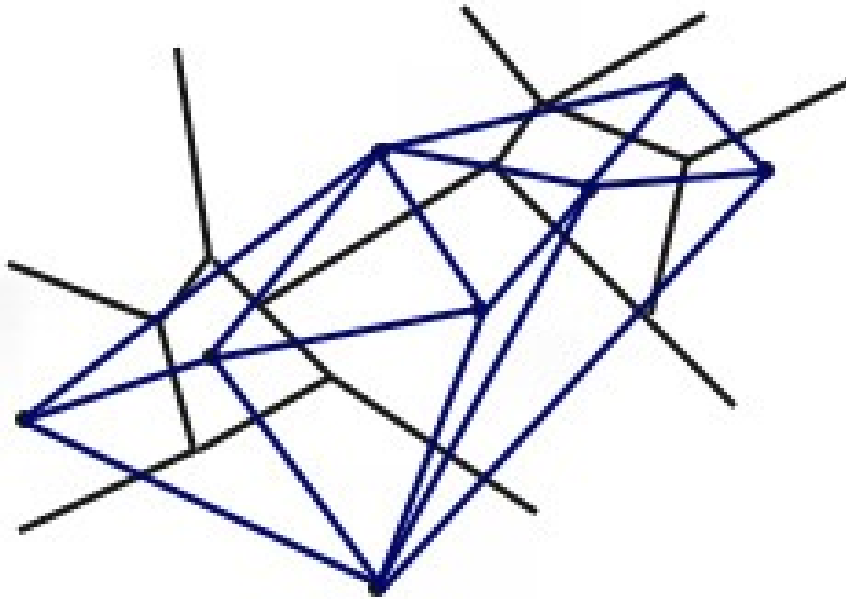
Figure 7 The dual Delaunay triangulation of the Voronoi diagram.

3.4 Results and Discussion

In order to verify the utility of the K-C model in a poly-disperse system, empirical flow rate was compared to predicted flow rate under the same operating pressure. Curve Fitting Toolbox (from MATLAB, command: cftool)(Mookiah et al. 2015) was used to evaluate the goodness of fit between data and predicted line.

3.4.1 Narrow Size Distributions

Figure 8 and Table 3 illustrates how well the predicted flow rates from K-C model match the empirical flow rates when the particle size distribution of the cake is narrow. Although the flow rates predicted by the K-C model were consistently a little lower than the empirical results in these narrow size distribution samples, the error between the empirical data and predicted data, in terms of the percent error, is less than 15 %.

Figure 9 shows how well the empirical flow rates fit with the predicted flow rates for different thicknesses of cakes for the same particle size distribution: $90 - 106$ μm. The flow rate decreases significantly with the increase of cake thickness; however, the errors between the empirical data and the predicted data are remain small. This quantitatively confirms that the K-C model can be applied in polydisperse systems with very narrow size distributions (deviation < 10 μm).

Table 3 Experiments: cake thickness, porosity in different narrow size distribution.

Narrow size distribution (µm)	53-63	63-75	75-90	90-106	500
Cake thickness (cm)	0.52	0.49	0.54	0.54	0.49
Porosity	0.36	0.36	0.34	0.35	0.35
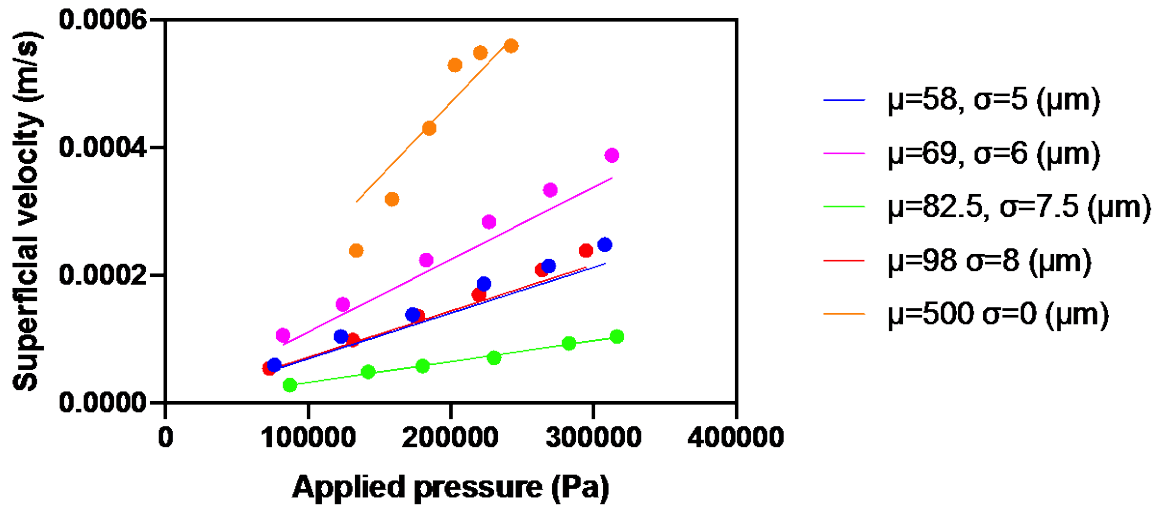
Figure 8 The relationship between the operating pressure and the flow rate with narrow size distribution particles (line: predicted flow rate, point: empirical flow rate).
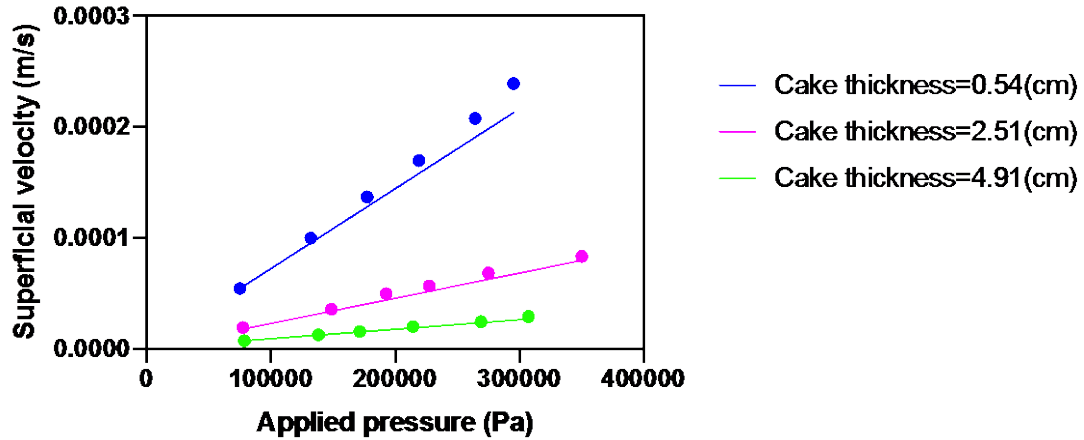
Figure 9 The relationship between the operating pressure and the flow rate in different thickness with narrow size distribution particles (line: predicted flow rate, point: empirical flow rate).

3.4.2 Wide Size Distributions

Unfortunately, when a cake is composed of particles that exhibit a wide particle size distribution, the flow rates predicted by the K-C model were consistently much lower than the flow rate obtained experimentally.

Figure 10 and Table 4 illustrates that the error between the empirical data and the predicted data is much larger. Even if we were to assume that the harmonic mean diameter is the wrong choice of average particle size and instead treat the average particle size as a fitting parameter we obtain an unrealistically high mean diameter (i.e., one that is beyond the limits of the distribution's sizes; see Table 5).

Figure 11 shows that the errors between the empirical data and the predicted data increase as we increase the cake thickness, again using the same particle size distribution: $50 - 100$ μm.

30

Thus, even if we introduce an unrealistically large mean particle diameter, 120 μm, we still need to modify the tortuosity as the cake thickness changes in order to maintain a good fit (see Table 6). These "ideal" quantities confirm that the K-C model cannot be used for beds of polydisperse particles with wide size distributions (standard deviation > 10 μm).

Table 4 Experiments: cake thickness, porosity in different wide size distribution.

Wide size distribution (μm)	50-75	50-100	75-100	155-177	180-210
Cake thickness (cm)	0.54	0.54	0.52	0.49	0.52
Porosity	0.35	0.36	0.35	0.35	0.36

We hypothesize that the increase in error observed for wide particle size distribution is caused by the change in cake structure that results in a multi-model pore size distribution (which is beyond the scope of the K-C model). The large error between empirical results and predicted results from K-C model demonstrates the influence of changing the void volume of the cake on the observed flow rate.
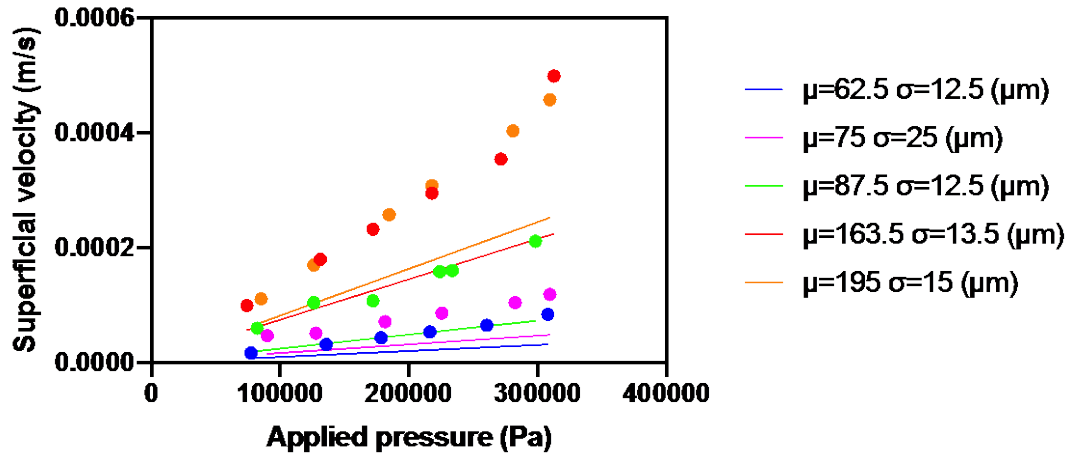
Figure 10 The relationship between the operating pressure and the flow rate with wide size distri- bution particles (line: predicted flow rate, point: empirical flow rate).
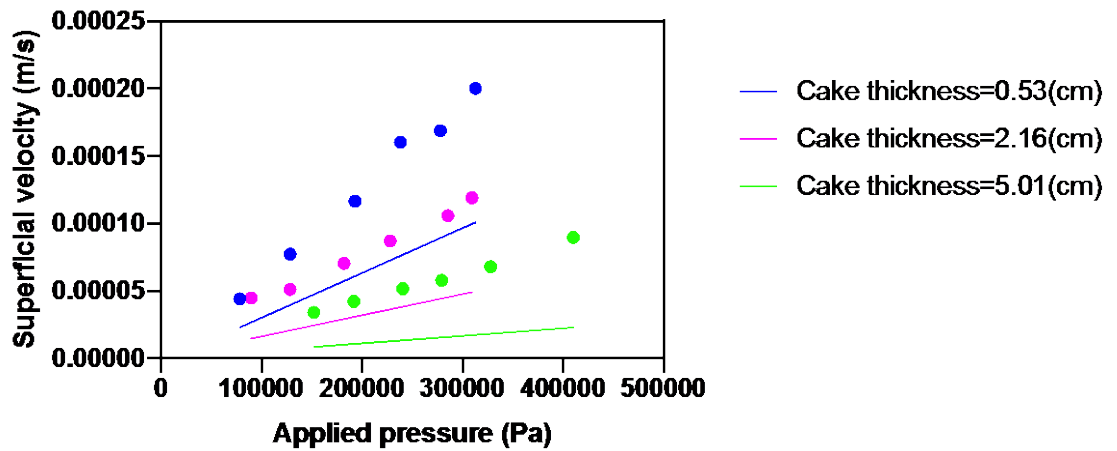
Figure 11 The relationship between the operating pressure and the flow rate in different thickness with wide size distribution particles (line: predicted flow rate, point: empirical flow rate).

Table 5 Fitted mean particle size for matching the predicted flow rate with experimental flow rate.

Real size (µm)	Fit size (µm)
50-75	92
50-100	120
75-100	171
150-177	223
180-210	239

Table 6 Fitted tortuosity for matching the predicted flow rate with experimental flow rate.

Cake thickness (cm)	Fit tortuosity
0.53	2.78
2.16	2.08
5.01	1.46

3.4.3 Binary Distributions

As shown in Figure 12, the errors between the empirical data and the predicted data are quite small for $R_{s/l} = 0.20$ and $R_{s/l} = 0.33$. However, the errors between empirical data and predicted data are much larger for $R_{s/l} = 0.50$ and $R_{s/l} = 0.84$ as shown in Figure 13. Therefore, the flow rate for a constant pressure filtration cake can be predicted by the Kozeny-Carman equation for small size ratios ($R_{s/l} = 0.50$), and it is inaccurate for large size ratios ($R_{s/l} = 0.50$). As previously explained, empirical results are influenced by particle distribution.
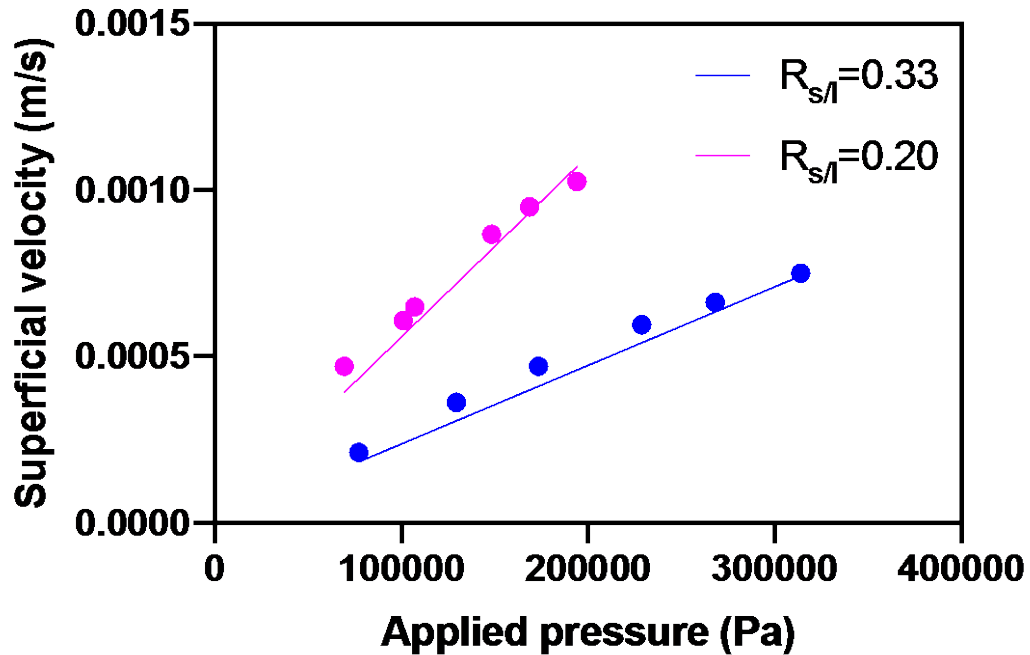
Figure 12 The relationship between the operating pressure and the flow rate with small size ratio (line: predicted flow rate, point: empirical flow rate).
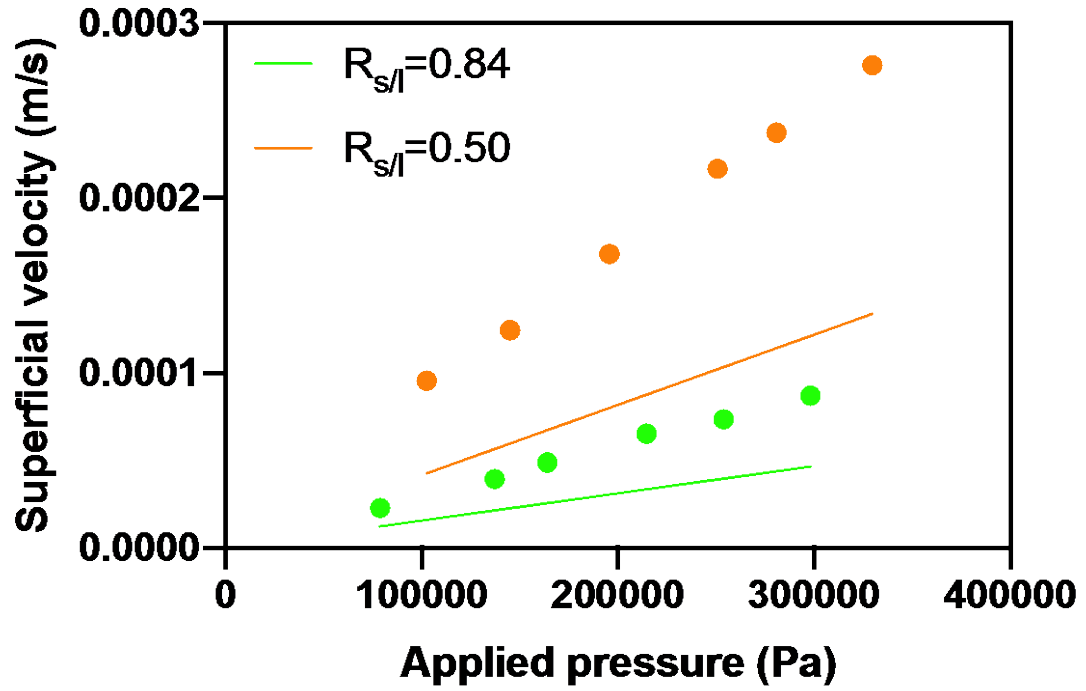
Figure 13 The relationship between the operating pressure and the flow rate with large size ratio (line: predicted flow rate, point: empirical flow rate).

Figure 14 shows the influence of number ratio in the prediction: the K-C model can only work for small size with different number ratio. Based on the work by Lash(Lash et al. 2015), for binary systems, particles with $R_{s/l} < 0.50$ can be packed efficiently, so the cakes have a tight distribution of void sizes; in contrast, particles with $R_{s/l} \geq 0.50$ cannot form ordered packings. Because the particles cannot form ordered packings for $R_{s/l} \geq 0.50$, we hypothesize that some voids are expanded by this disordered packing which can lead to channel formation and ultimately explain the much higher flow rate that is observed during filtration. Alternatively, for particles with a size ratio $R_{s/l} < 0.50$, we expect that the ordered packing that is achieved will behave much like a mono-model particle system (with a narrow size distribution). As a test of these two hypotheses, we endeavor to examine the void distributions observed in packings of binary systems in the next section.
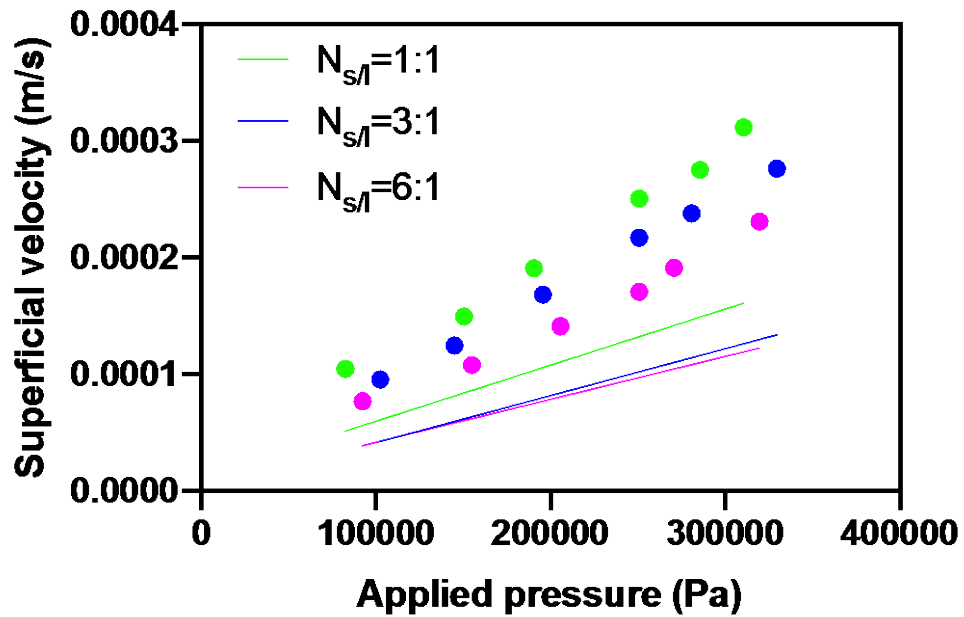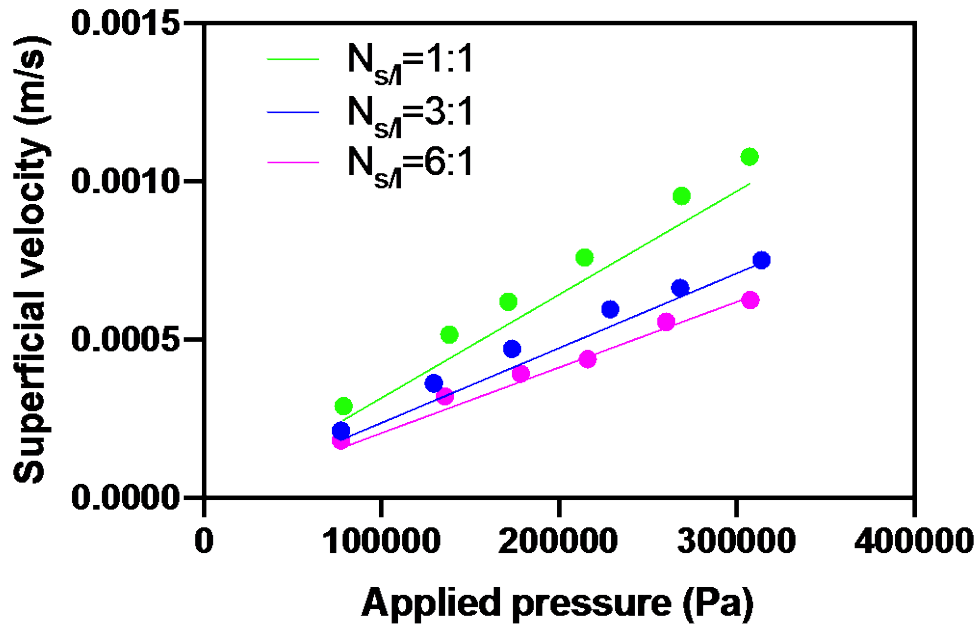
Figure 14 The relationship between the operating pressure and the flow rate with different number ratio. a.

Rs/l = 0.33; b. Rs/l = 0.50(line: predicted flow rate, point: empirical flow rate).

3.5 Modified Binary Model

Having established that the traditional K-C model fails to accurately account for the complex pore size distributions found in polydisperse (and other complex) packed beds, here we develop a modification that alleviates this shortcoming. Specifically, we introduce two quantities κ and β to describe this complexity. As mentioned earlier,we assume that the increase in the measured flow rate is caused by a disordered packing structure within the cake structure. This disorder, at a minimum, will lead to the formation of a non-monomodal distribution of effective void sizes. As such, as a simple first approximation, we introduce two quantities to describe the expansion: κ is the fraction of expanded voids; β is the ratio of void sizes. In order to determine the equivalent void tube diameter (D_{eq}) in a polydisperse medium, the surface area for n tubes should be equal to the surface-volume ratio times the particle volume(Carman 1956):

$$\kappa n\pi\beta D_{eq}L + (1-\kappa)n\pi D_{eq}L = A_{cs}L(1-\varepsilon')6/D_p \qquad (3\text{-}9)$$

$$\frac{A_{cs}L(1-\varepsilon')6}{D_p} = [\kappa\beta + (1-\kappa)]n\pi D_{eq}L \qquad (3\text{-}10)$$

Similarly, the void volume is equal to the total volume of tubes.

$$A_{cs}L\varepsilon' = \frac{1}{4}n\pi D_{eq}^2\kappa\beta^2 L + \frac{1}{4}n\pi D_{eq}^2(1-\kappa)L \qquad (3\text{-}11)$$

Combining these equations provides a new equation for D_{eq}:

$$D_{eq} = \frac{2}{3} \frac{\kappa\beta + (1-\kappa)}{\kappa\beta^2 + (1-\kappa)} \frac{\varepsilon'}{1-\varepsilon'} D_p \qquad (3\text{-}12)$$

Due to the fact that we have now assumed that the packed bed has two mean void size, D_{eq} and βD_{eq}, the actual velocity in each tube is no longer identical. We will take the actual velocity in a normal tube as v, so the actual velocity in an expanded tube should be βv. Then we can achieve the relationship between superficial velocity and actual velocity by match the same volumetric flow rate:

$$A_{cs} \times v_{sup} = \frac{1}{4} \pi n [\kappa\beta^2 v\beta^2 + (1-\kappa)v] D_{eq}^2 \qquad (3\text{-}13)$$

Again, combining these expressions gives

$$v_{sup} = \varepsilon \times v [\frac{\kappa\beta^4 + (1-\kappa)}{\kappa\beta^2 + (1-\kappa)}] \qquad (3\text{-}14)$$

Incorporating this model into the Hagen-Poiseuille equation:

$$\frac{\Delta p}{L} = \frac{32v\mu}{D_{eq}^2} \qquad (3\text{-}15)$$

Taking u to represent v_{sup}, therefore, we can obtain the modified Kozeny-Carman equation for multi-disperse systems:

$$\frac{\Delta p}{L} = \frac{72\lambda u\mu}{D_p{}^2 \varepsilon^3} \frac{[1 - \varepsilon[\kappa\beta^2 + (1-\kappa)]]^2}{[\kappa\beta + (1-\kappa)]^2} \times \frac{1}{\kappa\beta^2 + (1-\kappa)} \qquad (3\text{-}16)$$

Because we have assumed that some voids are expanded, the pathway through the cake can be more linear as fluid has more gaps to flow through. As a result, the tortuosity should be decreased. The tortuosity factor, λ, can be modified based on its definition. That is, the tortuosity is the ratio between the length of the real pathway and the distance between two ends. Based on Figure 15, the length of a real pathway can be calculated from the equation:

$$L' = D_{eq} + 2D_p \ (red \ path) \qquad (3\text{-}17)$$

Similarly, the distance between two ends is:

$$L = D_{eq} + D_p \; (black\; path) \tag{3-18}$$

Using this definition, we can calculate the tortuosity from the weighted average of the normal value and the expanded one,

$$\lambda_{tot} = (1 - \kappa)\lambda_{normal} + \kappa\lambda_{expanded}$$

$$= (1 - \kappa)\frac{D_{eq} + 2D_p}{D_{eq} + D_p} + \kappa\frac{\beta D_{eq} + 2D_p}{\beta D_{eq} + D_p} \tag{3-19}$$
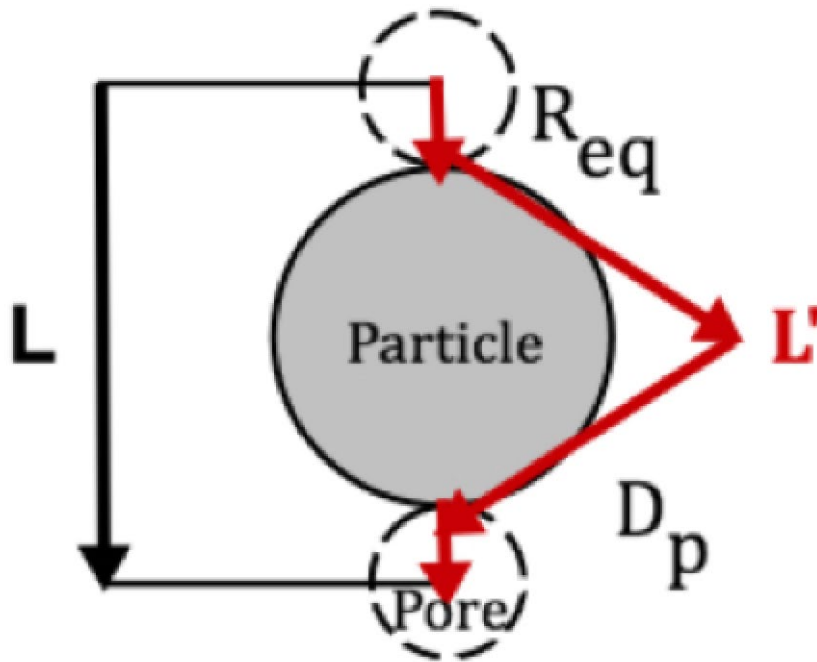
Figure 15 Determination of tortuosity through a particle.

Based on this equation, we can calculate the modified tortuosity with the modified quantities. It is important to note that, for a mono-modal distribution of pores, this equation predicts a value of the tortuosity equal to 2.1 (as is typically chosen empirically in K-C model). Nattavades and Gerald also try to measure the tortuosity based on the streamlines from the lattice Boltzmann method(Srisutthiyakorn and Mavko 2017). The tortuosity calculated based on our model are quite similar to those found in the simulation results from the Nattavades model as shown in Table 7.

We should note that this new model ostensibly has two total "fitting" parameters, κ and β. However, one way to verify the modified model is to use a DEM simulation to represent the pore size distribution and calculate the quantities κ and β (thus reducing the model to zero fitting parameters). Because the positions of the centers of particles in the cake are known by the DEM,

we can determine each void volume based on their positions in MATLAB(Reboul, Vincens, and Cambou 2008). The normal distribution and kernel distribution of the void size distribution can be determined by the MATLAB from the CurveFittingToolboxT M (from MATLAB, command: cftool). The bi-normal distribution of the void size distribution can be determined by the PDF function in MATLAB.

Table 7 Compare tortuosity between modified K-C model and LBM simulation with Ns/l = 3.

Particle size ratio	Tortuosity by modified model	Tortuosity by LBM(Srisutthiyakorn and Mavko 2017)
1	2.10	2.11
0.84	1.76	1.78
0.50	1.73	1.75
0.33	2.10	2.12
0.20	2.10	2.11

Table 8 AIC test of normal and bi-normal fit for the pore size distribution in different particle size ratio.

Rs/l	1	0.84	0.50	0.33	0.20
AIC of normal fit	-1971.67	-2767.57	-2444.90	-2554.70	-2643.16
AIC of bi-normal fit	-1921.56	-3516.19	-3093.52	-2510.21	-2578.27

For a mono-disperse medium and small size ratio, the void size distribution shows only one peak (see Figure 16 and Figure 17), which implies that the size of each void space is identical. Thus, one single average void size is adequate to predict the flow behavior by the modified model for mono-disperse medium ($\kappa = 0$ and $\beta = 1$).

In an effort to assess whether the additional (non-fitting) parameters increase the goodness of fit, we use the Akaike information criterion (AIC)(Akaike 1987). The AIC is an estimator of the relative quality of statistical models for a given set of data.

Table 8 shows the AIC of normal fit is small than the AIC of bi-normal fit for Rs/l = 1, Rs/l = 0.20 and Rs/l = 0.33, which indicates that the normal model fits better. For a normal model of void size distribution, $\kappa = 0$ and $\beta = 1$. In contrast, the AIC of normal fit is much larger than the AIC of bi-normal fit for Rs/l = 0.84 and Rs/l = 0.50. This indicates that the bi-normal fit is better. Hence, there is a significant impact of pore size distribution on the permeability of packed beds for certain binary particle size ratios. In short, we find that in systems that include large size ratio mixtures (Rs/l > 0.5), particle packings are disordered such that they lead to channeling in the packed bed. In these cases, void quantities determined by bi-normal distribution are based on different mean void sizes and probability density as shown in Figure 18. Using these distributions, we can calculate the predicted flow rate using the κ and β from the modified model. Void quantities (κ and β) that determined by fitting distribution are based on different mean void sizes and probability density as shown in Table 9.
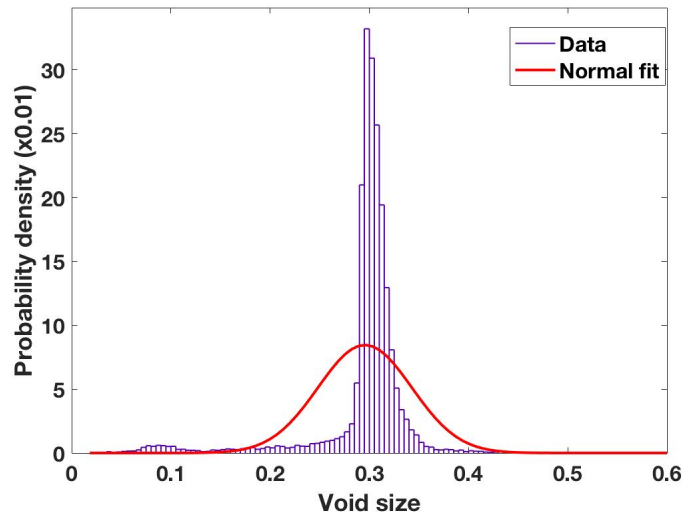
Figure 16 Probability density functions of the void size for mono-disperse system.
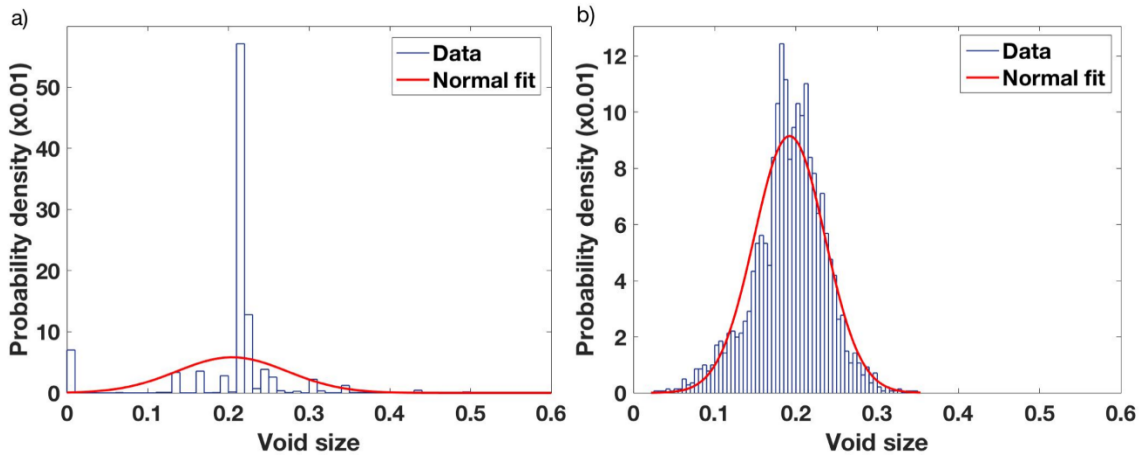
Figure 17 Probability density functions of the void size for binary-disperse system in small size ratio a. Rs/l = 0.20 b. Rs/l = 0.33.

Table 9 Void sizes and the percentages of the second peak for the void size bi-normal distribution of simulated beds.

Rs/l	Fitting method	Void size of first peak	Void size of second peak	Percentage of second peak
0.84	Bi-normal fit	0.1707	0.2224	20.54%
0.50	Bi-normal fit	0.1932	0.2199	45.86%

For both $R_{s/l} = 0.84$ and $R_{s/l} = 0.50$ in Figure 18 the error between the empirical flow rate and the predicted flow rate based on the K-C model is quite large. Conversely, the error between the empirical flow rate and the predicted flow rate using the modified model is much smaller. Similarly, the value of R-square is significantly increased with a modified model in Table 10.
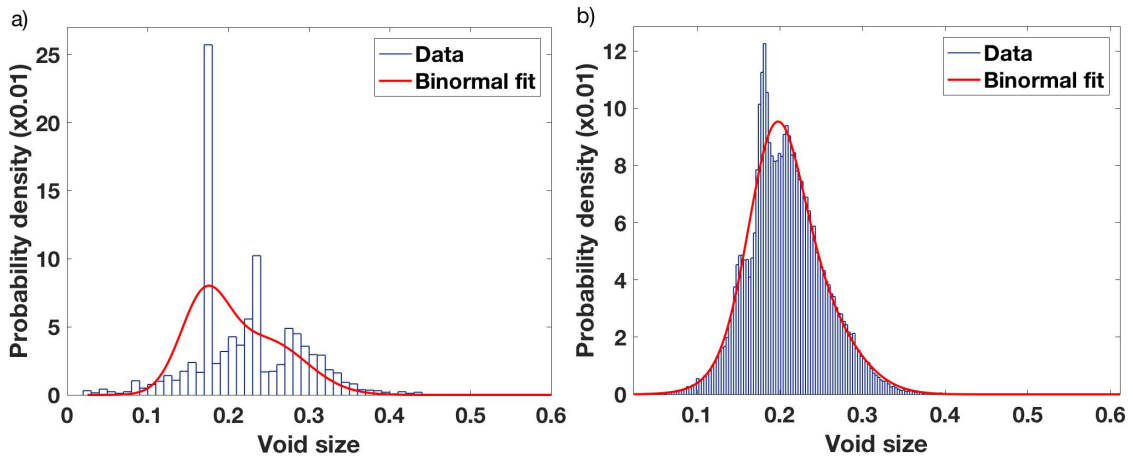
Figure 18 Probability density functions of the void size for binary-disperse system in large size ratio: a. Rs/l=0.50 b. Rs/l=0.84.

Table 10 Different between predicted flow rate and empirical flow rate.

Rs/l	Data	Error	R-square
0.84	K-C model	87.71%	0.7803
0.84	Bi-normal fit	25.68%	0.9557
0.50	K-C model	110.85%	0.7543
0.50	Bi-normal fit	40.37%	0.9415

The modified model predicts the fluid flow/pressure relationship to a higher degree of accuracy than the K-C model for our filtration experiment as shown in Figure 19 and Figure 20. We should note that, while the error between the predict flow rate from the modified model and the measured results from experiment are still larger than 10 %, we assume that this error is caused by a (small) difference in the pore size distribution observed in the experimental cakes relative to those in our simulated packed beds. In order to test this assumption, we mimic the flow through the simulated cake using LBM.

Figure 21 shows the simulation result. As in the physical experiments, our simulated flow shows that the K-C model can only predict the flow behavior in mono-disperse systems. The difference between the predicted results from the K-C model and the simulated flow rate is much larger in Rs/l = 0.84 and Rs/l = 0.50 systems, where the particle packing is observed to be disordered. What's more, the prediction from our modified equation in Rs/l = 0.84 and Rs/l = 0.50 system fit the simulated results extremely well.
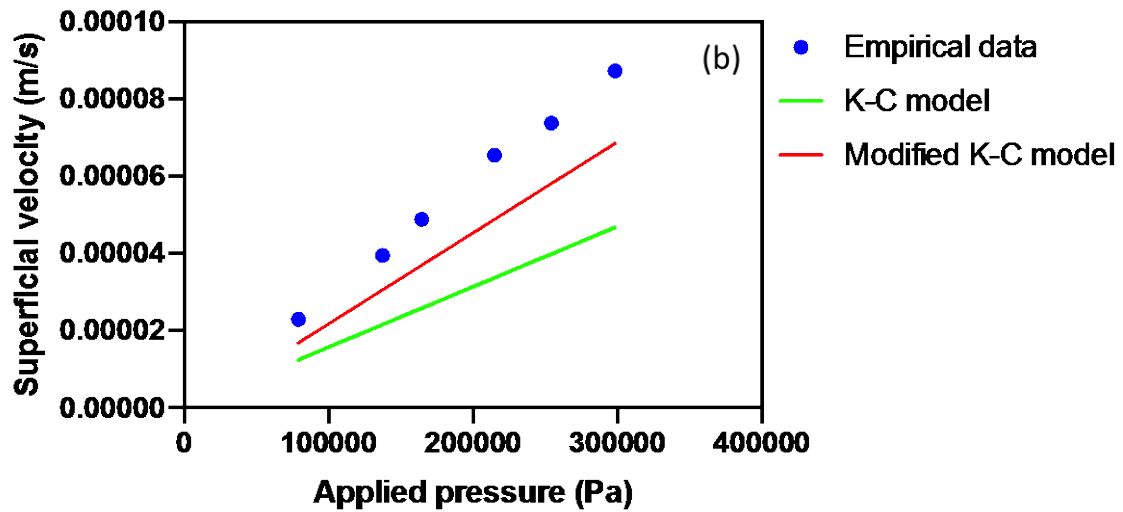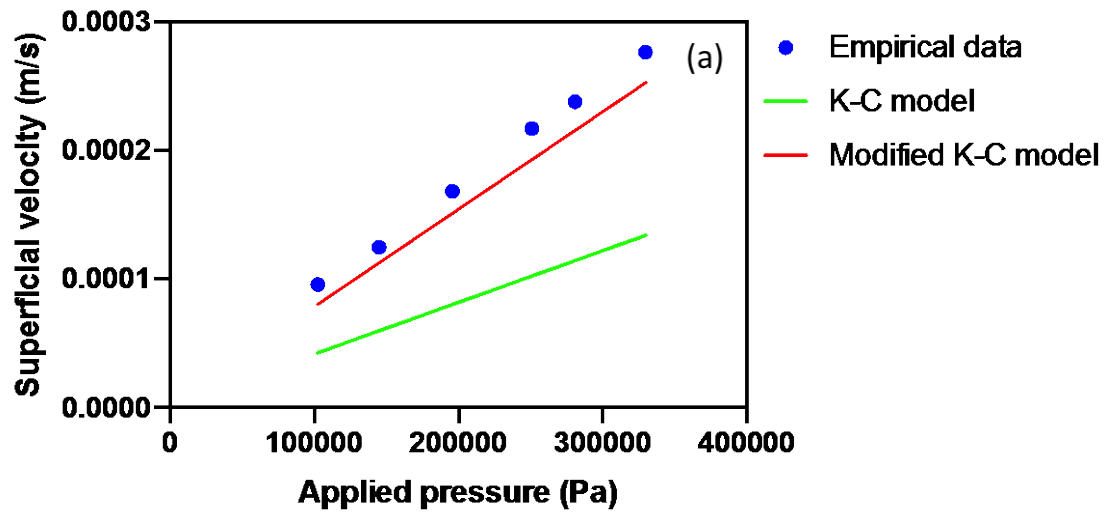
Figure 19 The relationship between the operating pressure and the flow rate of binary-disperse system with modified K-C model: a. Rs/l=0.50 b. Rs/l=0.84.
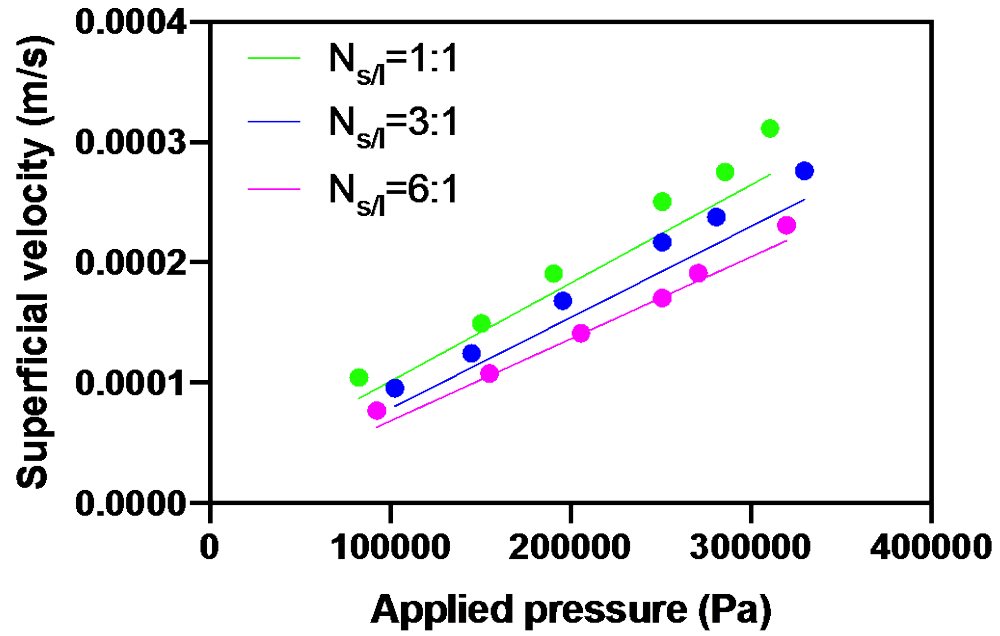
Figure 20 Verification of modified model in binary-disperse system with different number ratio, Rs/l =0.50.
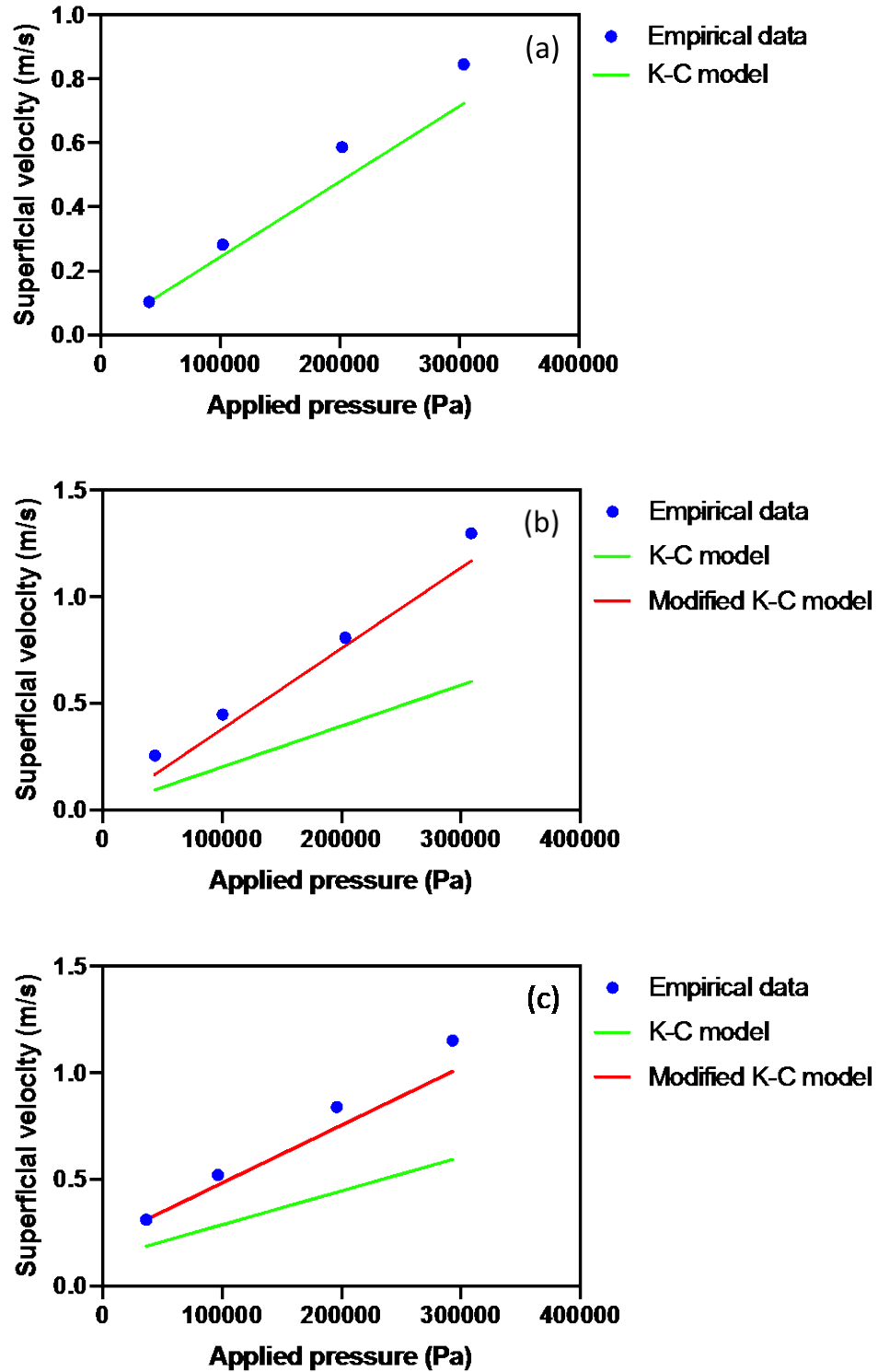
Figure 21 Verification of modified model with LBM simulation: a. mono-disperse b. Rs/l = 0.50 c. Rs/l = 0.84.

By comparing experimental results to those predicted from the K-C model, we assess the utility of this equation for application to systems that include polydisperse particles at moderate fluid pressure. We find substantial agreement between the model and the experiment only for systems that result in well-ordered particle packing. Dramatic disagreement is observed for particle beds that exhibit wide pore size distributions (deviation > 10 μm), as these particles cannot form ordered packings. The K-C model is failed to consider the complexity of the pore size distribution of a packed bed. Therefore, we introduce two quantities κ and β to describe this complexity. κ is the percentage of the expanded pores in the pore size distribution, which is influenced by the percentage of disordered particles; β is the ratio of the expanded pore size to the normal pore size, which is influenced by the expanded rate during the filtration. The predicted flow dynamics from the modified model are found to be much more similar to the experimental flow rates than those calculated using the K-C model. Prediction by the modified model also works much better in LBM simulations where we have direct access to the pore size distribution. In short, the effect of the pore size distribution on filtration cakes is important. The modified equation is deemed reliable at predicting the flow behavior, provided that an accurate representation of the pore size distribution is available. It will also be interesting to simplify the modified K-C model based on the analysis of the pore size distribution to reduce the redundant calculations.

4.0 Dynamic Modeling of Steric Filtration Including Surface- and Depth- Filtration Effects

From Chapter 3.0, we found that the increase of flow rate is caused by disorder within the cake structure. This disorder, at a minimum, will lead to the formation of a non-monomodal distribution of effective void sizes(Hulmes et al. 1995). We proposed a modified K-C model capable of predicting the flow behavior for a poly-disperse system by introducing two quantities to describe the pore structure. The modified model is deemed reliable at predicting the flow behavior, provided that an accurate representation of the void size distribution is available. However, the calculation of n-1 quantities can be extremely inconvenient with complicated pore size distribution. This modified model is also limited to static pressure drop predictions and is difficult to directly apply to any dynamic filtration process. In this section, a first-principles based model is developed to predict the cake dynamics, including a transition between depth/surface filtration, based solely on known physical quantities of the filter bed and contaminants. The model relies solely on the to-be-captured particle size distribution of contaminants as well as the pore size distribution of the filtration media with an output of all relevant process variables and parameters (superficial velocity, pressure drop, etc.). Experiments, including both cake filtration and depth filtration, are used to validate this model.

4.1 PSD Model

The current study develops experiments including both cake filtration and depth filtration are used to validate this model. Based on previous work, we found that the increase of flow rate is caused by disorder within the cake structure. This disorder, at a minimum, will lead to the formation of a non-monomodal distribution of effective void sizes(Lash et al. 2015). In order to capture this variation in pore size, we explicitly account for both the pore sizes and pore volumes to describe the expansion. We provide a model to predict the dynamic behavior for both the liquid and solid phase of a filtration process without the requirement of empirical parameters. Instead, our model relies solely on the to-be-captured particle size distribution of contaminants as well as the pore size distribution of the filtration media. In an effort to understand the relationship between flow dynamics and pore size distribution more fully, we built a dynamic filter cake model that continuously modifies the pore size distribution as contaminants (polydispere spheres) are deposited. The model is based on the following assumptions: (1) The filter cake is incompressible. (2) There is no chemical reaction during the filtration process. (3) The fluid flow should be a slow, viscous flow with a Reynolds number less than one. According to the Hagen-Poiseuille equation,

$$\Delta p = \frac{32\lambda L v_i \mu}{D_i^2} \tag{4-1}$$

where Δp is the pressure drop across the tube, L is the length of the tube, μ is the dynamic viscosity, v is the average velocity in the unhindered tube, and D is the diameter of the tube. We can calculate the linear velocity through each pore as:

$$v_i = \frac{\Delta p D_i^2}{32 \lambda L \mu} \tag{4-2}$$

where λ is the tortuosity of the pore channel. Tortuosity can be determined by its definition: that is, that the tortuosity is the ratio between the length of the actually path traversed by the fluid and the linear distance between the two measurement points. Assuming that the actual fluid pathway within a porous material includes traversing both the "empty space" within a pore as well as circumscribing the particles that make up the pore, we obtain

$$Real\ pathway = D_i + 2D_p \tag{4-3}$$

In contrast, the linear distance between the two corresponding measurement points is given as

$$Distance\ between\ two\ end = D_i + D_p \tag{4-4}$$

Thus, a first-principles expression for flow through an occluded pore may be written as

$$\lambda = \frac{D_i + 2D_p}{D_i + D_p} \tag{4-5}$$

If we employ the constraint that the overall volumetric flow rate may be written either in terms of a superficial velocity, v_{sup}, or in terms of the sum of all of the individual flows within the pores, we get:

$$A_{cs} v_{sup} = \sum_{i=1}^{m} \frac{1}{4} \pi D_i^2 v_i\, n_i \qquad (4\text{-}6)$$

where n_i is the number of pores of type i, m is the total number of pore sizes. We can obtain this value from a measurement of the total pore volume for each pore, i, using

$$n_i = \frac{V_i}{\lambda L \frac{1}{4} \pi D_i^2} \qquad (4\text{-}7)$$

where V_i is total volume of pore type i. Combining these expressions, we can get a final, first-principles description of the superficial velocity based on the pore diameters and pore volumes as

$$v_{sup} = \frac{1}{A_{cs}} \frac{\Delta p}{32 L^2 \mu} \sum_{i=1}^{m} \frac{D_i^2 V_i}{\lambda_i^2} \qquad (4\text{-}8)$$

The pore size distribution (PSD) model, shown in (4-8, allows the prediction/calculation of the overall flow (i.e., superficial velocity) through a complex bed that relies simply on knowledge of the fluid properties and a measurement of the pore size distribution (including pore volumes) of the cake itself.

4.2 Static Filtration

In order to verify the PSD model, a Nutsche Filter (Rushton, Ward, and Holdich 2008), which is a cake filter and performs filtration at constant operating pressure, was chosen for the experiments. Several validation tests were run, including constant pressure flow measurements through a cake, as well as both depth and depth/surface filtration of contaminants. The cake medium in these tests is either made of glass beads or a commercially available diatomaceous earth (FAX) material. The contaminant of choice was comprised of glass beads with regular, smooth surfaces (of varying size) and the viscous liquid used for the fluid phase is pure glycerol.

In our first suite of experiments, we ramp the operating pressure (drop) several times to not only test the repeatability of our results but also to ensure that our cake is not to be considered as compressible. We chose different grades of FAX (i.e., that we will label as 3, 5, and 7) that offer a variety of complex pore structures (see Figure 22). Our first set of validation experiments were run using six operating pressures (repeated 3 times). The cake thicknesses were 0.5cm and other factors were kept constant. The process for each filtration experiment was as follows:

1. Fix filter paper cloth at the bottom of the filter.

2. Pour a known volume and mass of dry filter aid into the filter.

3. Tap the outside chamber several times until the particles have to settle evenly.

4. Pour the fluid into the chamber; make sure the structure of the solid phase is not destroyed.

5. Apply a known pressure into the filter.

6. Allow the fluid flow through the filter continuous into a beaker, which posited on a scale.

7. Calculate the mass of fluid collected every 30 seconds.

8. Run six times for each cake with six different operating pressures.

9. Repeat step 8 two times.
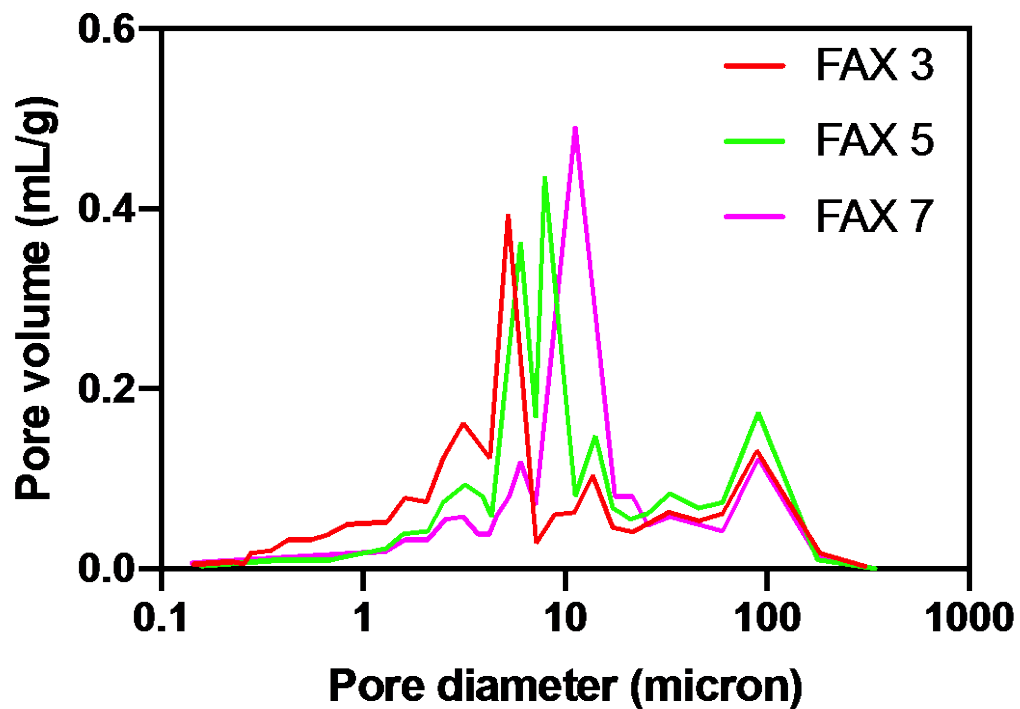
Figure 22 Pore size distribution of filter aid FAX3, FAX 5 and FAX 7 from mercury porosimetry, Lubrizol Corporation.

We employed both the PSD model and the K-C model to predict flow rates under the same operating conditions. Here we determine the number of pore sizes of the filter medium based on the number of peaks in its pore size distribution. From the pore size distribution, as shown in Figure 22, there are approximate seven pore sizes for FAX 3. As a means of refining the PSD model, we test our approach under three sets of assumptions Figure 23. The "7-model" assumes that all measurable pores contribute to the fluid flow, thus it combines all the pore modes observed from measurements of the FAX structure; the "6-model" omits the smallest measured mode of pore sizes; the "5-model" omits any pores whose mode falls below 3 µm.

Figure 24 shows a comparison of the simulation results and a series of experimental tests. One notes that the K-C model dramatically under-predicts the flow rate (perhaps due to the highly porous nature of FAX). The AIC test(Akaike 1987) also shows the "6 model" fits the experimental data best: the AIC of "7 model" is -1763.64, the AIC of "6 model" is -2412.02, the AIC of "5 model" is -2019.87. Of the PSD model varieties tested, it is clear that the "6 model" most accurately predicts the flow behavior.

This can be understood in the following way. The single-mode of pore sizes that is omitted from the analysis in this PSD variety are those with pore size < 2 µm; however, in examining the scanning electron micrograph of the material Figure 25, it is clear that it is not the absolute size of the pore that is critical, but instead the fact that the pores of that size are those that are intrinsic to the individual particles that make-up the FAX. We found the "6 model" fits the experimental data best when we only consider the peak of the pore size distribution.

Thus, we tried to extend the "6 model" with some pore sizes near these six peaks. The AIC of the extended "6 model" is about 2474.85, which is only a slightly lower than the AIC of the "6 model". That is, our PSD model works quite well we consider only pores (peaks in the pore size

distribution) that are created between particles of the cake/filter media, and omit those that are intrinsic (or "dead end") to the material (Hodgson et al. 1993, Koponen, Kataja, and Timonen 1997).
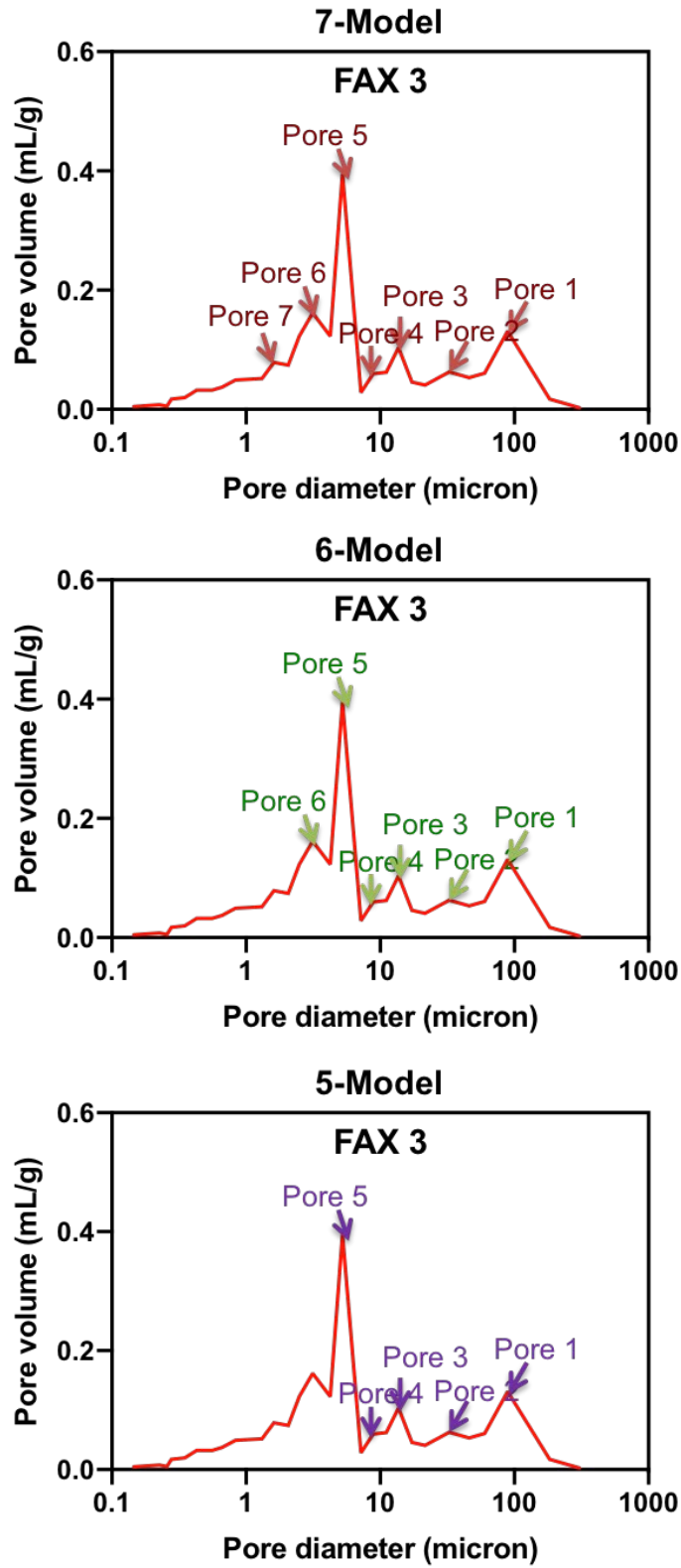
Figure 23 Selection of pore sizes for 7-PSD Model, 6-PSD Model, and 5-PSD Model.

60
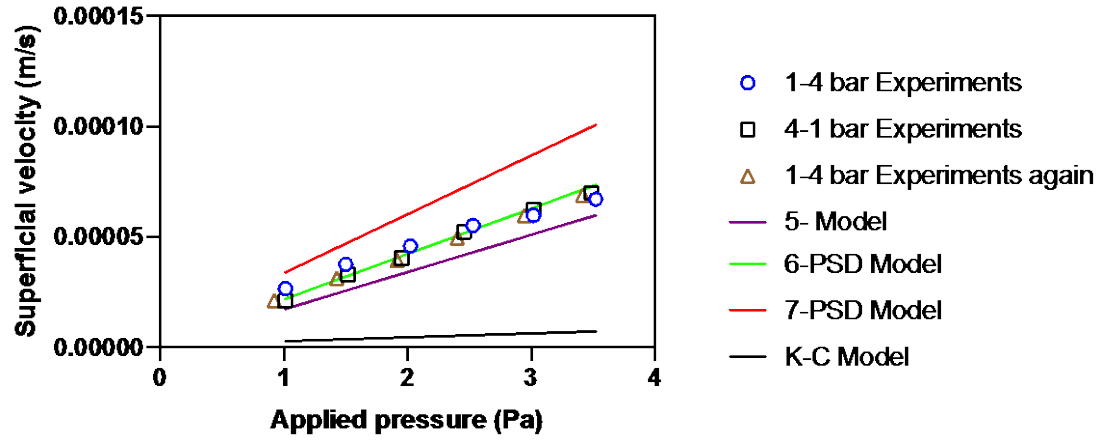
Figure 24 The relationship between the operating pressure and the flow rate of the FAX system with PSD

models. (Line: predicted results by simulaiton model. Points: experimental data)
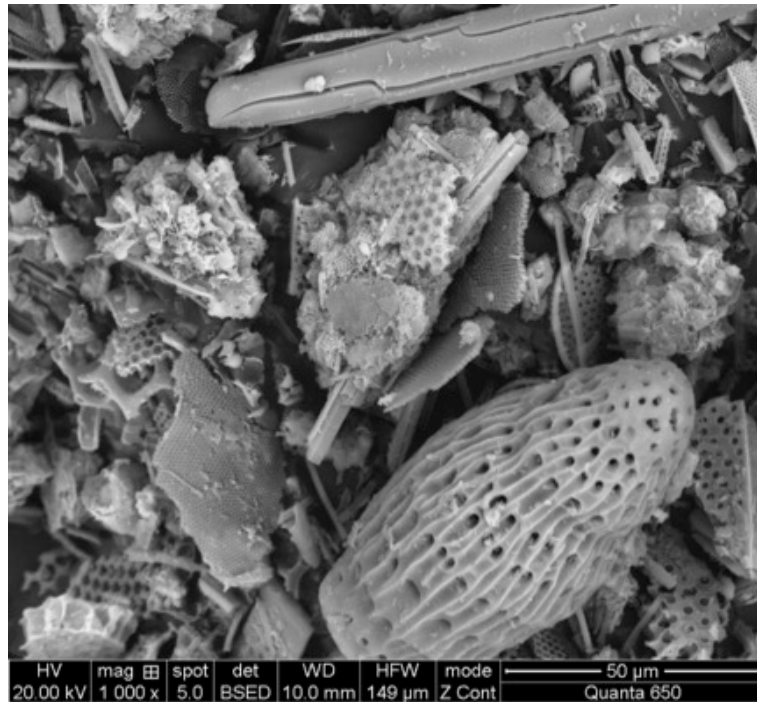
Figure 25 SEM image of FAX 3 with intrinsic pores (pore size < 2µm).

The comparison between experimental flow rate and prediction for FAX 5 and FAX 7 also show the 6-PSD model works best. Thus, the PSD model (6 model) can predict the flow behavior in high porous system very well without the consideration of intrinsic pores.

4.3 Dynamic Filtration

The next step is to verify the PSD model in a dynamic filtration, which separate solid particles from suspensions. Dynamic filtration can be separated into two parts: depth filtration and surface filtration. Depth filtration is typified by a porous layer that captures solid contaminants from the liquid phase within its embedded pore volume. Thus, the time dependency of volume flow J_v is given by (Chudacek and Fane 1984):

$$J_v(t) = \frac{J_v(0)}{(1 + Bt)^2}$$
(4-9)

where B is equal to Ku and K is the decrease in the cross-section area of the pores per unit of total permeate volume. The predicted time evolution of the total permeate volume is

$$V(t) = \frac{J_v(0)t}{1 + Bt}$$
(4-10)

While the characteristic equation of the depth filtration process should be

$$\frac{d^2t}{dV^2} = \frac{2B}{\sqrt{J_v(0)}}(\frac{dt}{dV})^{3/2} \quad or \quad \frac{d^2t}{dm^2} = k\left(\frac{dt}{dm}\right)^{1.5} \tag{4-11}$$

Instead, surface filtration involves the capture of contaminants at the surface of the media such that the filter cake height increases. Thus, particles will remain at the surface of the filter medium and create a new cake layer. For a surface filtration, the time law for the volume flow J_v is given by (Chudacek and Fane 1984, Bowen, Calvo, and Hernandez 1995):

$$J_v(t) = \frac{J_v(0)}{\sqrt{1 + Ct}} \tag{4-12}$$

where $C = 2R_rK_Cu_0$. $1/K_C$ is the total permeate volume per unit of membrane area and R_r is the hydraulic resistance. The predicted time evolution is given by:

$$V(t) = \frac{2J_v(0)t}{C}[\sqrt{1 + Ct} - 1] \tag{4-13}$$

63

Thus, the characteristic equation of the surface filtration process is:

$$\frac{d^2t}{dV^2} = \frac{C}{2J_v{}^2(0)}(\frac{dt}{dV})^0 \; or \; \frac{d^2t}{dm^2} = k\left(\frac{dt}{dm}\right)^0 \tag{4-14}$$
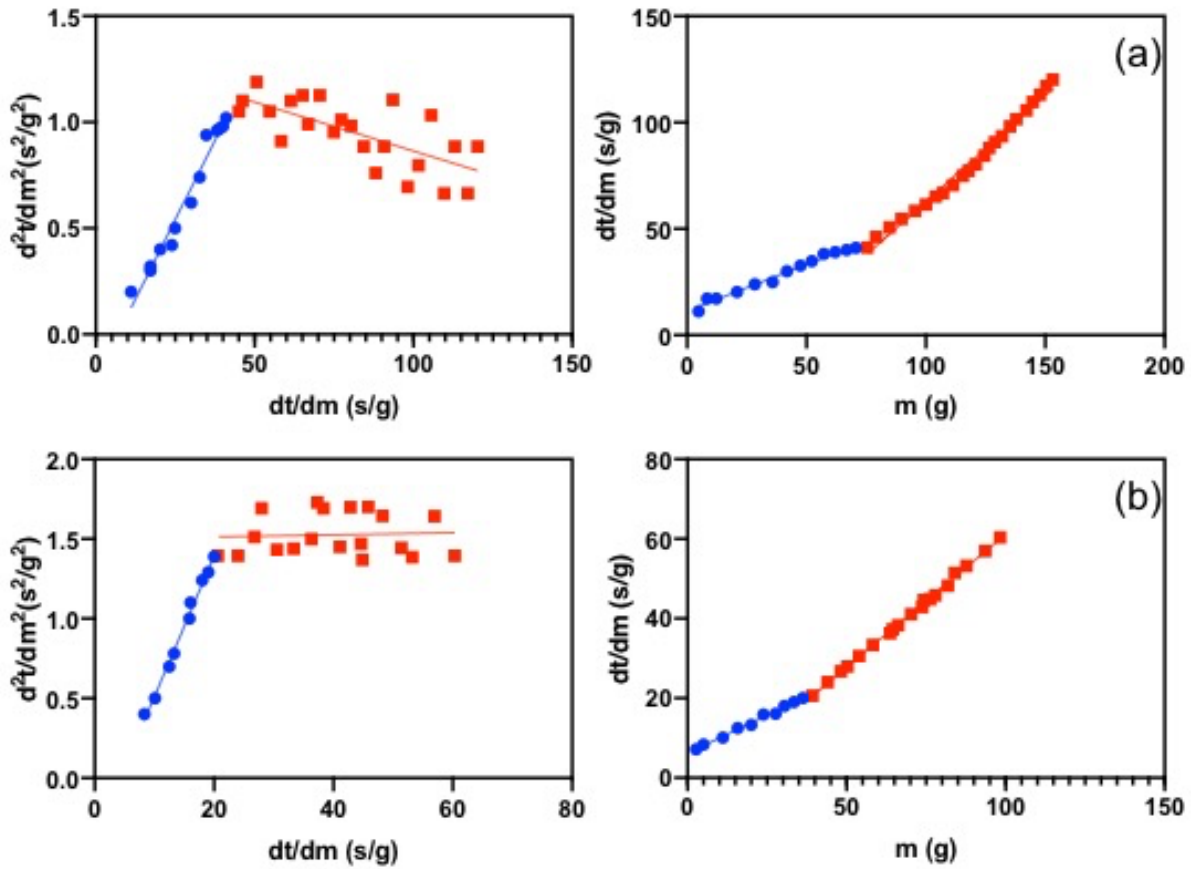
Figure 26 Determination of depth- and surface-filtration by experimental results of dynamic filtration process: a.3mm b.5mm c.10mm.

Based on (4-11 and (4-14, we can determine the filtration mode by plotting $\frac{d^2t}{dm^2}$ as a function of $\frac{dt}{dm}$ as shown in the Figure 26. In this figure, we show measurements made with varying thickness of a filter cake comprised of FAX 7 that are used to capture glass beads from a mixture of beads and glycerol. One notes that the blue points can be fit with an exponential index close to 1.5 which is indicative of depth filtration. In contrast, the red points show a roughly horizontal (i.e., zero slope) profile, which is indicative of surface filtration (Tien 2013). Also shown (on the right-hand side of this figure) is that the value of $\frac{dt}{dm}$ becomes proportional to the mass of output (m) during surface filtration(Tien 2006). By using both plots, one can identify the transition point where the filtration mode shifts from primarily depth to surface filtration. For these thin dynamic filtrations, the process starts with a depth filtration that most contaminant go into the filter medium and deposited at the bottom filter paper, resulting in the decrease of porosity of the filter medium. Then the filtration process changes to a surface filtration at a certain point, where contaminants remain at the surface of the filter medium instead of going through it.

To determine the "changing/switch" point, we create two types of the filter medium as shown in Table 11. (1) Pm cake: premix all glass beads with the filter aid. (2) Cm cake: premix a certain value of glass beads with FAX7 and then add additional mass of glass beads on the top of the cake.

Table 11 Sample of glass beads mixed with FAX 7 by different mass.

	Number	1	2	3	4	5	6
3mm	Pm (g)	0	0.65	1.17	1.60	3.68	4.19
	Cm (g)				1.17+0.43	1.17+2.51	1.17+3.02
5mm	Pm (g)	0	0.47	2.17	4.40	4.68	–-
	Cm (g)				2.17+2.23	2.17+2.51	–-
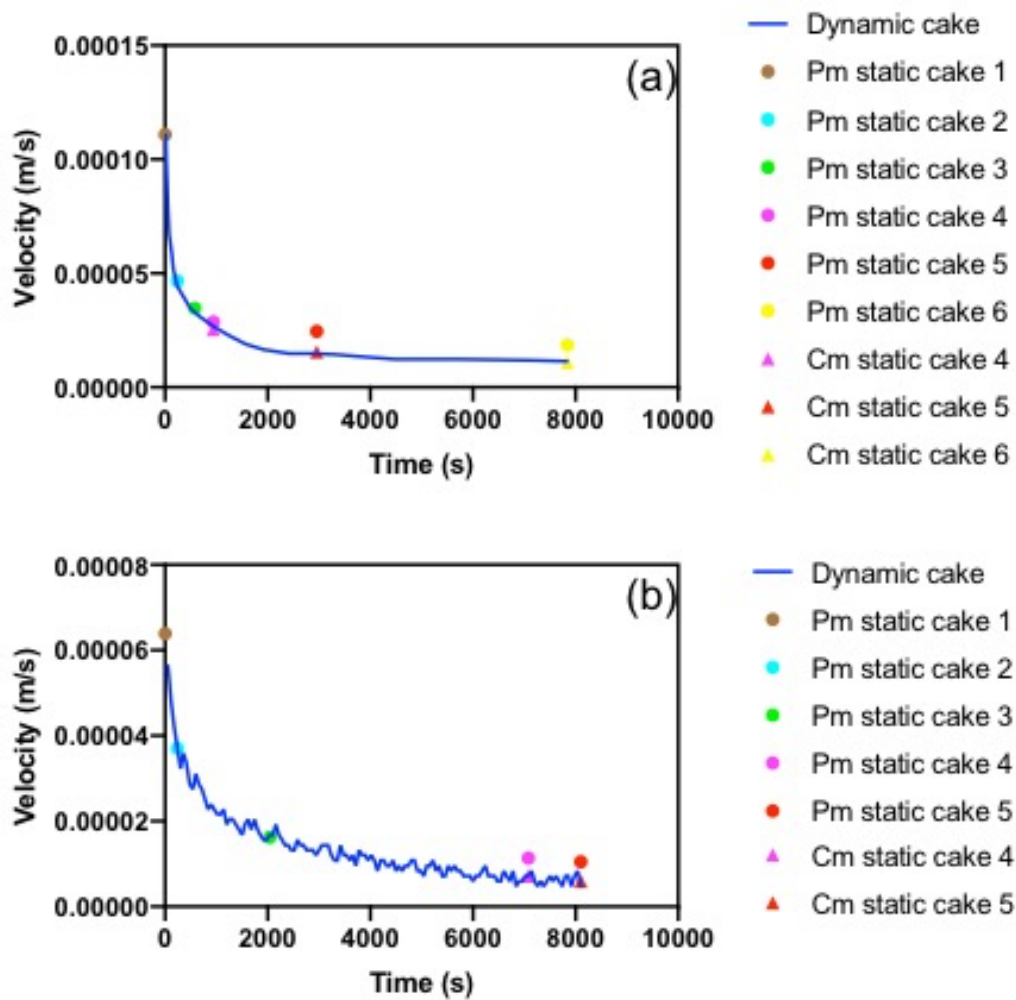
Figure 27 Experimental results between dynamic filtration process and static filtration process: a. 3mm b. 5mm.

66

Figure 27 shows a comparison of the dynamic PSD flow rate predicted from a dynamic filtration (lines) to the experimental results obtained from the series of individual static cases described above (Cubes for Pm and points for Cm). Because the Pm cake premixes more glass beads into the filter aid than would otherwise be expected to be captured by native depth filtration, it results in a more open structure and a flow rate that is larger than predicted by the PSD model. In contrast, the more realistic Cm cakes show the combined impact of depth and surface filtration and agree much more closely with the PSD predictions.

Figure 27 shows the flow rate of Pm cake after the changing point is always higher than the dynamic cake, that is because after all the pores are filled with glass beads, the pore size can be enlarged by adding new glass beads in to the system. Thus, the "changing/switch" point from depth filtration to surface filtration is the maximum filling point, which means all the open pores of the filter medium is filled with contaminants.

4.3.1 Dynamic Pore Size Distribution

In order to accomplish this, we must step forward in time such that, during one-time step, the pore size distribution is changed by the filling of contaminants that occurred during the intervening time. Our algorithm for pore filling is based on a series of probability functions: for contaminant particle identity, for pore flow, and for contaminant capture. That is, the likelihood of a particular size contaminant particle being considered for capture is based on the weighted frequency of occurrence of that particular size. Then, the pores into which the contaminant flows are explicitly related to the pore resistance. Finally, the likelihood of physical capture within that given pore is based on the ratio of contaminant to pore sizes (in the current study, for simplicity, this probability is set to unity).

At the end of each time interval, the pore size distribution is updated based on the resultant packing of contaminants within the selected pores. Note that contaminant capture can, therefore, lead not only to a reduction in the number of large pores, but also the creation of smaller pores (between capture contaminant particles). The packing within particular pores is based on the model established by Desmond (Desmond and Weeks 2014).

Ultimately, with the change of pore size distribution vs. time, we can finally predict the flow behavior during the dynamic filtration, as shown in Figure 28.
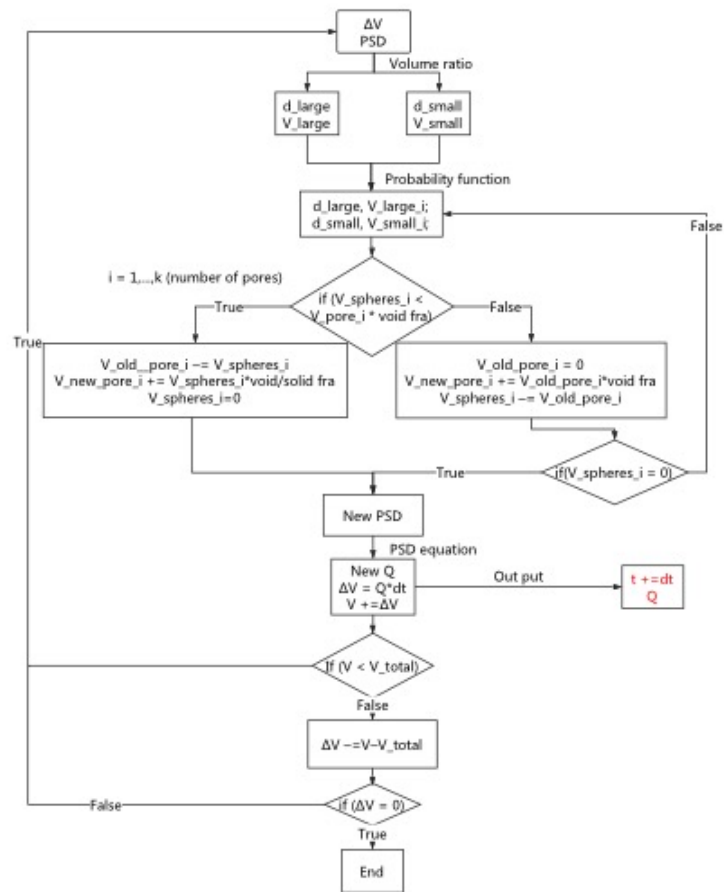
Figure 28 Chart of the dynamic PSD mode.

4.3.2 Mono Disperse Systems

Having validated the ability of the PSD model to capture the transition from depth to surface filtration via comparison with curated static flow measurements. Next, we turn toward testing fully dynamic filtration modeling. As mentioned earlier, here the critical component is to capture the change of the pore size distribution with time (Bryant, King, and Mellor 1993). As an initial test, we examine the filtration of a simple mono-disperse glass bead suspension from a stream of otherwise pure glycerol. As a test of the PSD model's efficacy for modeling dynamic filtration, a suspension composed of monodisperse spherical glass beads and glycerol is prepared.

Figure 29 shows the experimental process of the dynamic filtration. The filter medium is FAX 7 and varies with 5mm cake thickness. The suspension is 11µm glass beads that mixing in 180ml glycerol with a constant concentration: 30g/mL. Figure 30 shows the comparison between the predicted flow rate from the PSD model to the experimentally measured flow rate in the dynamic filtration process of mono-sized spheres. As one can see, the model captures the flow rate at a fixed pressure over the entire history of the dynamic filtration process while maintaining an error between simulation and experiment that is always smaller than 10%. The model works well to predict the flow behavior of dynamic filtration process in mono-spheres suspension since the error between simulation and experiment is always smaller than 10\%. The system changes from depth filtration to surface filtration can also be predicted.

Figure 31 shows the pore size distribution for different stages. Depth filtration dominates the filtration process from the initial phase through the blocking phase. During this stage, the volume of large pores is continually decreased as a result of the increasing particle loading. In contrast, the volume of some small pores increases during this stage as new pores that are created between the containment particles and the filter aid. After reaching the blocking point, some

contaminant remains at the top surface of the filter aid, creating new small pores and increasing the cake thickness.
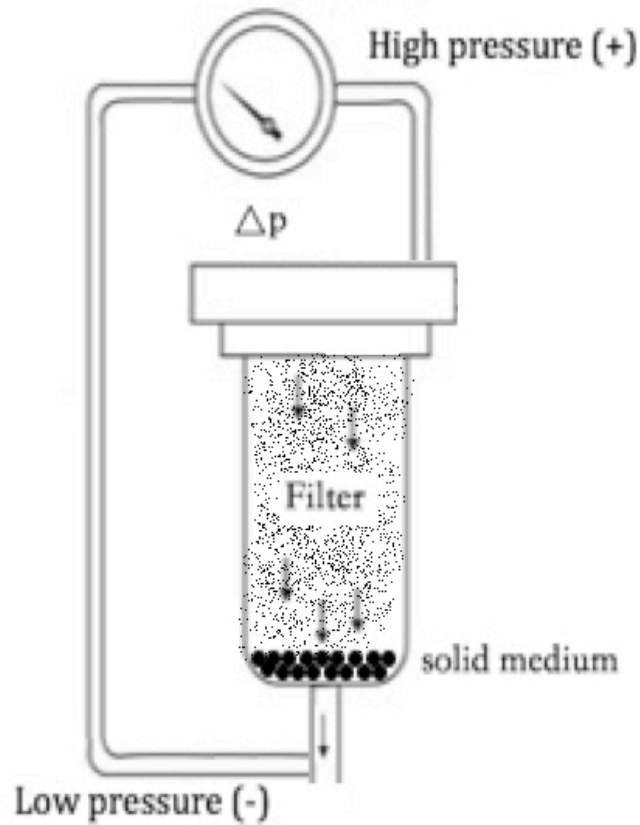
Figure 29 Sketch of the dynamic filtration.
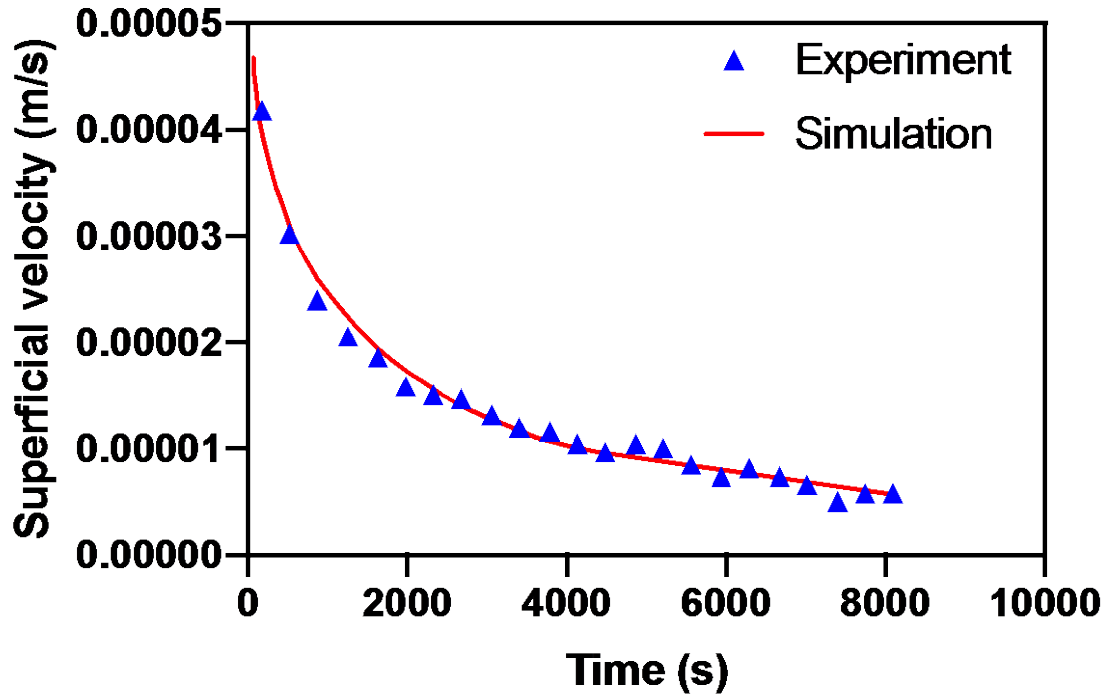
Figure 30 Comparison between predicted flow rate and experimental flow rate in dynamic filtration process of mono-spheres suspension.
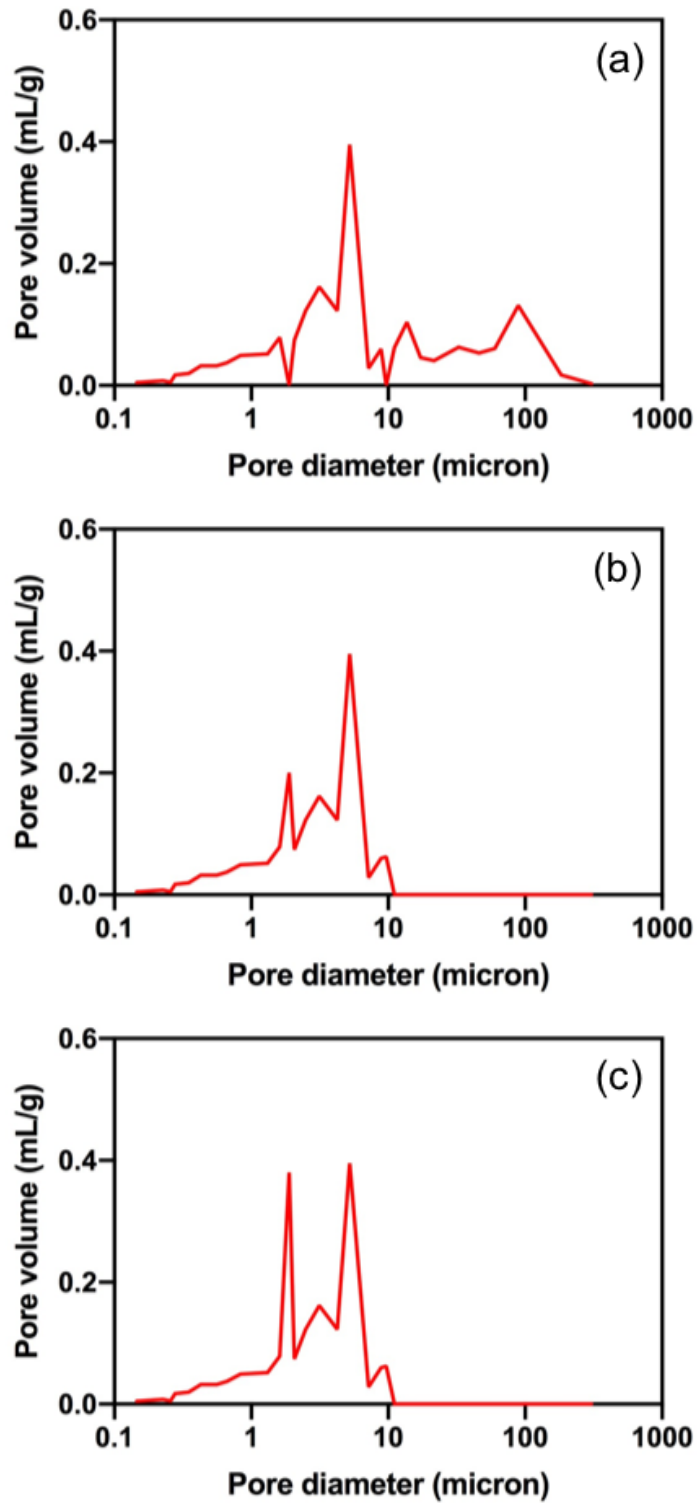
Figure 31 Dynamic pore size distribution of mono-disperse dynamic filtration: (a). Initial stage (b). Block stage (c). Final stage.

4.3.3 Multi Disperse Systems

The last step in testing the PSD model is examine dynamic filtration where the particle size distribution of contaminants is also complex. While it is more complex to predict the resultant pore size changes when filling a pore with polydisperse contaminants(Al-Raoush, Thompson, and Willson 2003), we do so by adapting the packing density model of (Desmond and Weeks 2014) where they suggest that: the packing density is influenced by the particle size distribution: $\Phi=0.634+c_1\delta+c_2\delta^2$, where Φ is the packing density, c_1 and c_2 are constant values that equal to 0.0658 and 0.0857, δ is the polydispersity. δ is determined by the particle size distribution as shown in Table 12(Furnas 1931, Farr 2013). Since we have already shown that we can obtain the flow behavior of a filter medium directly from its pore size distributions using the PSD model, now we simply need to predict the evolution of the pore side distribution. By modifying our mono-disperse approach with the more complex packing fraction outlined above, we can predict the dynamic changes in pores size distribution as shown in Figure 33. Then, to verify the PSD model in a more realistic dynamic filtration, a suspension that is composed of a mixture of glass beads of differing sizes and glycerol is prepared as shown in Appendix B.

Figure 32 shows the resulting comparison between the predicted flow rate from the PSD model and the experimentally measured flow rate from the aforementioned dynamic filtration process of a multi-disperse sphere suspension. Once again, it can be seen that the model predicts the flow behavior to within 15% error across the entire evolution of the process.

Table 12 Polydispersity fuctions.

Function	$P(R)=p_1\sigma(R-a)+p_2\sigma(R-b)+p_3\sigma(R-c)+\ldots+p_n\sigma(R-n)$
Number fraction	$p_i=P(i)/[(P(a)+\ldots+P(n)]$
Size ratio	$\eta_i=R_i/R_1$
Constrained	$a=\eta_1/(p_1\eta_1+p_2\eta_2+\ldots+p_n\eta_n$
Polydispersity	$\delta=[p_1(a-1)^2+p_2(b-1)^2+\ldots+p_n(n-1)^2]$
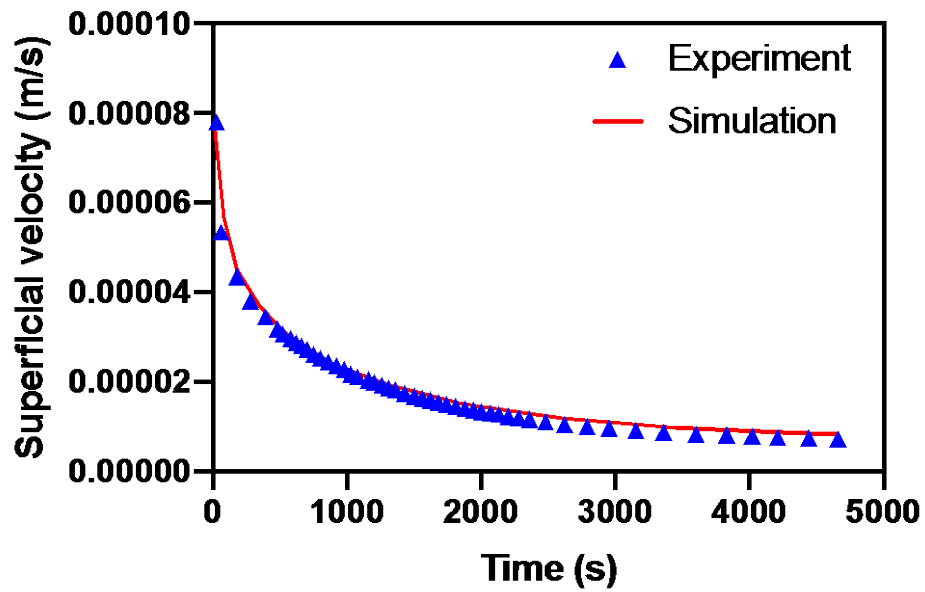
Figure 32 Comparison between the predicted flow rate and the experimental flow rate in dynamic filtration process of multi-spheres suspension.
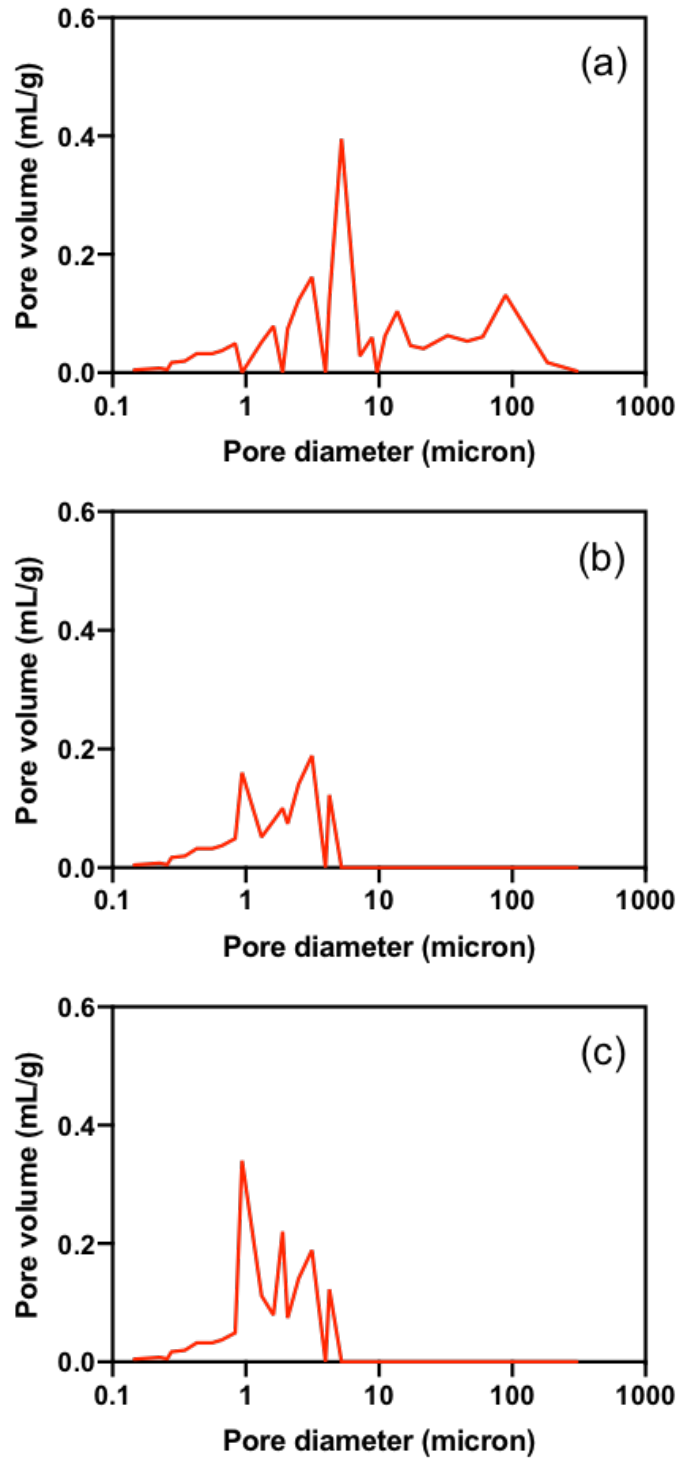
Figure 33 Dynamic pore size distribution of multi-sphere dynamic filtration: (a). Initial stage (b). Block stage

(c). Final stage

4.3.4 Optimization with the PSD Model

As a final application example, one might envision using the PSD model to perform an optimization of a particular filtration process, either attempting to conserve power, reduce the use of filter aid and/or reduce the filtration time. Here we examine a candidate contaminated stream that contains a known quantity (0.69g) of 11µm glass beads suspended in 35mL glycerol. Table 13 shows the predictions of a variety of quantities of interest from the filtrations when using alternatively FAX 3, 5, or 7. One notes that FAX 7 is the best filter aid for the separation based on operating time, the quantity of filter aid required, and total cake thickness used. Figure 34 shows the validation of the predicted screening of 11µm glass beads via a comparison of the measured and predicted superficial velocity (showing an accuracy similar to our earlier validation plots). In contrast, if one were to consider the cleaning of a suspension of 24mL of glycerol that contains 0.48g of 3-6µm glass beads, our prediction (and subsequent validation) show that FAX 5 is the best filter aid for this separation (see quantities of interest in Table 14).

Table 13 Screening for 11μm glass beads with FAX 3, FAX 5, and FAX 7.

	FAX3	FAX5	FAX7
Porosity(ml/g)	2.76	2.30	1.96
Mass of FAX (g)	1.96	1.51	0.83
Cake thickness (mm)	6.45	4.35	2.09
Time (s)	1078	561	180
Weight index	35.16%	56.46%	83.14%
Mass velocity (g/s)	6.11e-04	1.23e-03	3.83e-03
		Better	Best

Table 14 Screening for 3-6μm glass beads with FAX 3, FAX 5 and FAX 7.

	FAX3	FAX5	FAX7
Pore volume (ml/g)	0.88	1.21	0.76
Mass of FAX (g)	1.34	1.00	1.59
Cake thickness (mm)	4.19	2.88	4.00
Time (s)	580	240	350
Weight index	24.49%	48.00%	30.19%
Mass velocity (g/s)	1.21e-03	3.37e-03	1.98e-3
		Best	Better
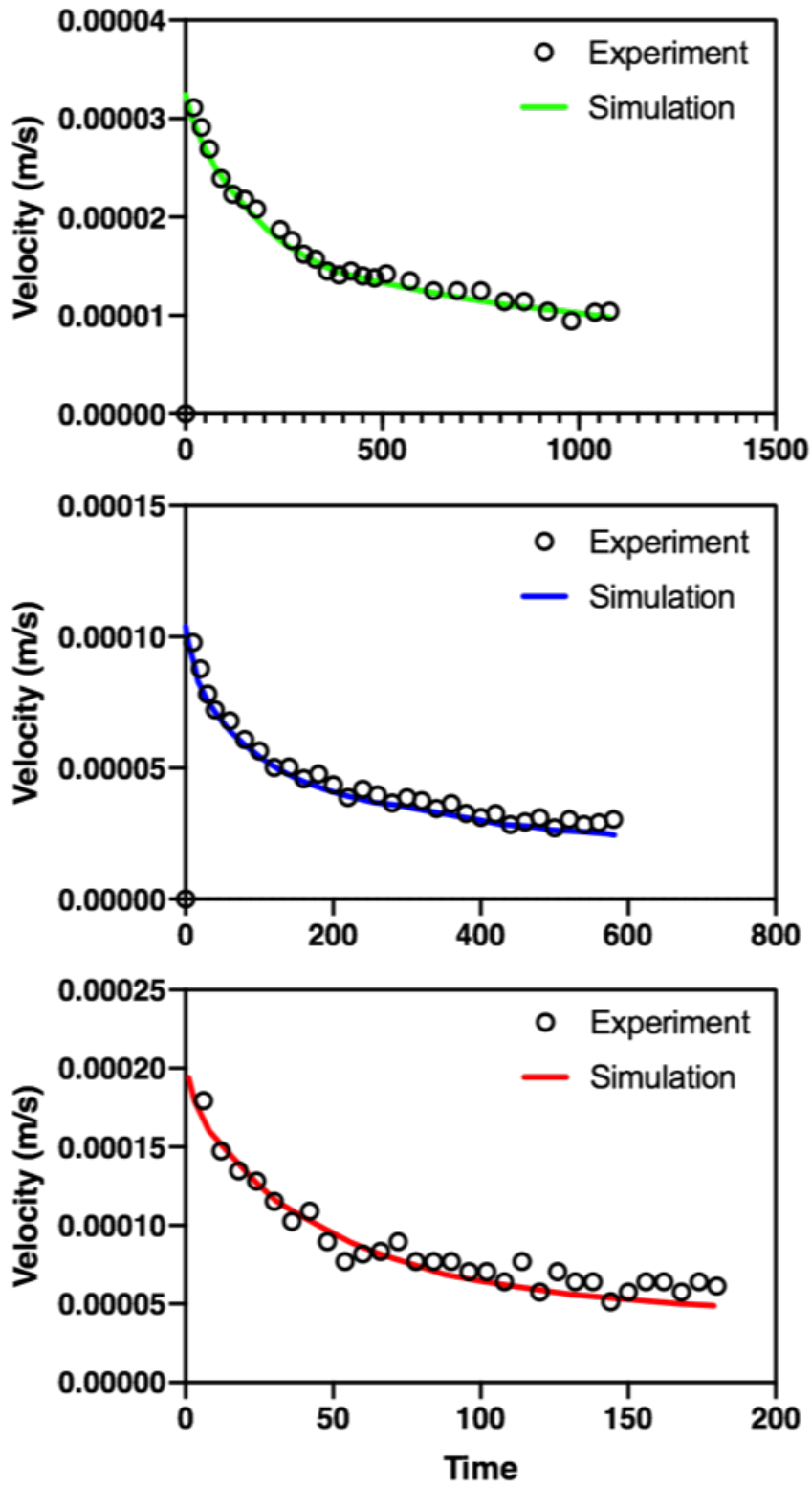
Figure 34 Screening for 11µm glass beads by surpefical velocity with FAX 3, FAX 5 and FAX 7.

In this chapter, we introduce a new model, the PSD model, that is capable of predicting the dynamic flow (or pressure) behavior for both the liquid and solid phases in a cake filtration process. It is important to note that the model accurately captures both depth and surface filtration, as well as the transition, without requiring any empirical quantities. That is, the model simply requires that one known the physical properties of the liquid and solid materials (including both the contaminant size(s) as well as the media pore sizes). With these data, the PSD model can provide an accurate estimate of the pressure drop, flow dynamics, resultant filter cake structure, and permeability in both static and dynamic filtration processes.

5.0 Numerical Simulation of the Particle Capture on A Dead-end Pore

Modeling of the filtration process in porous media is of considerable interest in natural and industrial systems, such as wastewater treatment(Busch, Cruse, and Marquardt 2007), petroleum engineering(Gitis et al. 2010), chemical engineering (Sambaer, Zatloukal, and Kimmer 2011) and aquifer contamination(Harvey and Garabedian 1991). A deep understanding of the mechanism of the transport and retention of colloidal particles through the filter medium is essential for predicting contaminant separation and fluid dynamics.

Researchers have been working on the prediction of particle capture within inter-connected pores with early attempts adopting a phenomenological point of view (Ison and Ives 1969). This approach generally employs empirical equations for the rate of particle retention and the subsequent change in pressure gradient. An approach espoused by Ives work (Ison and Ives 1969) uses conservation equations for the concentration of the contaminants and obtains the flow dynamics from an adaption of the Darcy's law; however, this approach is an empirical model in that it does not directly address the operating mechanisms of particle capture. An alternative and more accurate method of modeling particle capture phenomenon during the filtration process is to consider a filter medium as the combination of collectors/pores(Rubenstein and Koehl 1977). The mechanism of particle capture by each filter pore/collector then becomes the problem of interest. Thus, this approach involves setting up the equation of motion for the suspended particles with the addition of a physical description of each possible collection mechanisms(Tufenkji and Elimelech 2004).

Current recognized mechanisms of the transport of particles from the fluid phase to the pores of a porous filter medium include interception, gravitational sedimentation, and Brownian

diffusion. Transport of particles by interception occurs when a particle moving along a streamline comes into contact with the pore/collector due to its finite size (Overton 1973). Gravitational sedimentation refers to the settling of particles with densities greater than that of the fluid onto the pore/collector surface(Velamakanni and Lange 1991). Diffusion/Brownian motion of smaller particles result in contact with the pore/collector(Spielman and Goren 1968). Prieve and Ruckenstein(Prieve and Ruckenstein 1974) demonstrated that the rate of particle capture calculated by summing individual contributions from each transport mechanism was in close agreement with deposition rates obtained from a rigorous solution of the convective-diffusion equation.

Yao et al.(Yao, Habibian, and O'Melia 1971) proposed the first filtration model suggesting that the three transport mechanisms are additive.

$$\eta_0 = \eta_D + \eta_I + \eta_G \qquad (5\text{-}1)$$

where η_D is the single collector efficiency by diffusion, η_I is the single collector efficiency by Interception and η_G is the single collector efficiency by diffusion. Here, the separate correlation equation of η_D, η_I and η_G are first determined. Then, the overall single-collector efficiency is obtained by summing the individual contributions of each mechanism.

Despite its utility, Yao's model does not consider the influence of hydrodynamic (viscous) interactions or van der Waals attractive (surface) forces. The hydrodynamic interactions and van der Waals interactions are studied using a the numerical solution of the convective-diffusion equation (Elimelech, Gregory, and Jia 2013, Prieve and Ruckenstein 1974) and trajectory analysis for non-Brownian particles(Tien 2013). Due to the fact that the numerical solution is not straightforward, and hard to apply, Rajagopalan et al.(Rajagopalan and Tien 1976) provide a semi-empirical approach for predicting filtration performance with an empirical equation for the single-

collector efficiency. The correlation equation of Rajagopalan's model has been verified to accurately predict the particle retention during the filtration process (Ryan et al. 2000, Martin, Bouwer, and Hanna 1992) (Martin, Bouwer, and Hanna 1992).

Current models are focused on the particle retention in the inter-connected open pores; however, studies of the capture of particles within dead-end pores are rare, because of the complex pore structure and hydrodynamic conditions. Despite this fact, the mechanism of capture by the dead-end pore is essential for the prediction of the performance of the filtration separation process, especially for the prediction of the filtrate clarity, such as oil purification. To predict the actual flow behavior and clarity during a filtration process, a model should not only consider the flow behavior and ability of open pores to trap contaminants, but also consider the ability of intrinsic pores to retain smaller contaminants. This research is focused on the latter mechanism. That is, here we examine the ability of intrinsic pores to trap small contaminants during filtration.

In order to test the ability of intrinsic pores within a filter medium to capture particles of a smaller size, we examine a naturally occurring filter material comprised of diatomaceous earth. Diatomaceous earth (DE) is a highly porous filter aid that provides the opportunity to combine high porosity with essential properties such as high strength and a high thermal and chemical stability(Scheffler and Colombo 2006). This combination is very important for industrial applications such as filters for gases and molten metals, removal of heavy metal ions (Cr, Ni etc.) from sewage water, catalytic supports, and chromatography columns(Green and Colombo 2003). DE has intrinsic pores that smaller than 1.5μm(Al-Ghouti et al. 2003). Even though these pores do not contribute to suspension throughput, they still contribute to colloidal particle capture (Parfitt 1976). To predict the actual flow behavior and cake structure during the filtration process, the model should not only consider the flow behavior but also consider the capture ability of intrinsic

pores. This chapter is focused on the mechanisms and modeling of the capture ability of intrinsic pores in the filter aid.

5.1 Experiments

To test the pore trap ability of porous materials, we need to figure out the concentration of suspension before and after the filtration process. We use model contaminant particle that are made up of glass beads whose diameter are 500nm (or smaller, as noted below). For the filter medium, we use a 20μm mesh as the filter cloth since this will allow all of the contaminant particles to pass through (if the cake has not removed them). In this way, all of the loss of glass beads in the filtrate can be assumed to involve the glass beads being trapped within the filter aid. The filtration process is designed as follows:

1. Fix 20μm mesh at the bottom of the filter.
2. Pour a known volume and mass of dry FAX into the filter.
3. Tap the outside chamber several times until the particles have settled evenly.
4. Premixing a known mass of glass beads with 180mL pure glycerol.
5. Pour the suspension into the chamber; make sure the structure of the solid phase is not destroyed.
6. Apply a known pressure into the filter.
7. Allow the suspension flow through the filter continuous into a beaker, which posited on a scale.

To determine the change in concentration of the suspension, we first create a calibration curve from standard solution, using a UV-VIS apparatus (Haiss et al. 2007) as shown in

Figure 35 and therefore measure the concentration of the filtrate both before and after the filtration. Since the absorbance is proportional to the concentration of the glass beads, we can then determine the captured mass from a simple measurement (and material balance). Based on the calibration curve(Haiss et al. 2007): $C=a*A+b$, (where C is the concentration of suspension, A is the absorbance. a and b are the constant value that determined by UV-VIS tests) we can get the change of concentration: $\Delta C=a*\Delta A$. Thus, the captured mass should be equal to $\Delta A*a*V_{suspension}$.

Figure 36 shows the captured mass that is calculated from the UV-VIS absorbance for different trials with filter aid and varying (three different) cake thicknesses. The ability of the DE to capture these fine particles within the intrinsic pores appears to be proportional to the intrinsic void fraction and cake thickness.
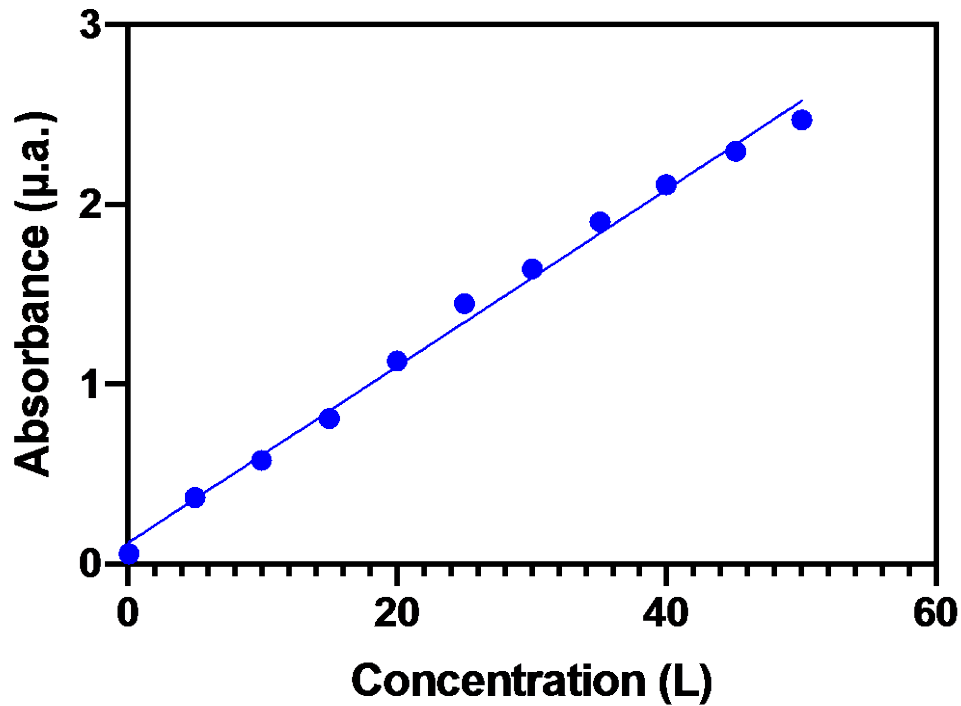
Figure 35 Slica calibration curve based on UV/VIS spectrophotometric method.
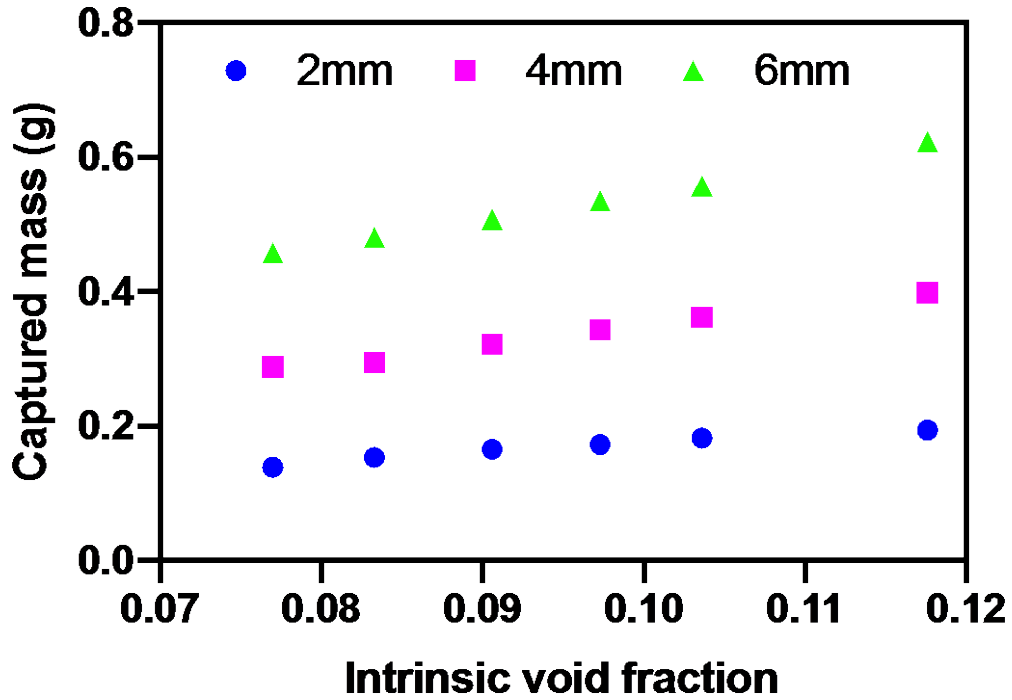
Figure 36 The capture ability of different FAX with different cake thicknesses.

5.2 Iwasaki Model

Iwasaki(Iwasaki 1937) made initial attempts at a mathematical description of granular media filtration, which assumes that the rate of the change of particle concentration along filter depth is proportional to the concentration along the filter depth. He proposed an equation based on first-order kinetics,

$$\frac{\partial C}{\partial l} = -\lambda C \qquad\qquad (5\text{-}2)$$

which was verified experimentally by Ison and Ives(Ison and Ives 1969). Here, C is the concentration of contaminants at a given time and depth, L is the cake thickness / filter depth, and λ is the filter coefficient.

Figure 37 shows the comparison of the form of the Iwasaki model with our experiments data. As can be seen, The $\ln(c/c^0)$ is nearly linear with the filter depth, as suggested by the model. At present, the value of λ cannot be predicted beforehand but is determined from the experimental results of the specific system. Here we examine a method of predicting the rate of colloidal particle capture by forming an expression for the theoretical description of λ.

Yao suggested that the performance of the filter coefficient is related to the porosity, particle diameter, attachment efficiency and a single spherical collector efficiency(Yao, Habibian, and O'Melia 1971).

$$\lambda = \frac{3}{2}\frac{\varepsilon}{d}\alpha\eta \qquad\qquad (5\text{-}3)$$

The porosity ε (here taken to be the intrinsic porosity) and the particle diameter d are both known properties. The attachment efficiency α is the number of contacts which produce a particle collector adhesion divided by the number of particle-collector collisions. The single collector efficiency η is the at which particles strike a collector divided by the rate at which particles flow toward the collector. Thus, it's important to figure out α and η.
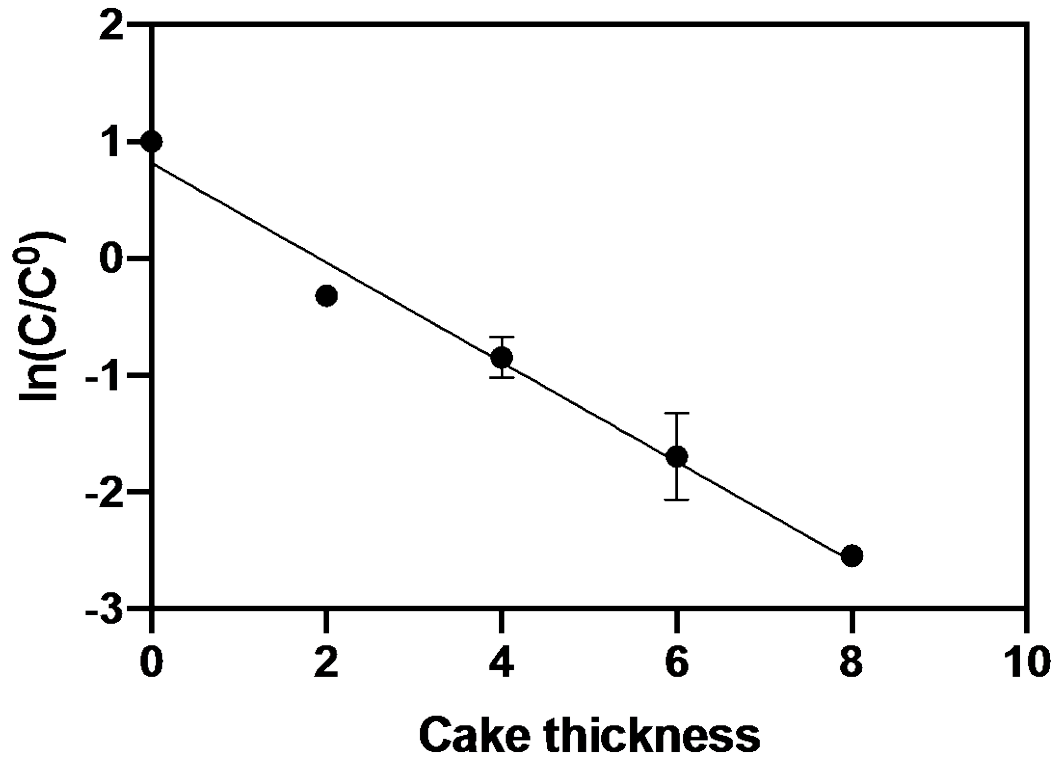
Figure 37 Verificaiton of the Iwasaki Model with experimental results.

5.3 Capture Mechanisms

In order to understand the mechanism of particle capture we consider two candidate phenomena, as shown in Figure 38. One possible mechanism involves the physical adsorption of the contaminants onto the surface of the DE via van der Waals (or other surface) forces(Aparicio, Prado, and Durán 2006, Parfitt 1976). The other mechanism involves the capture of the particles via entrainment caused by the transport of particles across the streamline that separates the flow within the main channel from the fluid entrained within the intrinsic pores (due to hydrodynamic forces and the finite size of the contaminant particles)(Luo et al. 2013). The fluid entrainment is tested by comparison of experimental results to a simulation of particle transport using DEM-LBM(Ma et al. 2012, Halama and Spliethoff 2016, Zhang and McCarthy 2019).
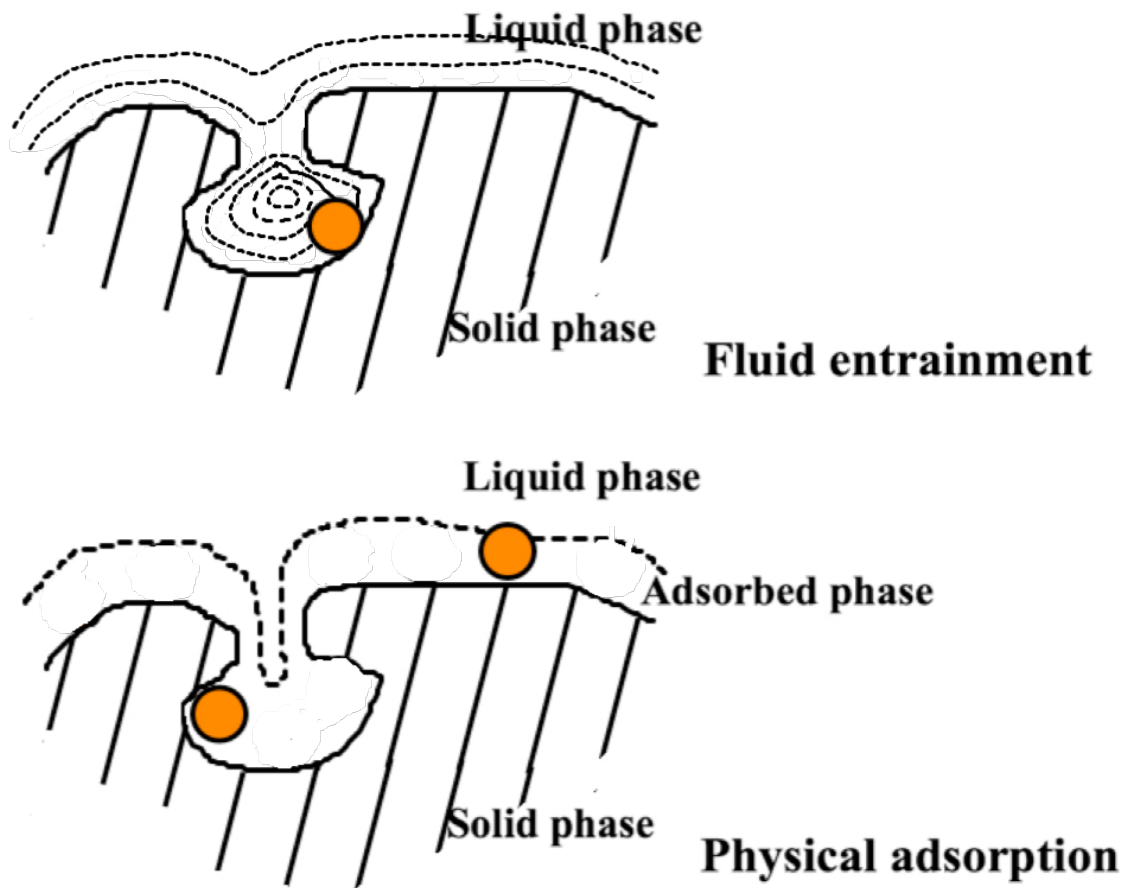
Figure 38 Two different capture mechanisms: a. fluid entrainment b. physical adsorption.

5.3.1 Physical Adsorption

The silica surface can be easily modified from the silanol groups, Si-OH, to different functional groups like treating with organotrialkoxysilane (RSi(OR')3) compounds or methallylsilanes together with catalyst(Yeon et al. 2008), and surface modification of the silica

nanoparticles with biorecognition molecules can make a specific interaction with receptor sites. APTEST, 3-aminopropyltriethoxysilane, were widely used for the modification of silica surface with (RSi(OR')3) compounds and also widely explored by many researchers(Chiang, Ishida, and Koenig 1980). Caravaja et al. investigated the surface modification of silica in the bulk surface of micron size silica(Caravajal et al. 1988). The surface modification process is below (Luo et al. 2013):

1. Suspend 800 mg of nano silica in 50 mL of MeOH.

2. Add 3 mL of 3-aminopropyltrimethoxysilane (APTES).

3. Stir the mixture at room temperature for 10h.

4. Centrifuge the product with 8000 rpm 10 min.

5. Wash the product with methanol five times.

6. Dry the product under vacuum.

Upon modification of the model contaminant particles, we use zeta potential measurements to assess the impact pf the surface modification on potential surface forces present under the experimental conditions. The zeta potential is caused by the net electrical charge contained within the region boundary. Thus, it can be used to quantify the change of the surface charge of the contaminants. We obtained the zeta potential by electrophoretic light scattering: first determine the particle mobility by the known applied electric field and measured particle velocity. Then the zeta potential can be performed with a pH titration. The blue points are the untreated silica and the red points are the surfaced modified silica as shown in

Figure 39. As can be seen, under our experimental conditions (where the operating pH is roughly 7.3), there is a significant change in the contaminant surface properties imparted by the surface modification. Despite the fact that the zeta potential test has shown that the surface

modification successfully alters the sign of the surface charge under experimental conditions, we

note that the concentration of the output does not change much in Figure 40. This suggests that the

physical adsorption mechanism is not prevalent for our experimental setup.
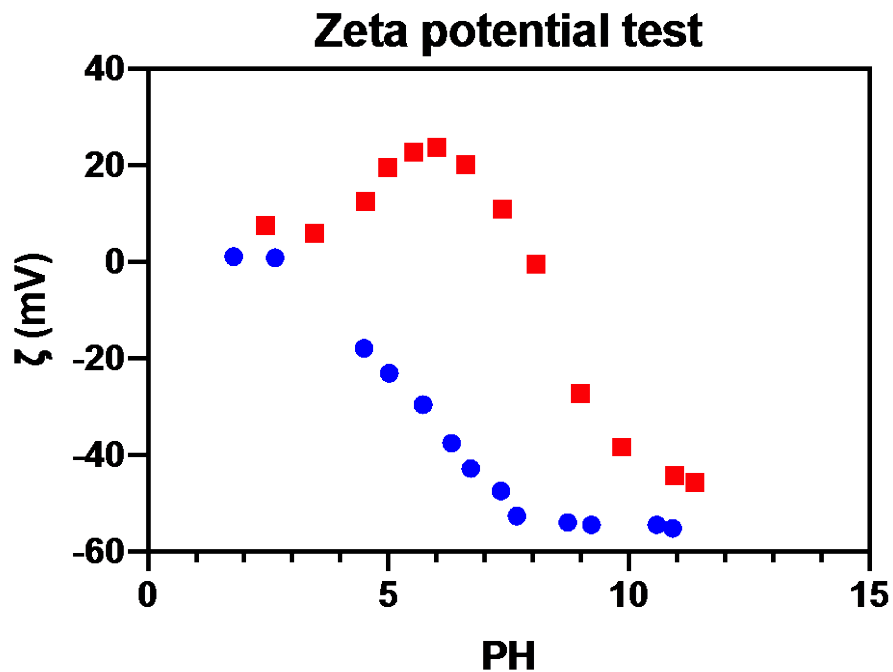
Figure 39 Zeta potential test for both treat and untreated 500 nm silica. Blue points: untreated silica; Red points: surface-modified silica.
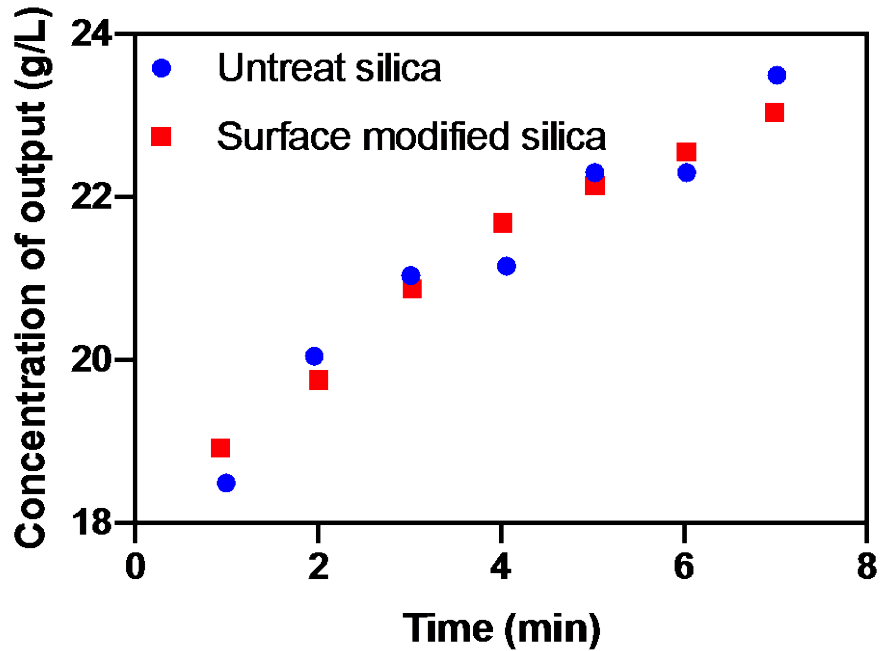
Figure 40 Capture ability test for both treat and untreated 500 nm silica with the same cake thickness and operating pressure.

5.3.2 Fluid Entrainment

The fluid entrainment is tested by the results of simulation using DEM-LBM(Zhang and McCarthy 2019) to experimental observations. The DEM is used to mimic the particle motion and the LBM is used to simulate the fluid motion past a simple pore-containing channel.

Figure 42 shows some particle (near the pore) has been "pushed" into the dead-end pore and remain there. Additionally, as discussed below, simulations examining single-particle transport are effective at estimating the scale of the hydrodynamic forces required to mimic our experimentally observed contaminant capture rates. Thus, we anticipate that fluid entrainment is

the dominant capture mechanism under the operating conditions examined in this study. Here a lift force is generated by the gradient of the shear rate. Thus, η should be related to the lift forces generated from the shear gradient and wall effects. (Martel and Toner 2014). Figure 41 shows the shear gradient lift force due to the curvature of fluid velocity profile(Di Carlo et al. 2009):

$$F_{WL} = \frac{C_{L\_WL}\rho U_{max}^2 d_{particle}^6}{d_{pore}^4} \tag{5-4}$$

and the wall lift force that is a result of wall-induced disturbance on the flow field around the suspended particles (Di Carlo et al. 2009):

$$F_{SGL} = \frac{C_{L\_SG}\rho U_{max}^2 d_{particle}^3}{d_{pore}} \tag{5-5}$$

94
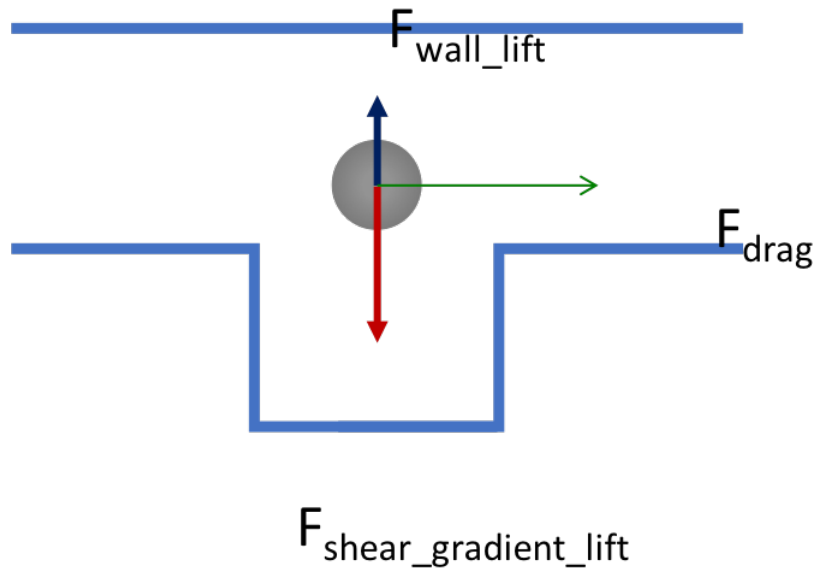
Figure 41 Schematis describe the lifing force induced bye shear gradient and wall effect.
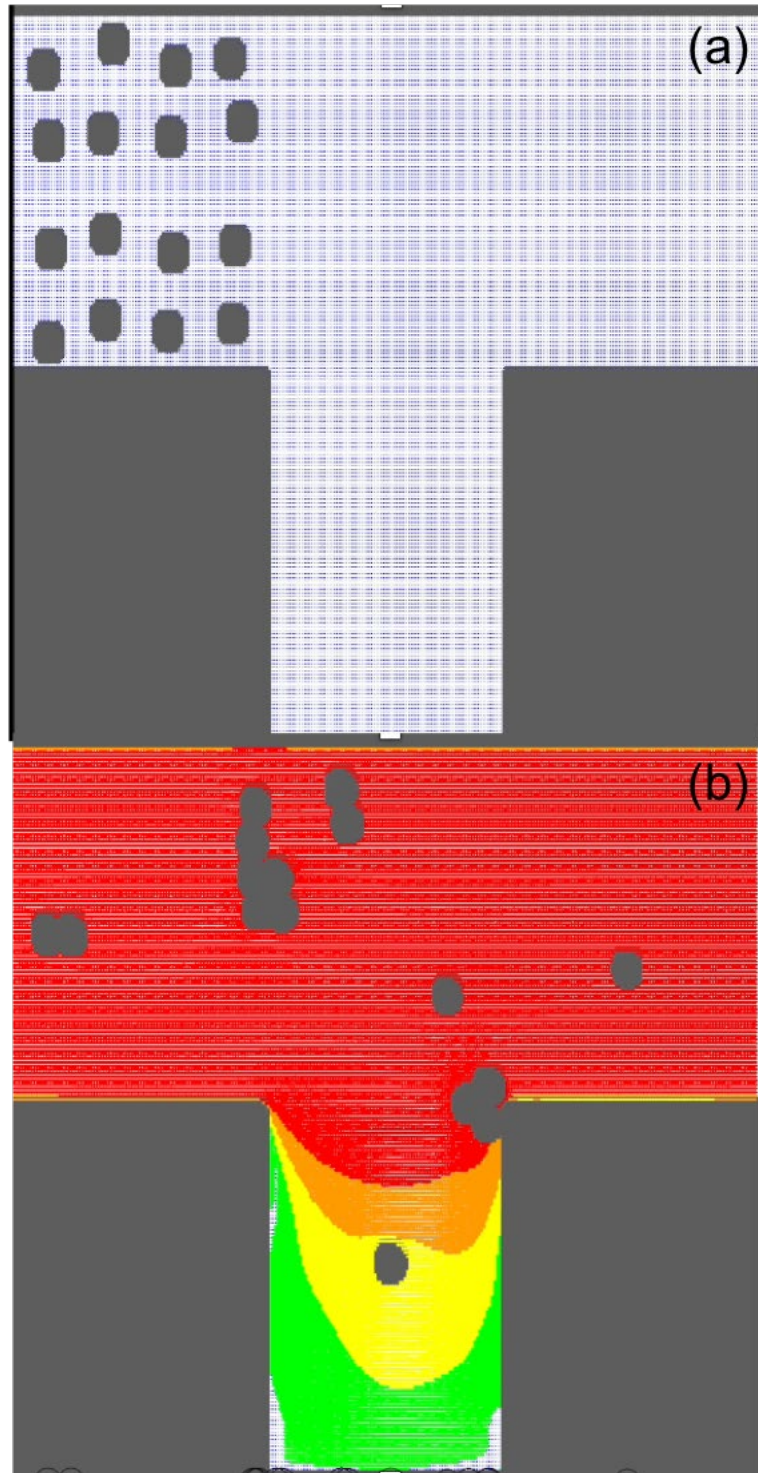
Figure 42 DEM-LBM simulation of particles go cross a dead-end pore.

5.4 Capture Model

In chapter 5.3, we conclude that the attachment efficiency should be equal to 1 should be assumed to be equal to 1 for the filter aid filtration with silica as there was no impact of surface forces on the rate of particle capture. Thus, the only significant parameter of interest in predicting the capture of colloidal silica with DE is that of the single collector η. The contact efficiency of a single media particle or collector η is a ratio of the rate at which particles strike the pore (or collector) divided by the rate at which particles flow past the pore/collector. The rate of particles flow across the pore can be predicted by the drag force:

$$v_D = \frac{F_D t}{m} = \frac{6\pi\mu d_{particle} U_{max} t}{m} \tag{5-6}$$

where F_D is the drag force, t is the time of the fluid flow cross the pore, m is the mass of the particle. The rate at which particles ``strike'' a pore should be calculated from the hydrodynamic forces acting on the contaminant. The rate at which particles flow strike a pore can be determined based on the Newton's law:

$$v_l = \frac{F_l t}{m} \tag{5-7}$$

where F_l is the total lift force. That is, we must examine the lift forces acting on the particle (in this case including a lift force arising from the local shear gradient as well as that arising from the proximity of walls):

$$F_l = F_{SGL} - F_{WL} \qquad (5\text{-}8)$$

Thus, the single collector efficiency is equal to:

$$\eta = \frac{\dfrac{C_{L\_SG}\rho U_{max}^2 d_{particle}{}^3}{d_{pore}} - \dfrac{C_{L\_WL}\rho U_{max}^2 d_{particle}{}^6}{d_{pore}^4}}{6\pi\mu d_{particle} U_{max}} \qquad (5\text{-}9)$$

As shown in (5-4) and (5-5), the lift force is related to the maximum velocity, U_{max}, density, ρ, pore diameter, d_{pore}, and particle diameter, $d_{particle}$, via the lift coefficients, C_L. To determine the lift coefficients, we examined two simple DEM/LBM simulations of single-particle flows. Figure 43 shows a model that includes a single wall at the left-hand side with a particle is flow parallel to the wall. Figure 44 shows the change of the forces of the moving particle in y-direction. The lifting coefficient is calculated from (5-5) with the average lift force.

98
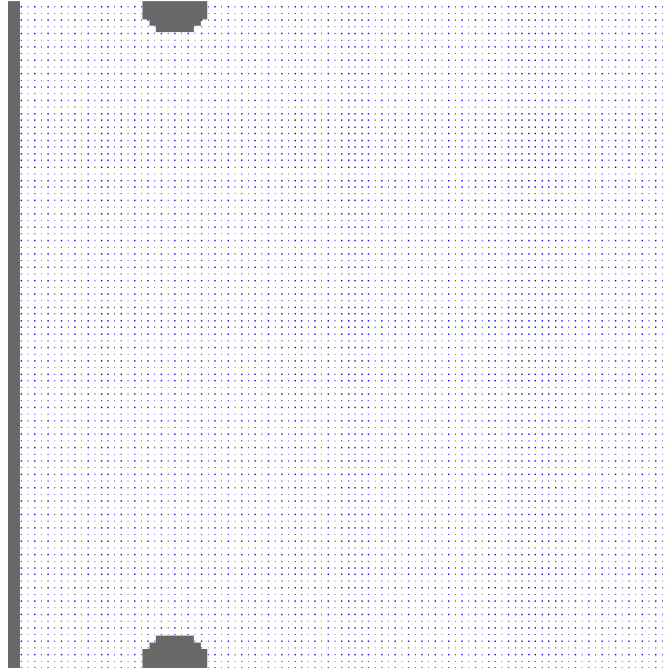
Figure 43 DEM-LBM model of a single wall with a particle moving parallel to the wall.
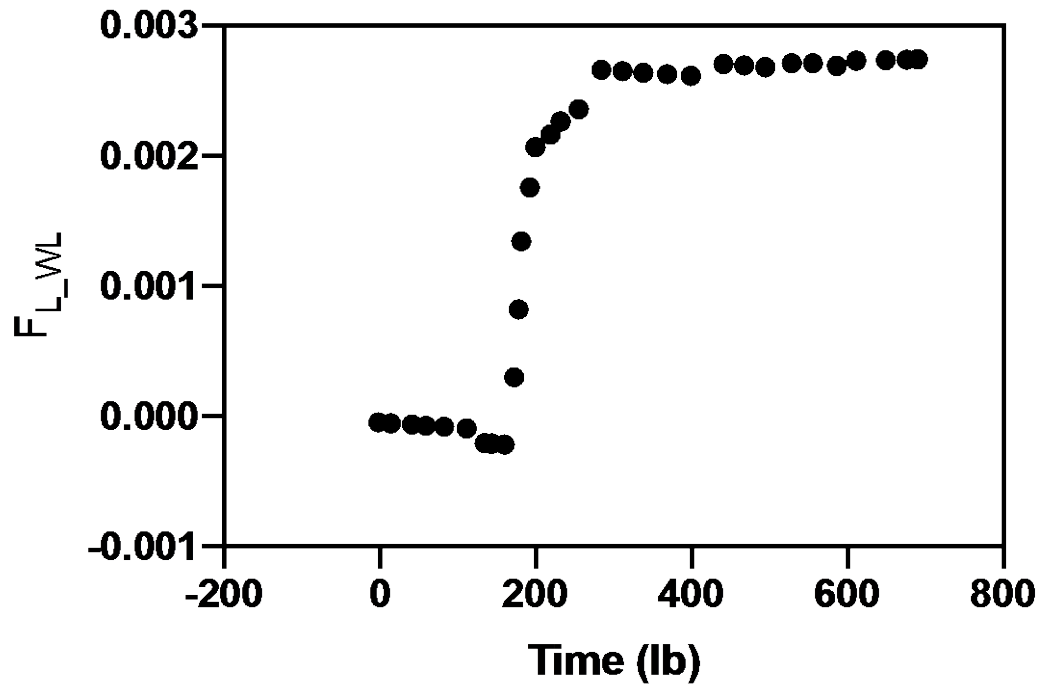
Figure 44 DEM-LBM simulation of the lifting force by the wall effect.

Figure 45 shows a model that includes a dead-end pore with a particle flow crosses the pore. Figure 46 shows the change of the forces of the moving particle in y-direction. The lifting coefficient is calculated from (5-4) with the maximum lift force.
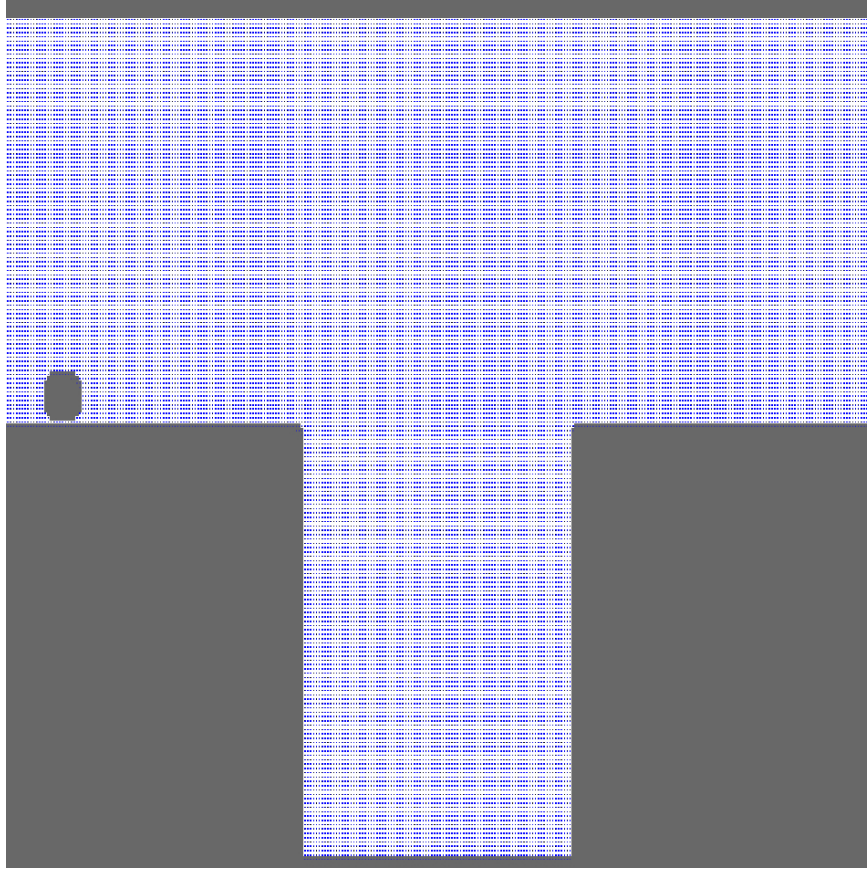
Figure 45 DEM-LBM model of a dead-end pore with a particle moving cross the pore.
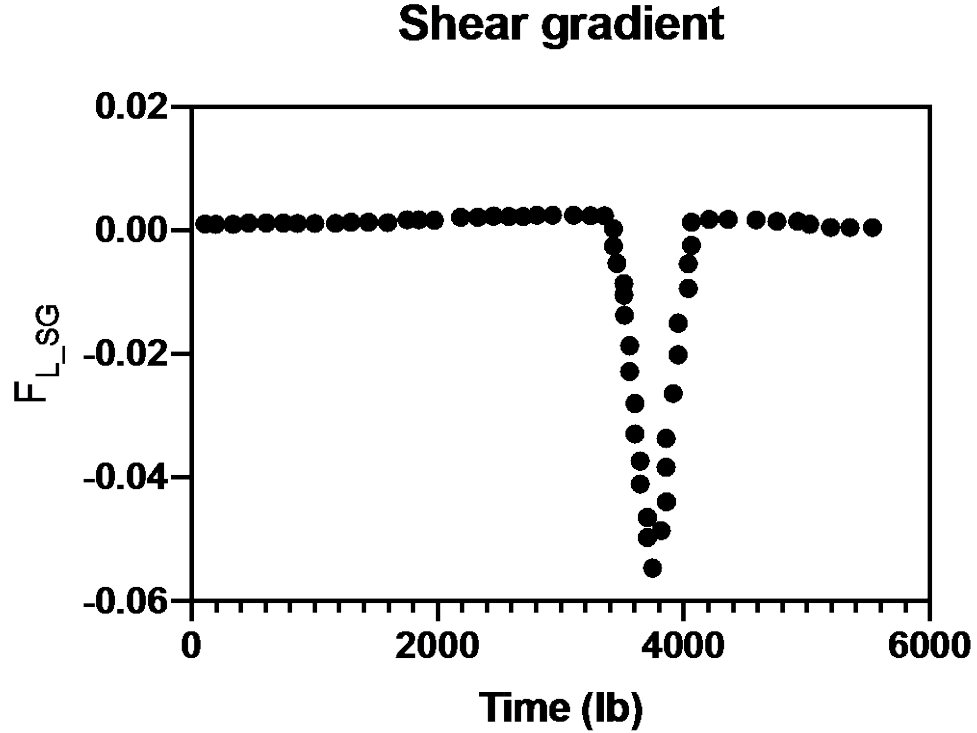
Figure 46 DEM-LBM simulation of the lifting force by the shear gradient.

By changing the Re in the DEM/LBM simulation, Table 15 and Figure 47 show that, for the range of conditions that are typically encountered in our filtration operations, the lift coefficient for both shear gradient and wall effect lift forces may be assumed to be a constant. Incorporating these measurements into an expression for the contact efficiency, (5-9), then yields a capture model as below with CLSG = 0.42 and CLWL = 0.22.

$$\ln\left(\frac{C}{C_0}\right) = -\frac{l}{4d_{particle}} \sum_{i=1}^{n} \varepsilon_i Re_{p,i}\, \alpha_i{}^2 (C_{L_{SG},i} - \alpha_i{}^3 C_{L_{WL},i}) \frac{d_{pore,i}^2}{d_{channel,i}^2} \qquad (5\text{-}10)$$

102

Table 15. Simulation tests of lifting coefficients with different pressure drop and Re.

Trial#	1	2	3	4	5
Pressure	1e-5	5e-5	1e-4	3e-4	5e-4
Re	0.12	0.65	1.32	3.97	6.56
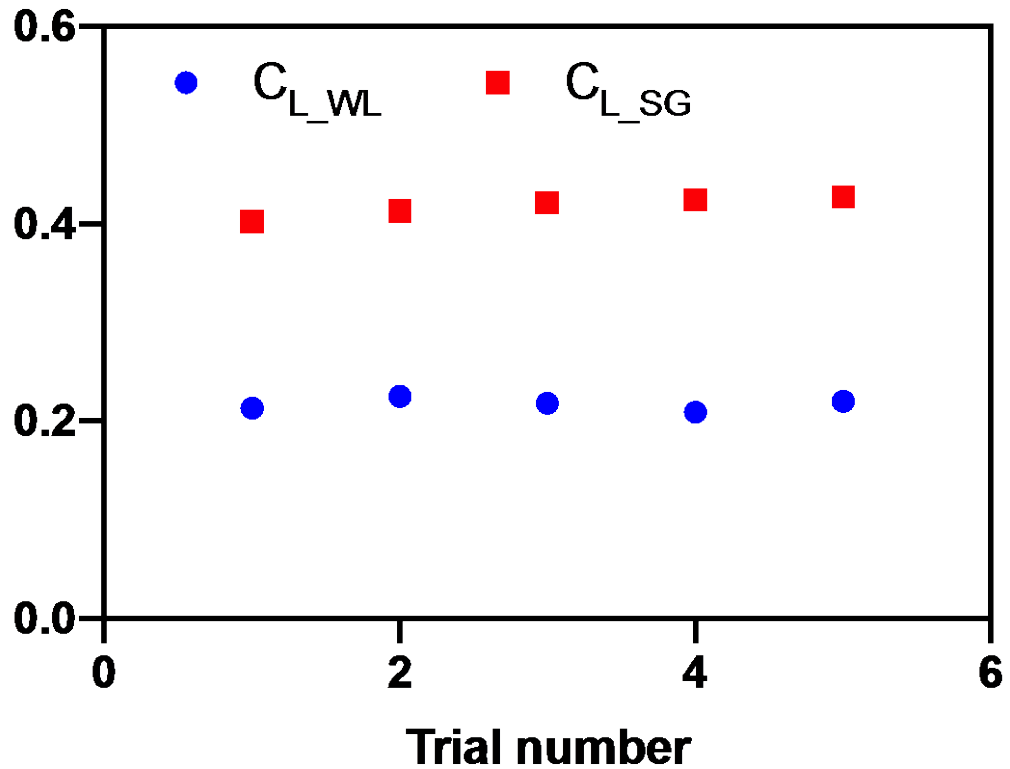
Figure 47 Lifting coeffcient of wall effect and shear gradient with different Re.

5.4.1 Mono Disperse Systems

To verify the capture model in a dynamic filtration, a suspension that is composed of mono-size nano-scale spherical glass beads and glycerol is prepared. The filter medium is a

commercially-available DE called FAX 3 built to a 10mm cake thickness. The suspension is 500nm glass beads mixed into 180ml glycerol with a constant concentration: 15g/mL. We can predict the flow behavior during the dynamic filtration from the previously reported PSD model.(Zhang and McCarthy 2019) Combining the flow dynamics from the PSD model with the capture kinetics outlined here, we obtain, in Figure 48, a prediction of the output concentration from the aforementioned filtration. As one can see, the capture model works well to predict the capture rate for a colloidal suspension since the error between simulation and experiment are always smaller than 18%. Figure 48 also illustrates that the ability of the filter media to capture contaminants decreases with the increase of filtration time due to the decrease of the intrinsic pore volume.
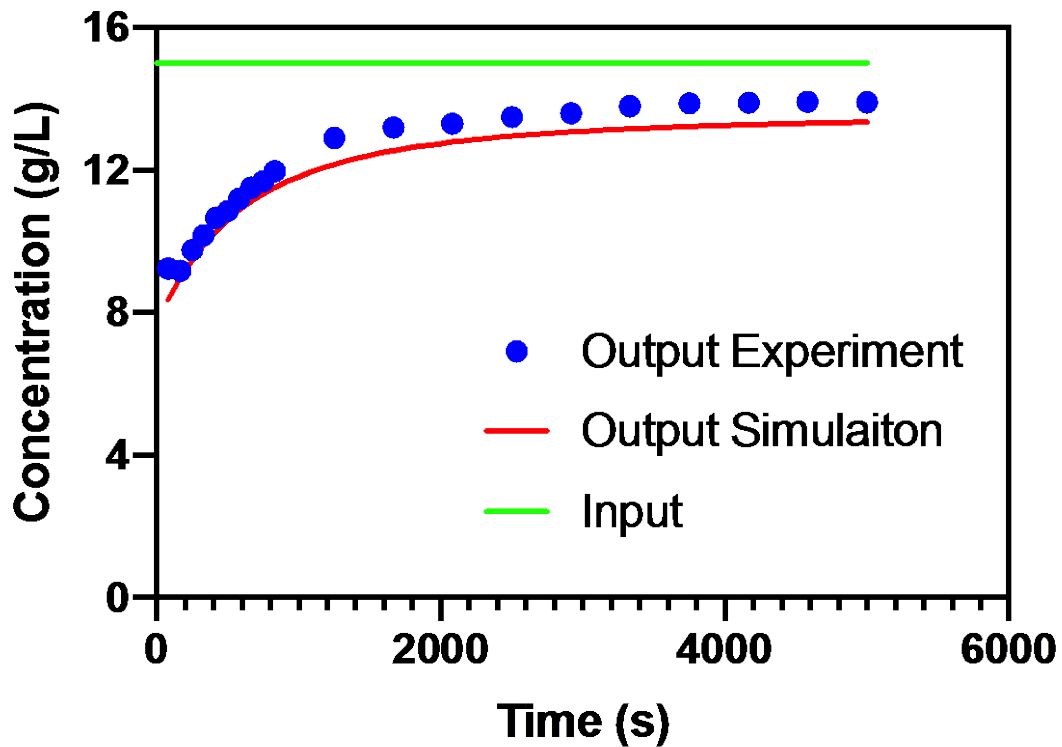
Figure 48 Comparision between the predicted capture ability (concentration of output) with the experimental results for mono-disperse contaminants.

104

5.4.2 Multi Disperse Systems

The last step in testing the capture model is predicting the capture of a more realistic array of contaminants. To test this, we construct a complex contaminant model by premixing 200μm 500μm and particles in varying number ratios. Again, the flow dynamics is obtained from our earlier PSD model, thus the probability of a particle to flow within a particular pore is related to both the pore size (i.e., the pore resistance) as well as the and particle size and number ratio (Di Carlo et al. 2009). The prediction of the model is still quite good as shown in Figure 49.
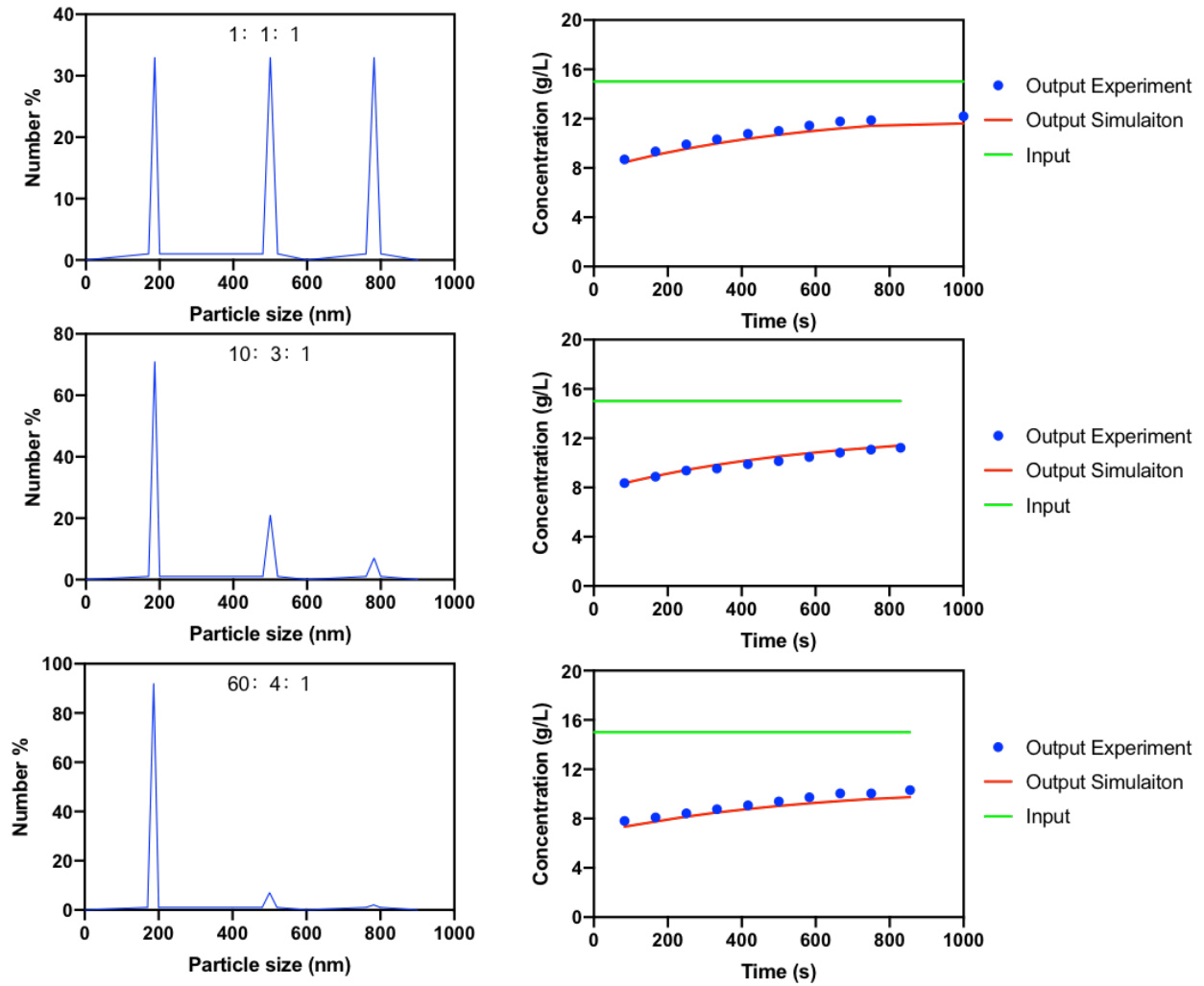
Figure 49 Comparision between the predicted capture ability (concentration of output) with the experimental results for multi-disperse contaminants

In this chapter, we test the mechanism of the describe the capture of spherical particles within dead-end pores. A 3D discrete element method-lattice Boltzmann method (DEM-LBM) coupling approach is applied to investigate the particle capture under conditions of different particle sizes and pore structures. We introduce a model to predict the ability of intrinsic pores capture semi-nano/nano particles. Both the pressure drop and the fluid density are examined to indicate this capture performance. The simulated results illustrate that the capture performance is dependent on the intrinsic pore structure and contaminant sizes.

6.0 Future Studies: Deep Depth Filtration

The process of particle transport and retention within porous media during deep bed filtration are widely applied(Mackie and Bai 1992, Bedrikovetsky et al. 2002, Jegatheesan and Vigneswaran 2005, Chi and Payatakes 1979)in natural and industrial system, such as the petroleum industry, wine purification and environmental treatments(Svarovsky 2000), Relatively high permeability is essential for a filtration process. However, the permeability is reduced because of particle retentions (particle deposit on or block the pore space). Thus, it is important to predict the particle retention/permeability reduction during a filtration process.

Mathematical models of predicting particle retention can be divided into two scales: macroscopic and microscopic(Jegatheesan and Vigneswaran 2005). Macroscopic models predict the particle transport through a filter medium via a continuous transport equation (Rege and Fogler 1988). The particle retention rate is assumed to be proportional to the particle advective flux (the movements of contaminants/particles along with flowing fluid), cU(Rege and Fogler 1988). The filtration coefficient is typically an evolving (rather than constant) parameter that depends strongly on the pore size distribution, surface properties (of both the contaminant and filter media), and fluid velocity(Herzig, Leclerc, and Goff 1970b, Chiang and Tien 1985). Then, Liu et al.(Liu and Civan 1996) provide a macroscopic model to predict the particle retention within two-phase flow. This model includes empirical parameters that require identification before any simulation process is possible. Van Oort et al. (van Oort, Van Velzen, and Leerlooijer 1993) propose a model that relates the permeability reduction with the particle retention, volume fraction of captured particles. Although convenient and straightforward, the macroscopic approach to date has been limited in its utility due to the strong dependence on fitting parameters (Yuan and Shapiro 2010).

Microscopic models, on the other hand, allow for the first-principles investigation of particle transport at the pore/particle scale. Properties of the fluid, contaminants and filter medium are discussed to model the transport and retention of each particle (Mirabolghasemi et al. 2015). The existing microscopic models can be subdivided into a direct numerical model and pore-network model. Direct numerical models, such as a CFD-DEM model(Mirabolghasemi et al. 2015), predict the flow dynamics and particle transport equations from the geometry of the filter medium directly by employing detailed (and expensive) computational calculations. Pore network models, on the other hand, start with one simplified pore represent the structure of filter medium by an interconnected network of pores. Fatt,(Fatt 1956) first introduced a pore network model by assuming simple pore shapes in an effort to reduce the computational costs of microscopic filtration modeling. Despite the simplification, pore network models have proven useful(Joekar-Niasar and Hassanizadeh 2012) in predicting particle transport since critical physical properties of the filter medium, contaminants, and fluid are preserved. Todd et al.(Todd, Somerville, and Scott 1984) employed a network model to simulate permeability reduction caused by particle retention with a regular cubic lattice. Many current pore network models are hampered by a lack of direct connection between the model and the physical mechanisms of particle retention that are at play in their application (such mechanisms can include straining by pore throat, Brownian motion and interception (Burganos, Paraskeva, and Payatakes 1992) as will be discussed in more detail below).

In this chapter, we develop a microscopic model for particle retention and penetration length. The particle retention model is determined through macroscopic experiments and verified by consideration of several potential particle-scale retention mechanisms. The penetration length is predicted based on the combination of the particle retention model and a pore network model.

6.1 Experiments

In order to examine particle retention, we perform experiments using a Nustche Filter to operate constant pressure filtration. A diatomaceous earth-based filter aid (here called FAX) is chosen as the filter medium. 5µm and 11µm spherical silica are used as the model contaminants to be removed. Before the filtration process, we calculate the maximum mass of the silica/contaminants that would be required to completely fill the available pores within the filter aid through a geometric analysis of the pore size distribution of the FAX being used as a filter medium (this quantity allows use to employ a somewhat unique scaling when couching our results in dimensionless terms).

The process for each filtration experiment was as follows:

1. Measure the volume of the filter aid.

2. Calculate the maximum mass of the (fixed size) contaminants.

3. Premix the contaminants with a known volume glycerol.

4. Put a 20µm mesh support at the bottom of the filter (to retain the filter media, but not hamper contaminant transport).

5. Pour the filter aid into the filter and then pour in the contaminated suspension.

6. Apply a known pressure to the filter.

7. Allow the fluid flow through the filter to be continuously collected within a beaker.

8. Measure absorption via UV-VIS for determining the concentration within the effluent.

Finally we run the test with different filter aid cake and maintain the same operating pressures as shown in Table 16 and Table 17. Here we still use the UV calibration curve to calculate the concentration of output as shown in Chapter 5.1.

Table 16 Experiment tests of different filter aids and the size ratios ($d_{particle}/d_{pre}$) for 11µm contaimiants.

	1	2	3	4	5
FAX3		0.776		0.328	0.119
FAX5		0.774		0.323	0.118
FAX7	0.938		0.501	0.326	0.118
FAX3+FAX5		0.775		0.325	0.118
FAX5+FAX7	0.938	0.774	0.501	0.325	0.118

Table 17 Experiment tests of different filter aids and the size ratios ($d_{particle}/d_{pre}$) for 5µm contaimiants.

	1	2	3	4	5	6	7	8	9
FAX3	0.919			0.538		0.353		0.149	0.054
FAX5		0.809	0.611			0.352		0.147	0.054
FAX7		0.816			0.426		0.228	0.148	0.054
(FAX3 +FAX5)*5	0.919	0.809	0.611	0.538		0.352		0.148	0.054
FAX5+FAX7		0.812	0.611		0.426	0.352	0.228	0.148	0.054

6.2 Probability Function

Figure 50 shows the ratio of the measured concentration of the filtrate, c, made dimensionless using the maximum concentration that could be captured (c^0; note that the value of c0 varies with cake thickness). The concentration ratio of c/c^0 always reaches a constant value when the cake thickness/filtration length is larger than some finite value (typically about 0.4cm). That is, after a certain "entrance length" region, the rate of particle retention becomes a constant, provided that the relative saturation of available contaminant is fixed. Mathematically, we can

write the number of particles retained within a given pore as $n_i P_i P_i^*$ where n_i is the number of particles that enter the pores of size i, P_i is the probability of flow passing through pores of size i (and is related to the resistance to flow within pore i as R_i) and P_i^* is the probability that a particle is captured within pore i (as will be seen, this value increases quickly to a value $P^*_{max,I}$, after passing the "entrance region"). In this way, the total amount of particles retained can be expressed as the sum over all pores of the particles captured within each pore. Noting that this value is constant after passing the entrance length, we can write:

$$\sum n_i P_i P_{i,max}^* = Constant \qquad (6\text{-}1)$$

$$P_i = \frac{\frac{1}{R_i}}{\sum \frac{n_i}{R_i}} \qquad (6\text{-}2)$$

Based on the pore size distribution, we can extract the Pi values as they completely determined by the pore size and pore volume. We hypothesize that P*i is a function of the size raito($d_{particle}/d_{pore}$) which we will denote as α_i. Given the contaminant and filter media used in our experiments, there are five pores with sizes larger than the contaminant (11μm glass beads). Thus, five unknown values of P*max, i are required for each filtration trial to be determined mathematically. Five filtration tests were therefore run, each with different filter medium combinations so that we may create a system of linear equations for our five unknows. Figure 52 shows the value of $P^*_{max,i}$ (the results from Table 17 see Appendix D) for a variety of contaminant

112

and pore combinations. Note that the value of $P^*_{max,i}$ may be extracted from the results shown in Figure 52 for the capture of the contaminants for a variety of combinations. As can be seen, it appears that $P^*_{max,i}$ is solely a function of the size ratio $d_{particle}/d_{pore}$ for both 11 and 5µm contaminants.
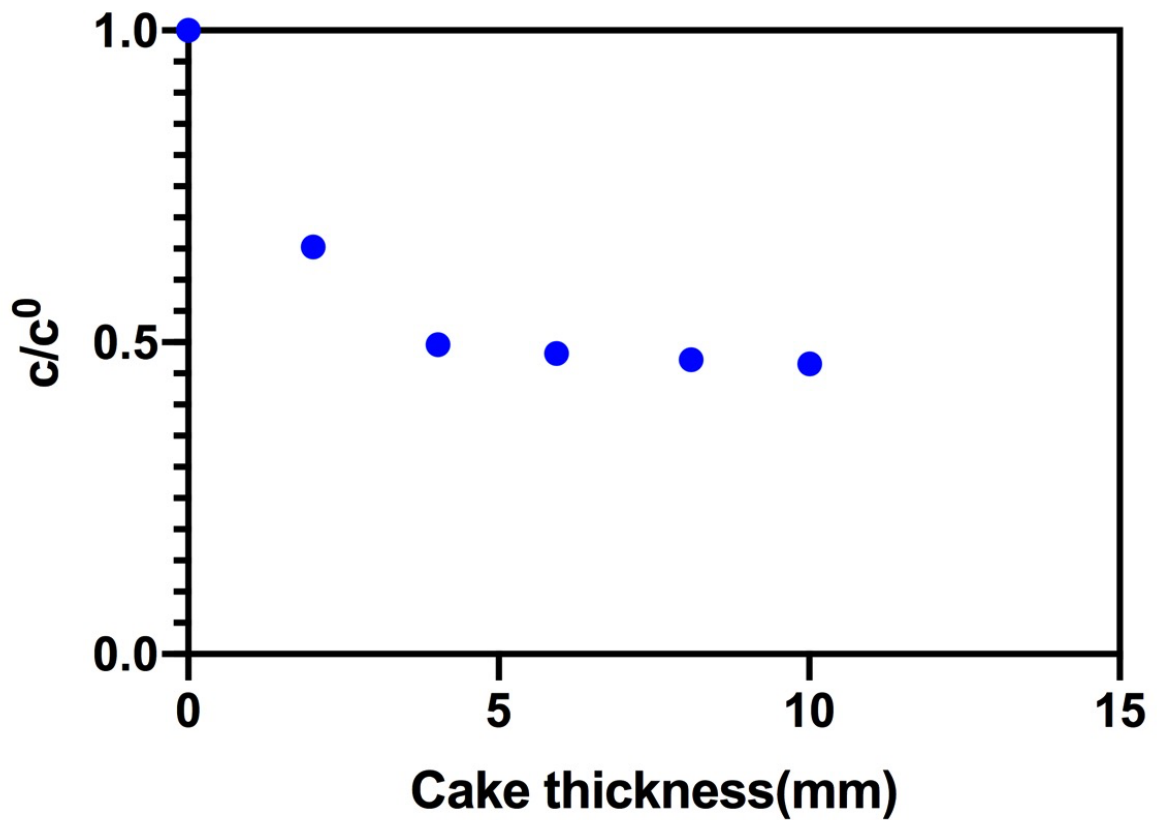
Figure 50 Concentration of output over the maximum concentration vs. the cake thickness of FAX 3.
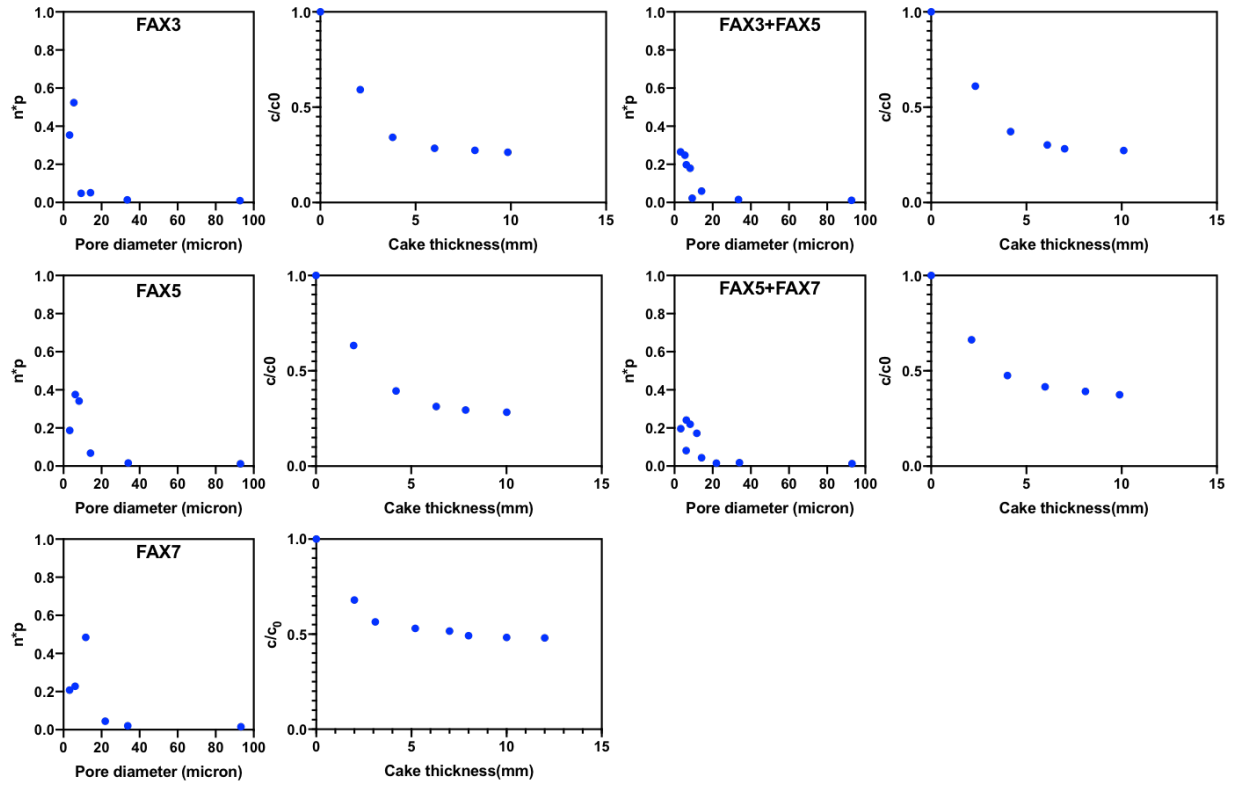
Figure 51 Probability of flow go through pore i with the change of concentration ratio c/c^0 in the same size ratio d$_{particle}$/d$_{pore}$.
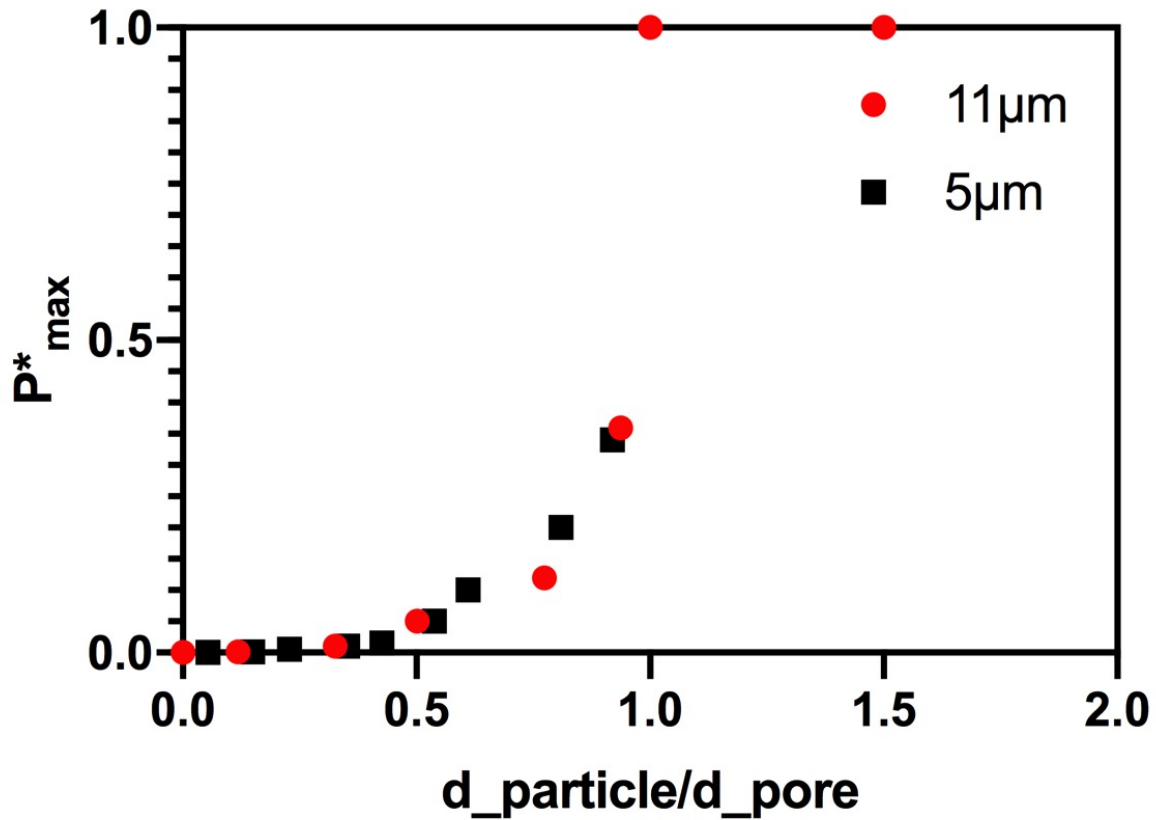
Figure 52 The maximum probability of a pore "capture" a contaminant with the change of size ratio d_particle/d_pore.

6.3 Deep Depth Model

To better understand the relationship between dynamic (or spatially varying) P^* and pore size / particle size. we run tests with a bed of spherical particles as the filter medium such that we simplify the bed structure. The pores formed by the mono-disperse large particles are well understood and, in general, lead to gaps that are roughly 0.18 * the large particle size. Thus, the size ratio $d_{partile}/d_{pore}$ is $d_{small\_particles}/(0.18d_{large\_particles})$.

Figure 53 shows the influence of the cake thickness on P^* (i.e., it shows the effective length of the entrance region) which we can fit to an exponential expression as:

$$P^* = P^*_{max} * \left(1 - exp^{-\frac{x}{k}}\right) \tag{6-3}$$

where P^*_{max} is the maximum probability of pore i capturing the particle of interest and k is a capture coefficient that that is related to size ratio $d_{particle}/d_{pore}$.
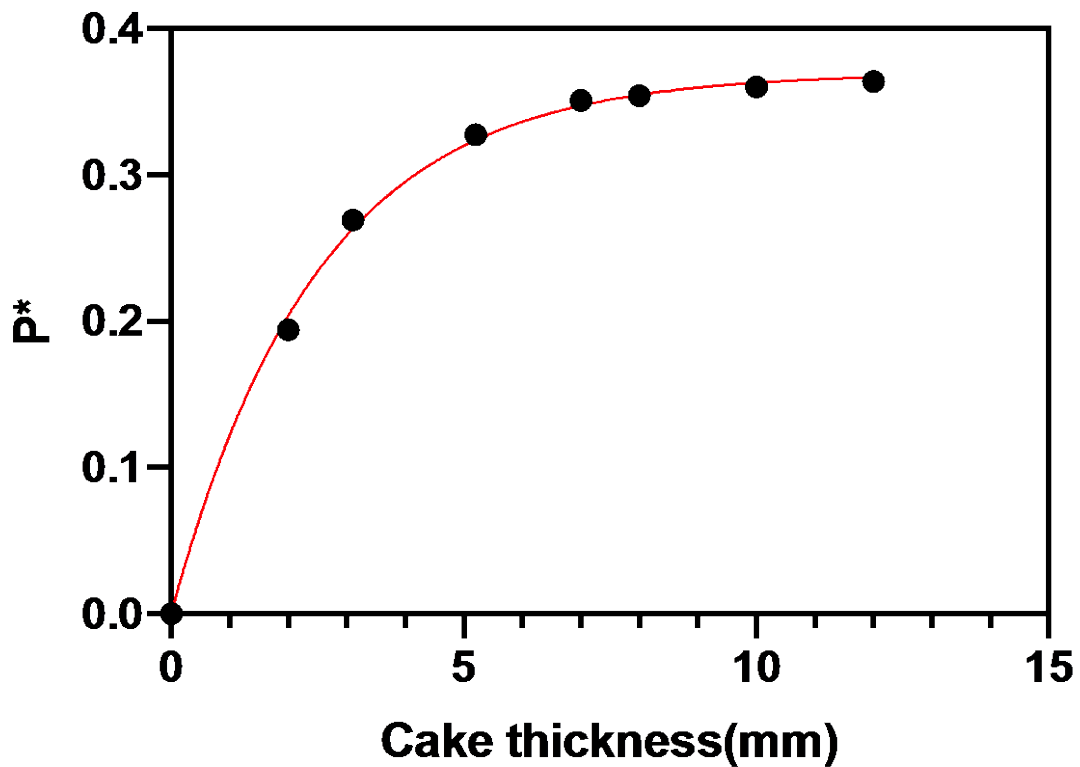
Figure 53 Probability of pore i capture particle j vs. cake thickness (size ratio is 0.917).

Table 18 Deep depth model tests with sphererical particles.

Particle size (μm)	Pore size (μm)	Contaminant size (μm)	R_c/R_p	K
500	90	μ=82.5, σ=7.5	0.917	2.496
500	90	μ=69, σ=6	0.766	3.151
500	90	μ=58, σ=5	0.644	3.503
500	90	μ=11, σ=6	0.122	3.918
μ=98, σ=5	17.64	μ=11, σ=6	0.624	3.543
μ=82.5, σ=7.5	14.85	μ=11, σ=6	0.741	3.207
μ=69, σ=6	12.42	μ=11, σ=6	0.886	2.636
μ=98, σ=5	17.64	μ=5, σ=5	0.283	3.901
μ=82.5, σ=7.5	14.85	μ=5, σ=5	0.337	3.873
μ=69, σ=6	12.42	μ=5, σ=5	0.403	3.775
μ=58, σ=5	10.44	μ=5, σ=5	0.478	3.692

Figure 54 Dynamic capture coefficient vs. size ratio $d_{particle}/d_{pore}$.

Figure 54 shows the relationship between capture coefficient k vs. size ratio. Note that (6-3 is, itself, a function of the size ratio (where in Figure **53**, it is given as 0.917).

6.3.1 Particle Retention Mechanisms

Despite the fact that the prediction from the deep depth model for the superficial velocity fits our experimental results well, the performance of the prediction relies significantly on the empirical values of both the capture coefficient k and the measured values of $P^*_{max,i}$. While, at present, k will still need to be determined experimentally based on the size ratio $d_{particle}$ / d_{pore} as shown in Figure 54, theoretical analysis of $P^*_{max,i}$ can lead to an first-principles model such that

we increase the generality (and accuracy) of the deep depth model. Toward that end, we test three sources of particle retention mechanisms and compare them with our measured results for deep depth filtration: direct interception, inertial impact, and straining. Direct interception or engagement, results in the capture of all particles that are moving along flow lines that are within a particle radius of a capture surface. The interception coefficient obtained from Lamb's solution of Navier-Stokes flow equations for low Re numbers (Re<1)(Lamb 1993) gives:

$$\eta = \frac{1}{2(1 - lnRe)}[2(1 + \alpha)\ln(1 + \alpha) - (1 + \alpha) + 1/(1 + \alpha)] \qquad (6\text{-}4)$$

where α is the size ratio $d_{particle}/d_{pore}$.
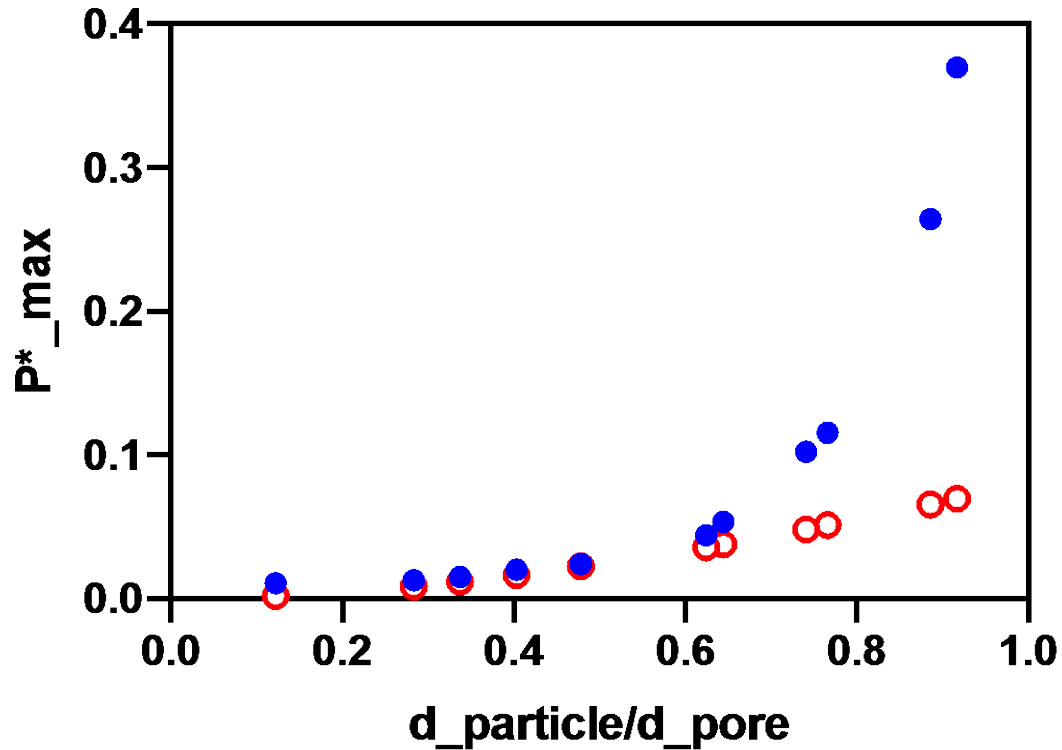
Figure 55 The p$^{*}_{max}$ obtained from Lamb's solution (red circle) compared to the experimental results (blue points)

Figure 55 shows that the p$^{*}_{max}$ obtained from Lamb's model fits well with the empirical data when the size ratio is smaller than 0.6. One conjecture, therefore, is that the direct interception is of primary importance as a retention mechanism in deep depth filtration when size ratios are small. Clearly, particle retention at higher size ratios must involve another mechanism(s).

The Inertial impact caused by the displacement of particles with a finite mass from the flow lines near curved regions of the flow (i.e., typical near capture surfaces) can also lead to retention (Shaw 1978). The corresponding expression for the capture coefficient is given as:

$$\eta_I = \frac{St * f}{2Ku^2} \tag{6-5}$$

where f is an empirical factor and Ku is the Kuwabara hydrodynamic factor. Shaw proposed that this mechanism is not significant under conditions where St $\ll$ 1. Since our study is restricted to conditions that lead to very small values of the Stokes number, we will ignore the effect of inertial impact in this study.
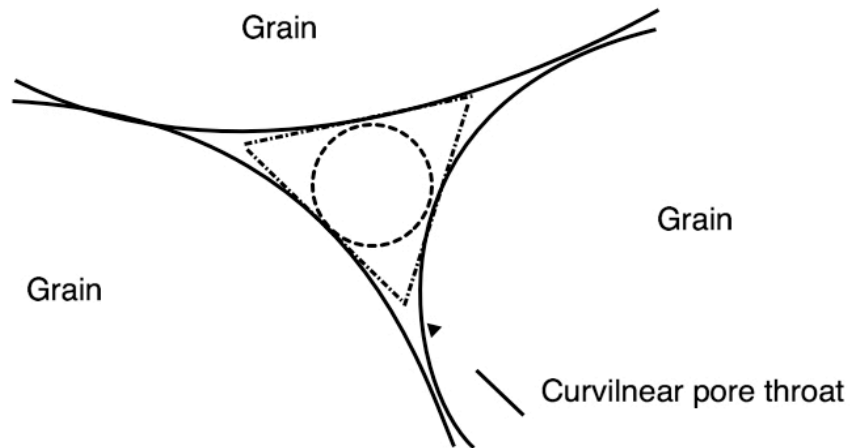
Figure 56 Schematic representation of a constricted pore throat.

Finally, pore blocking is often caused by straining and occurs when the particle size is larger than some portion (but not necessarily the largest part) of the pore space. Particles may block the pore even if the particle size is smaller than the average pore size because the complex pore structure (as shown in Figure 56) can lead to constrictions that are locally smaller than the average.

121

You et al. (You, Badalyan, and Bedrikovetsky 2013) presented a microscale model for particle straining, which is the stochastic parallel tube model (PTM). The medium is represented by the model of triangular parallel capillaries alternated with mixing chambers. The analytical model for $d_{particle} / d_{pore}$ filtration is derived and the steady-state solution is obtained as:

$$C_e(r_s) = C_0(r_s)[f_a(r_s) + f_{nl}(r_s)]\exp[-f_{ns}(r_s)\frac{L}{l}] \qquad (6\text{-}6)$$

where r_s is the injected particle size. f_{ns} is the flow fraction through the inaccessible small pores: $f_a + f_{nl}$ is the flow fraction through large pores. L is the length of the column. l is the distance between two chambers. C_e and C_0 are the outlet and inlet concentrations. When the particle size reaches the maximum pore size, C_e becomes zero. Here we introduced the mono-size PTM model to achieve an expression for $P^*_{max,I}$ based on this mechanism:

$$1 - P^*_{max,i} = [f_a(r_s) + f_{nl}(r_s)]\exp[-f_{nl}(r_s)\frac{L}{l}] \qquad (6\text{-}7)$$

Figure 57 shows how the capture coefficient obtained from the PTM model fits the empirical data. It is clear that the predicted data is consistently lower than the measured red values; however, when we combined the Lamb model with the PTM model we are able to predict the P*max,i as shown in Figure 58.
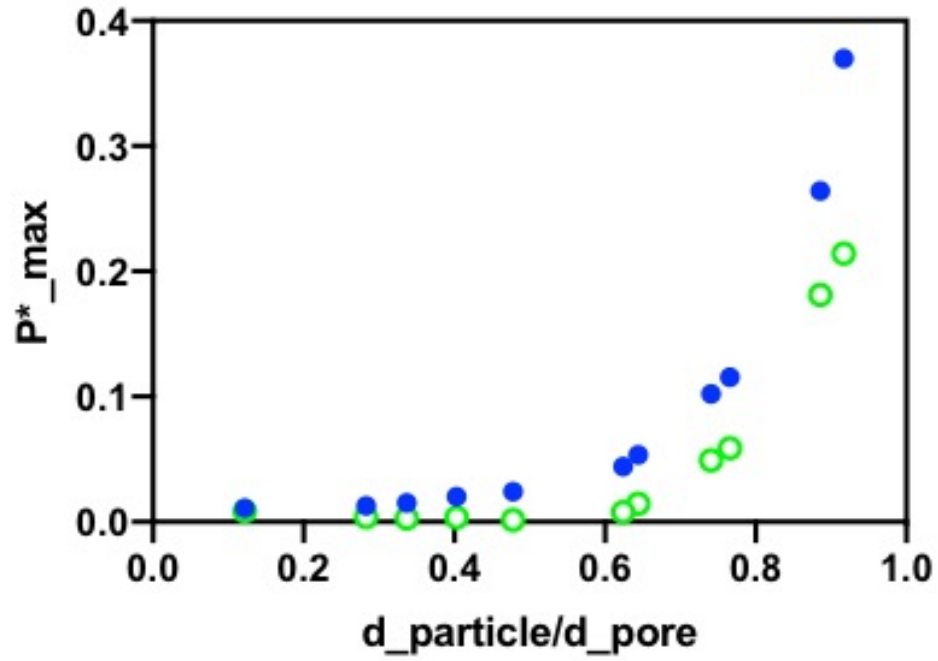
Figure 57 The capture coefficient obtained from PTM model (green circle) compare to the experimental results (blue points).
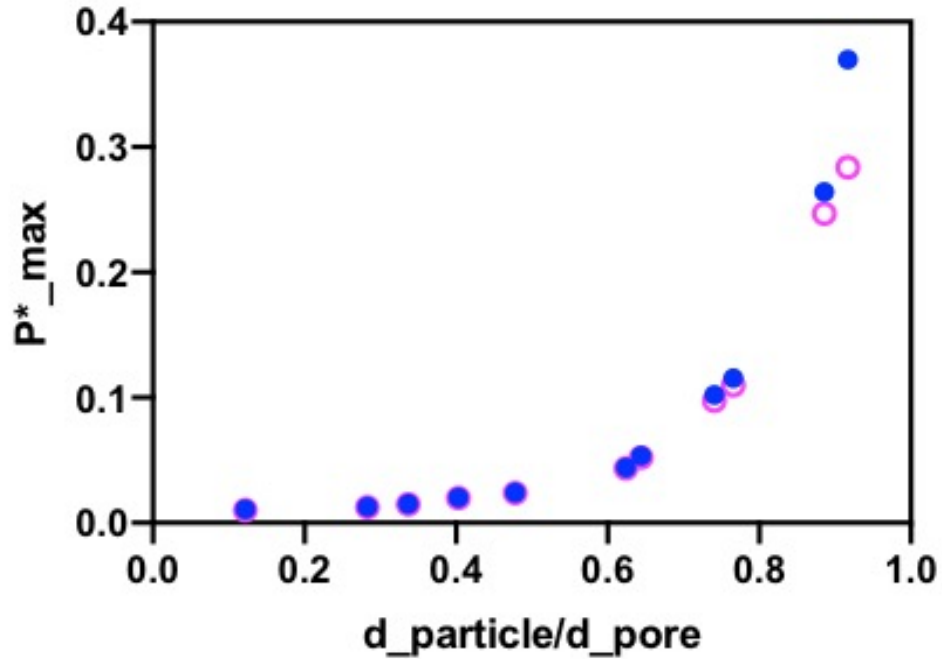
Figure 58 The capture coefficient obtained from the coupled Lamb-PTM model (purple circle) compare to the experimental results (blue points).

Despite the fact that Figure 58 shows significant agreement between a first principles model and our experimental measurements of $P^*_{max,i}$ there are several shortcomings of this approach. First, our model must still rely on the empirical measurements of the value of the k (i.e., the entrance length) parameter. Moreover, due to the complicated pore geometries, it is considerably more difficult to derive an analytical expression for $P^*_{max,i}$ for more realistic filter media materials (such as FAX) from the PTM portion of the model.

6.3.2 Penetration Length / Particle Deposition Distribution

Nevertheless, as a means of validating the predictive capability of our proposed model, we examine particle deposition during a deep depth filtration process performed for small spherical contaminants being captured by a bed of larger spherical filter media. In capturing the dynamics of the deposition process, we obtain the trajectory of individual contaminant particles from a time discretization of the (deep depth-modified) PSD model such that:

$$x_{p_{i+1}} = x_{p_i} + \frac{u_{p_i} + u_{p_{i+1}}}{2} \delta t \qquad (6\text{-}8)$$

where x_p is the particle position, δt is the time step and the particle velocity at both the present $u_{p_{i+1}}$ and the previous time steps u_{p_i} can be calculated by the PSD model. Based on the particle retention model, the change of the particle velocity at pore i +1 reduces to 0 ($u_{p_{i+1}} = 0$) is equal to the probability of the particle being deposited at that pore, P^*_{i+1}. The time step δt is chose to be 0.01s as this is the value at which we find that the result of the particle deposition distribution is independent of further reductions in the time step.

To test the prediction of particle location from the deep depth model, we chose 500μm glass beads as the filter medium and 11μm glass beads as the contaminants. Thus,

$$p^* = 0.011 * \left(1 - e^{-\frac{x_p}{k}}\right) \qquad (6\text{-}9)$$

Figure 59 shows the prediction of the spatial distribution of the deposition of 10,000 contaminant particles passing through a 4cm bed of filter medium using the deep depth model. As one can see, particles are retained at 0.4cm and the probability of particle deposition decreases dramatically after that poin. In order to verify the prediction of the deep depth model, a 3.92cm filter cake is built with 500µm glass beads. The suspension is composed of 11µm glass beads with glycerol. Then, the filtered cake is cut into sections of length step δl=0.3 cm along with the cake depth. Particles in each section are separated using a 10µm sieve.

Figure 60a shows the mass of the 11µm glass beads in each section vs. the position of that section of the filtered cake. This figure also compares the experimental particle deposition distribution with the prediction from the deep depth model. Similarly, we compare the cumulative distributions between the prediction from the deep depth model with the experimental results, as shown in Figure 60b. We also chose the 500µm glass beads as the filter medium and 11µm glass beads as the filter contaminants, to test the prediction of the concentration with different cake thickness. Table 19 shows the prediction of the dimensionless concentration of the output by the deep depth model and shows that these results still fit the experimental test quite well. Overall, the proposed deep depth model fits the experimental results and theoretical calculations quite well.
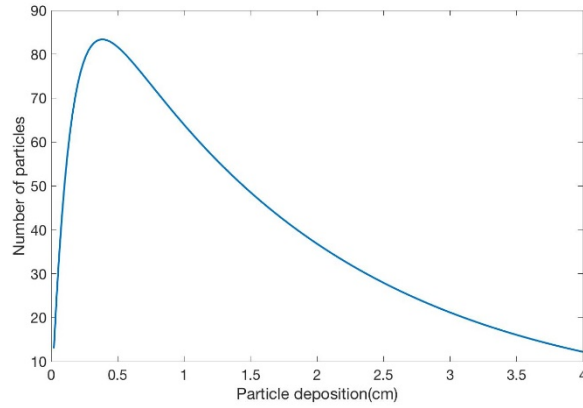
Figure 59 The prediction of particle deposition length distribution / particle penetration depth with 10,000 particles by the deep depth model.
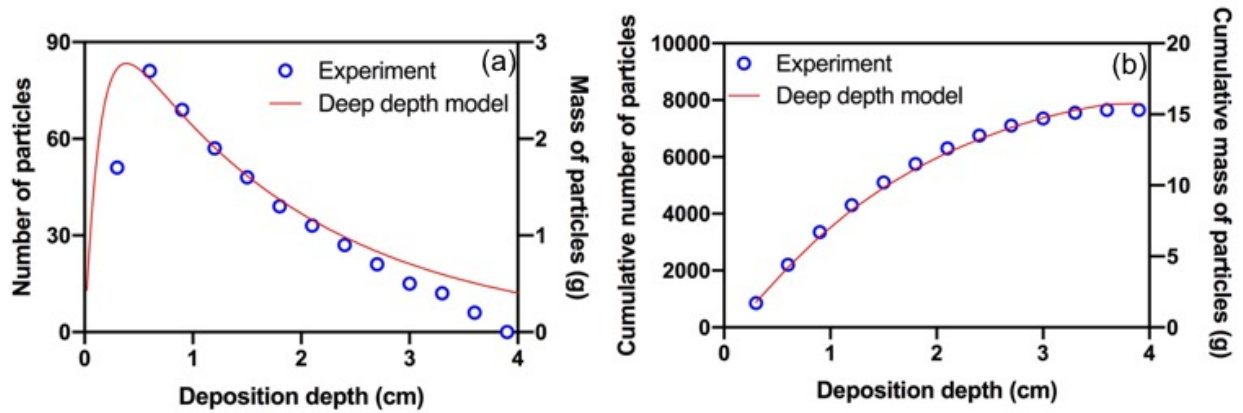
Figure 60 Verification of the deep depth model by experimental filtration results. a. Comparison between the predicted particle deposition distribution with the experimental particle deposition distribution. b. Comparison between the predicted cumulative number distribution with the experimental mass distribution.

Table 19 Compare the dimensionless concentration of output between the prediction by the deep depth model and the experimental test with different cake thickness.

Cake thickness(cm)	0.5	1	2	4
Deep depth model(c/c^0)	0.704	0.559	0.170	0.001
Experiment(c/c^0)	0.712	0.562	0.176	0

In this chapter, we develop a deep bed filtration model to predict the migration of micro- and semi microparticles in porous media. A transport probability function P(i) is proposed to predict the probability of flow go through a pore based on the analysis of pore resistance. The model also includes a deposit/capture probability function P^*(i) to describes the probability of particles deposit in a pore. The P^*(i) is calculated based on the change of concentrations during filtration tests with different pore structures and particle sizes. Because of the size exclusion of large particles in smaller pores, P^*(i) equal to 1 when $d_{particle} \geq d_{pore}$. Based on the experimental results, we also find finite particle retention when $d_{particle} < d_{pore}$. The empirical P^*(i) shows the probability of particle deposit/ pore capture is highly related to the size ratio ($d_{particle}/d_{pore}$) and flow velocity. P^*(i) is positively correlated to the size ratio. P^*(i) is negatively correlated to the flow velocity due to the shorter residence time and exhibit both a transient and steady-state stage. During the transient stage, P^*(i) increases rapidly since some particles start to deposit in a pore. During the steady-state stage, P^*(i) is constant since the particle concentration in that pore reaches a constant (particle retention limitation). Particle retention is mainly influenced by direct interception when the size ratio is smaller than 0.6. Particle retention with higher size ratio may be influenced by the particle geometry (straining). However, the pore geometry is hard to predict.

Future work may start with the expression of pore structures like diatomaceous earth with a computational method, to better understand the mechanism behind the particle retention.

7.0 Conclusion and Future Perspective

Solid-liquid filtration is a long-standing engineering practice and has been widely used in the chemical, process and mineral industries. Current models are semi-empirical in nature; thus, they require significant experimental and/or computational resources in order to determine the empirical quantities. In contrast, in this dissertation, we provide a model to predict the dynamic behavior for both the liquid and solid phase of a filtration process without the requirement of empirical parameters. Instead, our model relies solely on the to-be-captured particle size distribution of contaminants as well as the pore size distribution of the filtration media. Our new algorithm is capable of describing filtration based on both "'steric" capture of contaminants as well as capture within dead-end pores in the material.

Particle capture by a collecting medium is a common process, which can be applied to industrial applications (e.g., solid/liquid filtration). Ideally, the capture of contaminant particles by a porous filtration medium can be accomplished even when the radius of the particle is smaller than the pore radius. Several studies have been proposed to describe particle clogging within inter-connected (open) pores; however, studies of the capture of particles within dead-end pores are rare, because of the complex pore structure and hydrodynamic conditions. Despite this fact, this mechanism of capture is preferable due to the significantly smaller impact on overall flow behavior. Thus, in this work, we describe a simulation model capable of describing the capture of spherical particles within dead-end pores. A 3D discrete element method-lattice Boltzmann method (DEM-LBM) coupling approach is applied to investigate the particle capture under conditions of different particle size and pore structures. The DEM is used to describe the particle dynamics, whereas the LBM is employed to describe the fluid flow through the filter medium. Both the pressure drop and

the fluid density are examined to indicate this capture performance. The simulated results illustrate that the capture performance is dependent on the pore geometry and the Stokes number.

We show the performance of this model in modeling beds comprised of high void fraction materials (diatomaceous earth) that is used for the removal of multi-modal mixtures of contaminant. By formally accounting for the complex pore size distribution, we predict flow dynamics that are much closer to our experimental results than the predictions of the traditional Kozeny-Carmen (KC) model and show that this approach is viable for both statically formed and evolving (dynamic) beds. In an effort to understand the relationship between flow dynamics and pore size distribution more fully, we built a dynamic filter cake model that continuously modifies the pore size distribution as contaminants (polydisperse spheres) are deposited. In short, the predicted flow dynamics of this new model match the dynamic experimental results remarkably well, setting the stage for a priori prediction of filtration times, flow-rates, particle capture, and pressure requirements from simple measurements of the size distribution of both the filter media pores as well as the contaminant particles/droplets.

7.1 Perspective on Industrial Use

For the industrial use of the PSD model and the Capture model, the only information we need to perform these simulations is the physical properties of the fluid product and a characterization of the contaminant sizes. As shown in the

Figure 61, based on the particle size distribution of crude oil, we use the PSD model to predict the superficial velocity by considering particle size $> 2\mu m$. The red line shows the simulation results. We combined the PSD model with the capture model to predict the change of

clarity. In this dissertation, NTU test is used as the experimental clarity measurements and this is compared with the predicted c of output.

Figure 62 shows the result of 20mL crude oil filtrate with five clean 3mm filter aid passes. Since we have a fixed filter paper at the bottom, we have separated the large particles at the first pass, resulting in a dynamic decrease of velocity and decrease of the NTU. For the second to the fifth pass, the superficial velocity is almost constant because there is no larger contaminant that can block the through-transport pores. The NTU/c of output continuously decreases as a result of small contaminant being captured by the dead-end pores as shown in Figure 63.
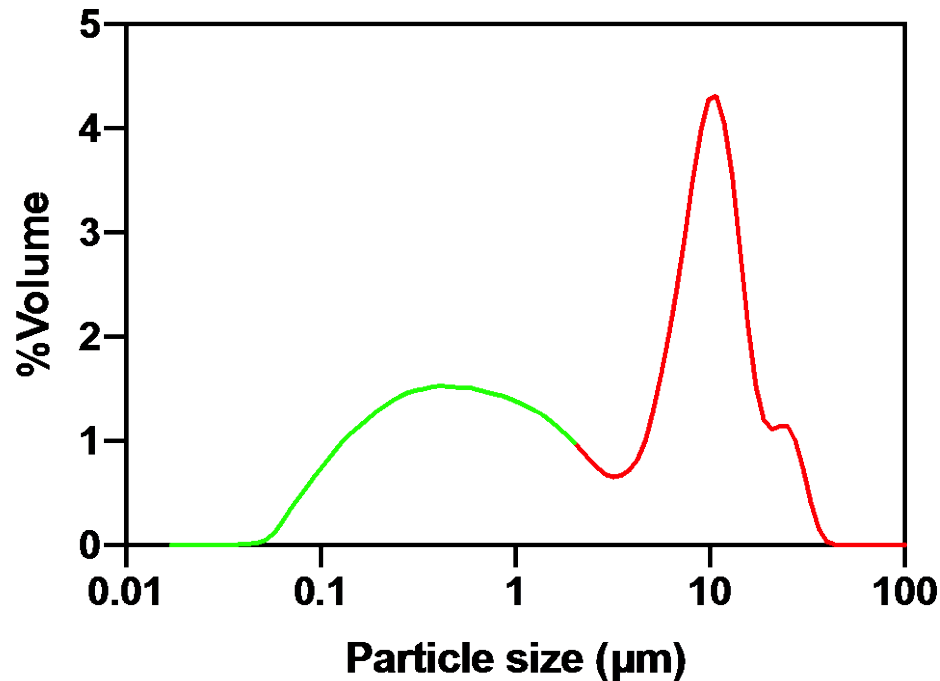
Figure 61 Particle size distribution of the contaminant in Detergent A.
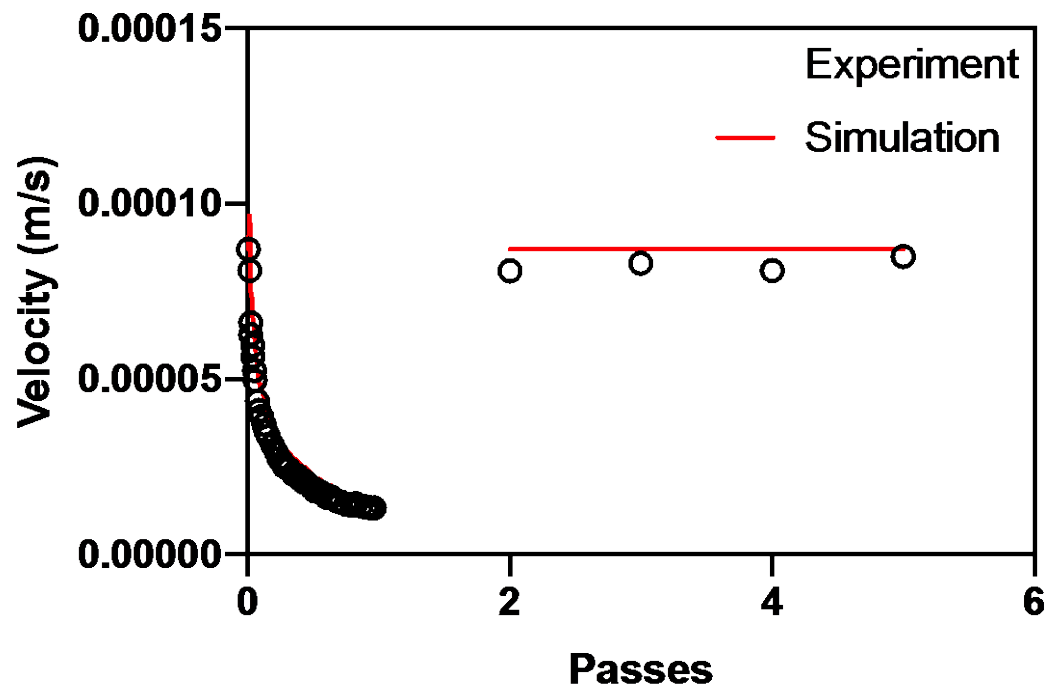
Figure 62 Comparision between the predicted flow rate by the PSD model with the experimental data (five recycle times).
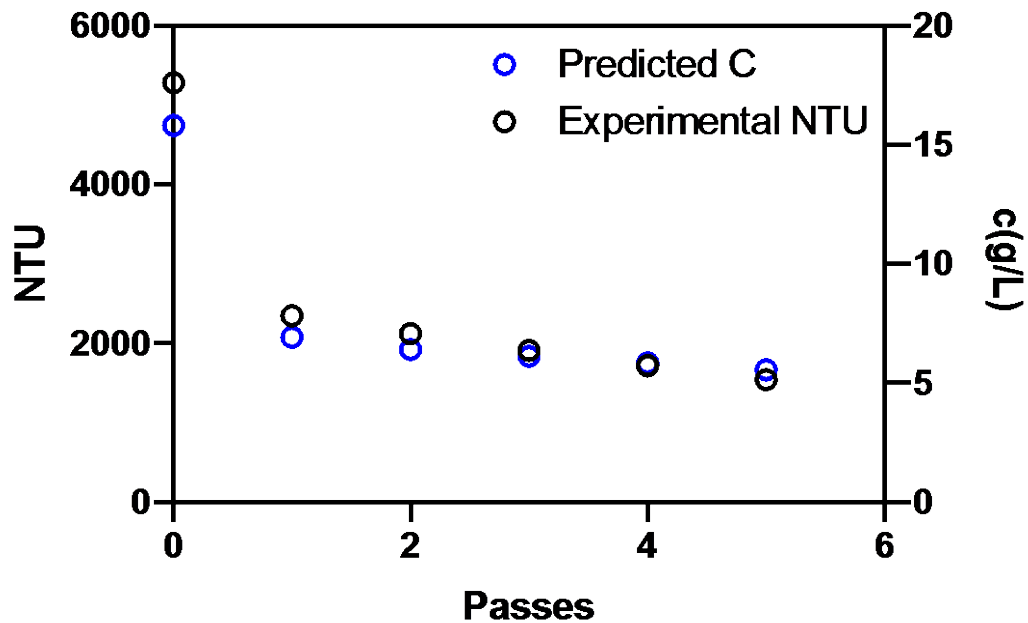
Figure 63 Comparison between the prediction concentration of output by the Capture model with the NTU test（five recycle times）.

Combined the PSD model and the Capture model with the requirements of the oil industry, we provide a SoLiFi software based on the MATLAB platform as shown in Appendix C. SoLiFi provides a computational modeling tool that can be used to enhance correctness of fluid dynamics simulations as well as to optimize solid-liquid separation processes. It mimics the filtration process, enabling a user to find the most efficient filter aid. It can, for instance, give a process engineer an accurate prediction of when a filter would need to be changed based on the inputs to that filter, or by an engineer designing filters to make the optimal filter aid selection at each stage in an industrial processing pipeline. This would reduce costly downtime from failure to change a filter at the right time, as well as reduce the time needed for making many experiments. It can also, for example, be used by a software engineer developing a fluid dynamics application to produce

134

more accurate simulations without needing to conduct many experiments to verify the correctness of the simulation.

The software provides a function that takes as input the intrinsic physical properties of the liquid and solid materials being tested and produces as output predictions of the dynamic behaviors of the liquid and solid phases for a bounded duration of the process. These dynamic behaviors include: pressure drop; flow dynamics; filter cake structure; effluent concentration; permeability of porous materials. The most closely competing models are based on many repeated experiments, which cost more time and money. In contrast, this model is based on first principles and simple physical characterization experiments. Therefore, the model can be used to rapidly simulate many possibilities to screen out bad inputs, rather than manually experimenting on every input.

The software has been tested with several oil industrial samples. Optimization of detergent samples has been tested via SOLIF software. Table 20 shows FAX7 works best to clean the crude detergent by maintain the same recycle times. Other filter aid may work better, which is depending on the industrial requirement, such as highest clarity, smallest recycle times, lowest power and time.

Figure 64 also shows the screening results by compare the flow rate during the filtration process. It also shows the predicted lines fit experimental circle points very well.

Table 20 Optimization of detergent A from oil company.

	FAX3	**FAX5**	**FAX7**
Porosity(ml/g)	2.76	2.30	1.96
Recycle times	2	2	2
Cake thickness (cm)	5.24	4.67	4.12
Time (s)	5260	4620	3800
		Better	Best
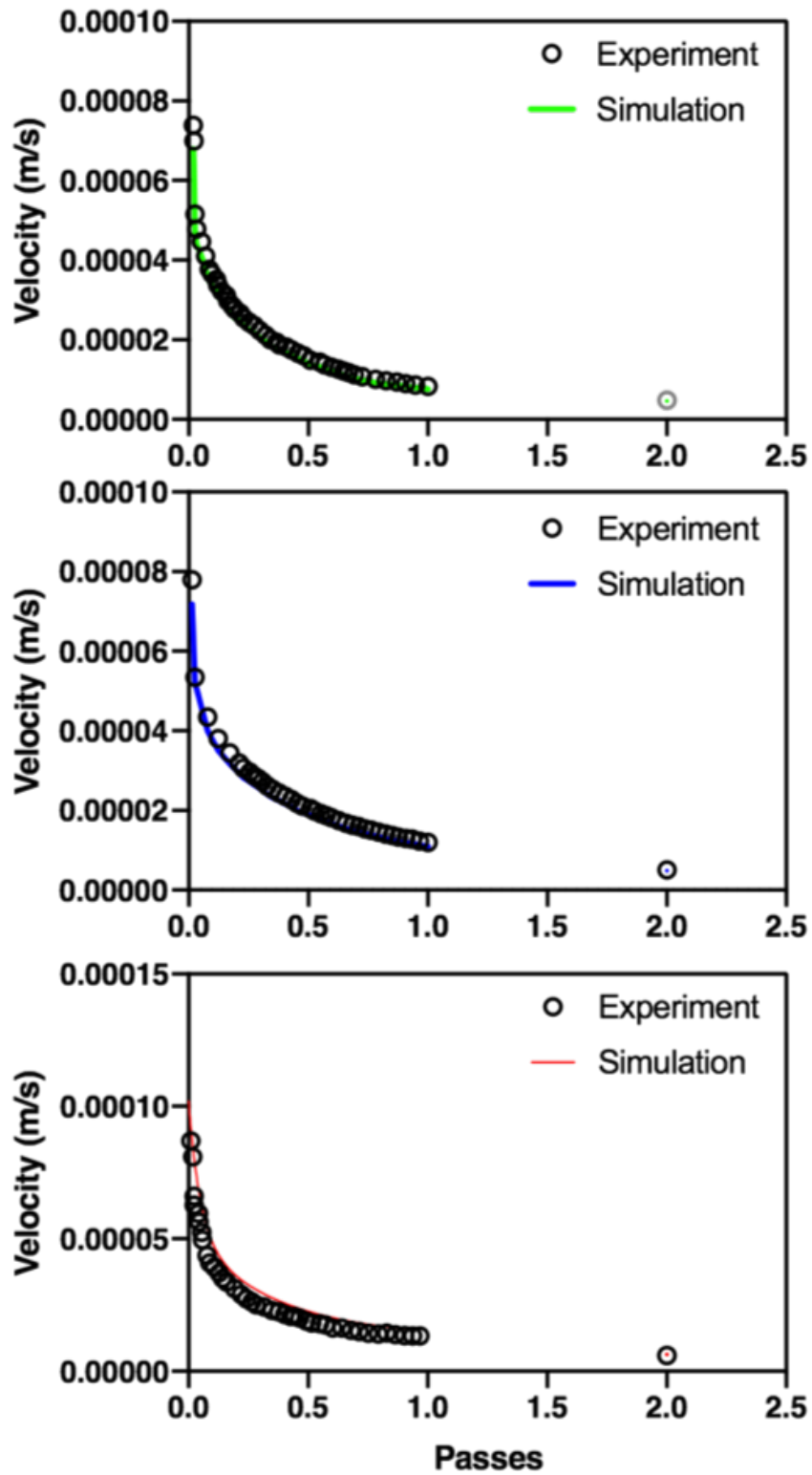
Figure 64 Screeening of detergent A with FAX 3, FAX 5 and FAX 7 with the same recyle times.

Another industrial test is the ZDP, Zinc dialkyl dithiophosphate. We test five clean ZDP samples and compare the almost constant experimental superficial velocity with the predicted velocity by the PSD model as shown in Figure 65.
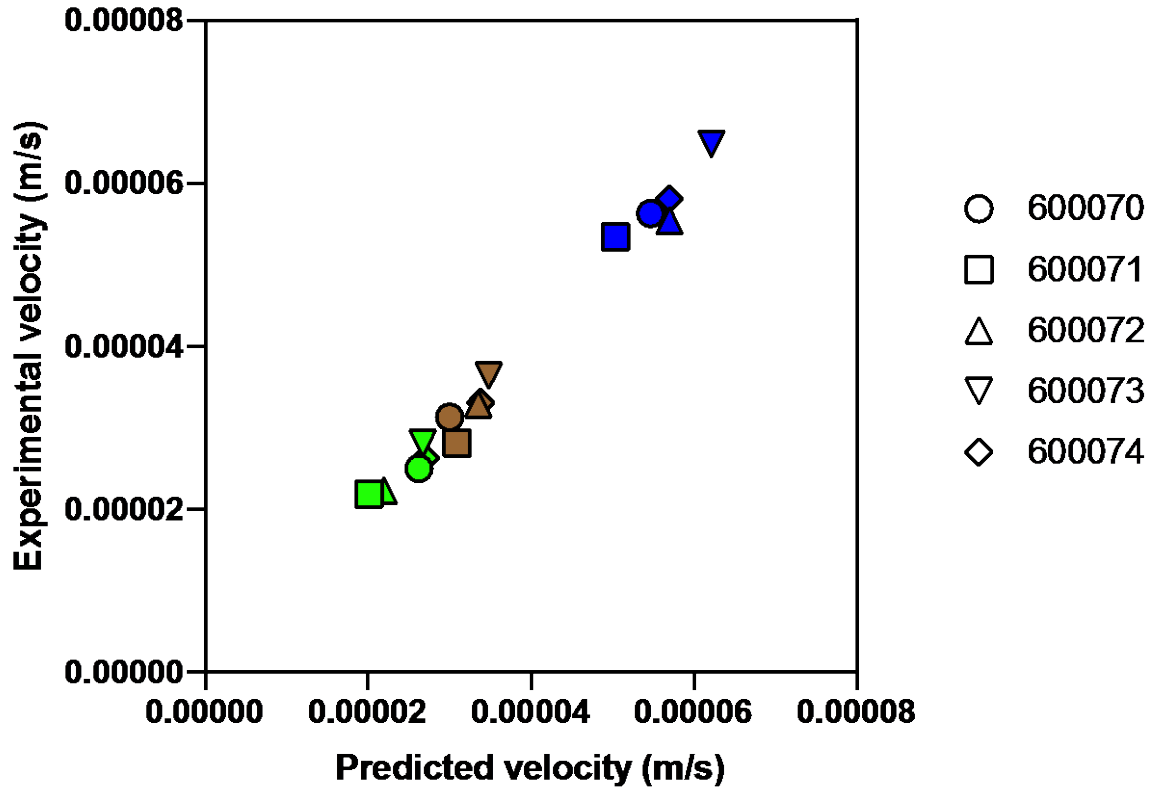
Figure 65 Comparision between the predicted velcotiy by the PSD model and the experimental velocity with clean ZDP samples.

Extensive R&D work will be needed to be done for the deep depth model. 1) Trying to figure out the theoretical description of k. 2) Derive the probability capture function into the filter medium with complicate structure. 3) Applied the coupled PSD, Capture and deep depth model

into the petroleum industries. This software should also broaden to other industries. Our current model can be worked for a slow viscous fluid. Analysis may be changed to the wastewater treatment, by consider the change of fluid dynamic and "clogging" problems.

Appendix A Prediction of the Change of Pore Size Distribution

d_{sphere}=4 μm

	6μm	11μm	22μm	34μm	93μm
Final d_p	2.44	2.24		1.21	
Final φ_p	0.70	0.57		0.36	

d_{sphere}=11 μm

	6μm	11μm	22μm	34μm	93μm
Final d_p	---	0	10.52	2.29	
Final φ_p	---	0	0.50	0.36	
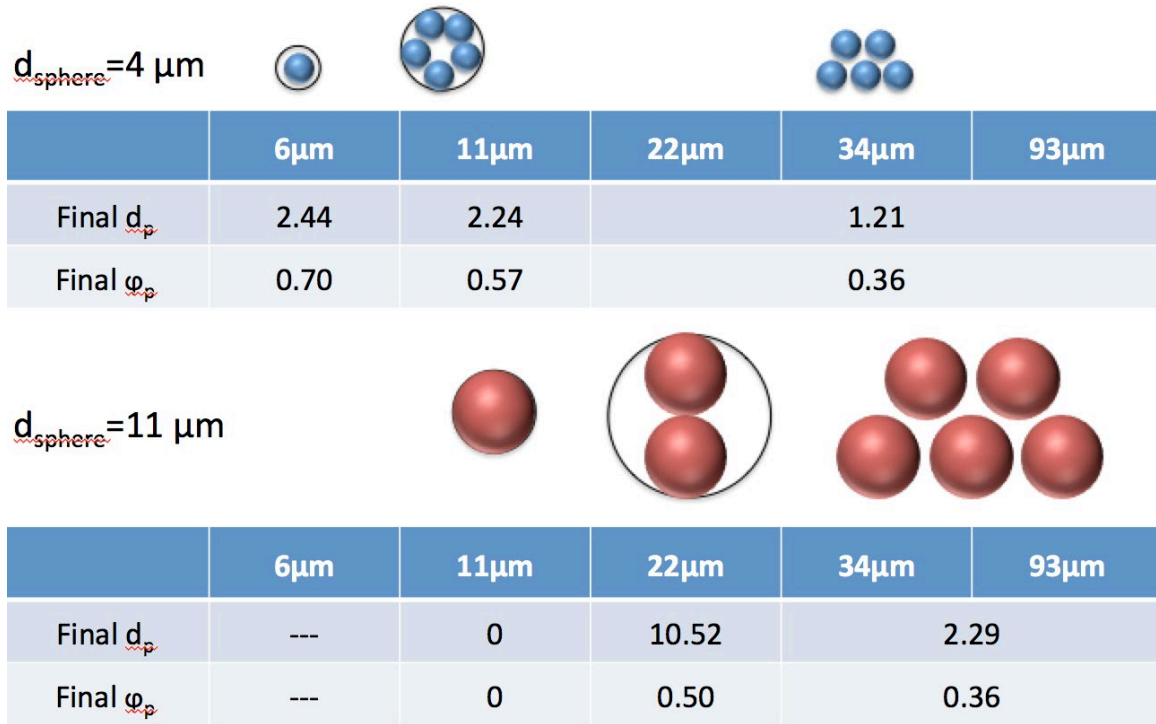
Figure 66 Prediction of the change of pore size distribution with monosphere contaminants.

$N_{s/l}=1:1$
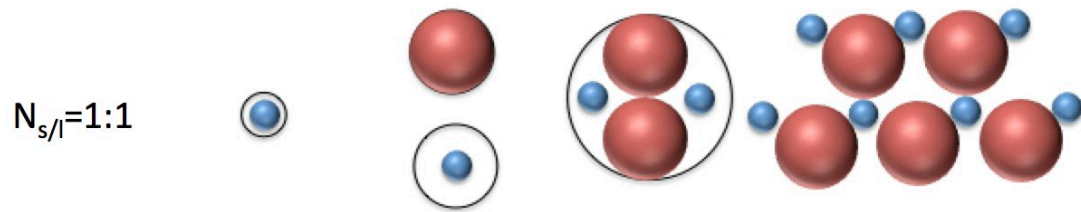
	6µm	11µm	22µm	34µm	93µm
Final d_p	2.44	0|10.25	10.32	7.01	
Final φ_p	0.70	0| 0.95	0.48	0.64	

$N_{s/l}=3:1$
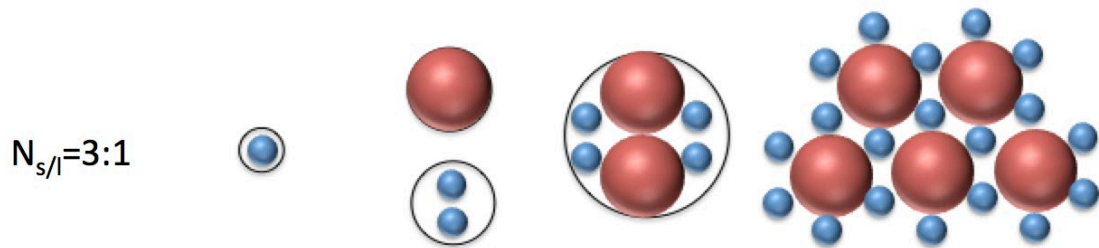
	6µm	11µm	22µm	34µm	93µm
Final d_p	2.44	0| 9.43	9.18	2.95	
Final φ_p	0.70	0| 0.86	0.43	0.42	

Figure 67 Prediction of the change of pore size distribution with multisphere contaminants.

Appendix B Preparing of Polydisperse Spheres
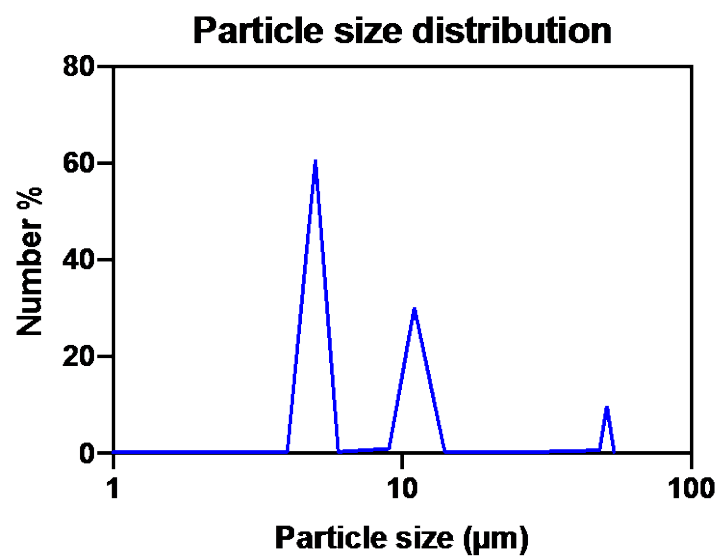
Figure 68 Particle size distribution of the mixed sample.

Appendix C SOLIFI Beta 1.1 User Innerface
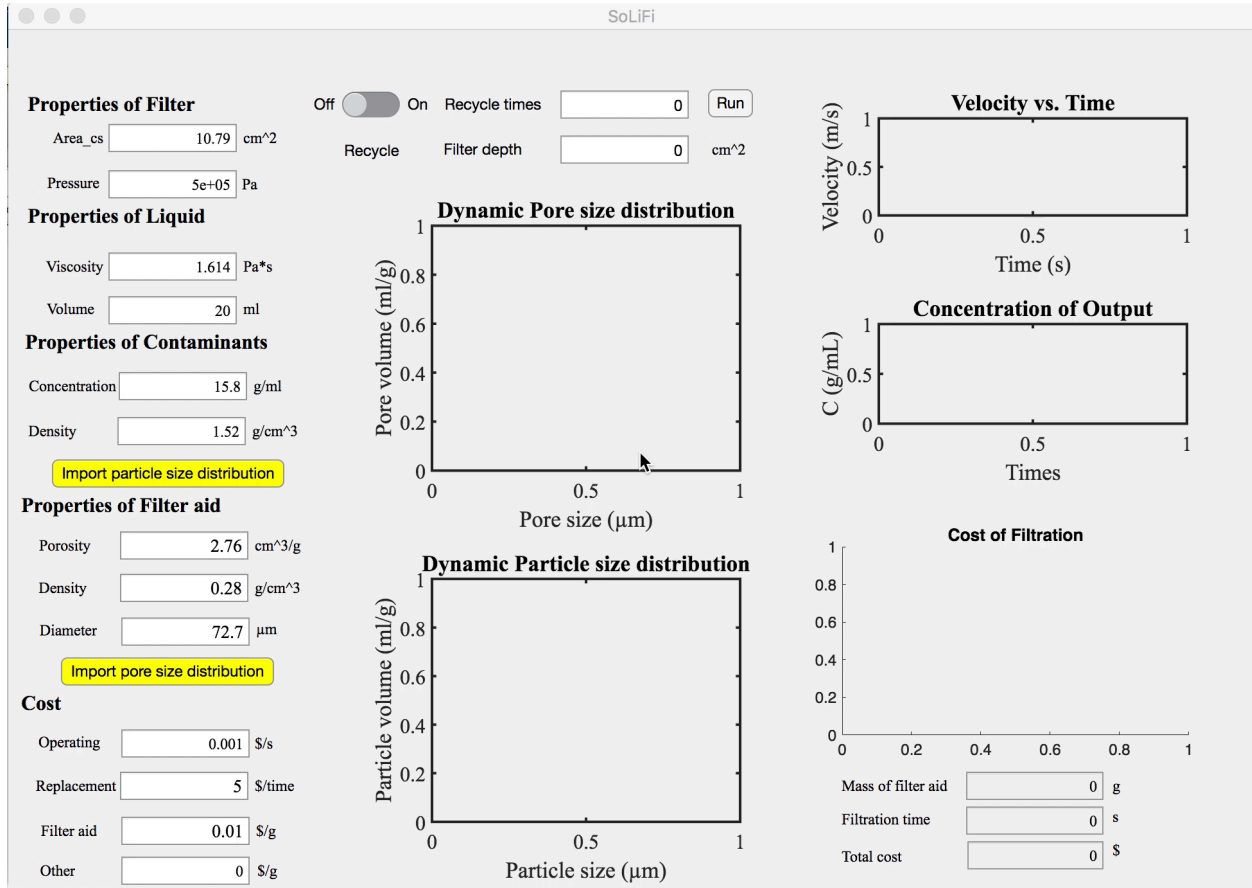
Figure 69 SOLIFI software user innerface.

Appendix D Probability of the Pore I Capture A Silica
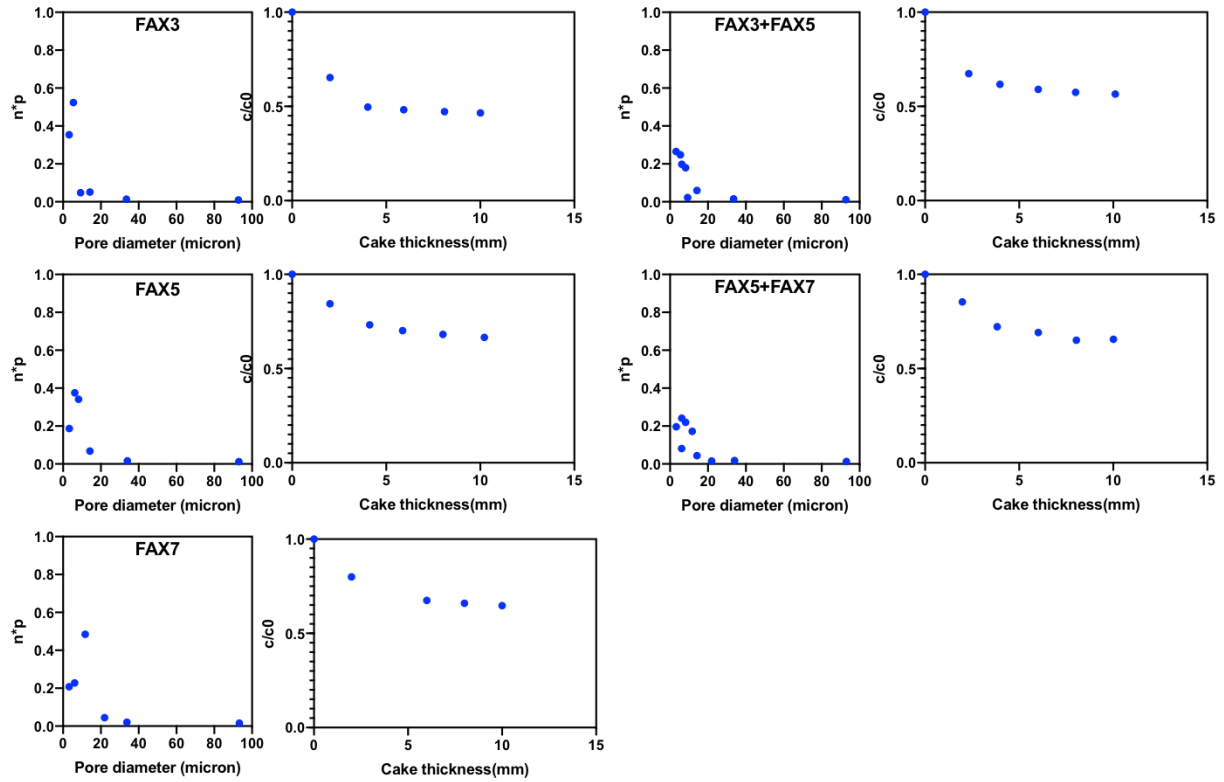
Figure 70 Probability of different size pores to capture a 5µm silica sphere.

Bibliography

Akaike, Hirotugu. 1987. "Factor analysis and AIC." In *Selected papers of hirotugu akaike*, 371-386. Springer.

Al-Ghouti, MA, MAM Khraisheh, SJ Allen, and MN Ahmad. 2003. "The removal of dyes from textile wastewater: a study of the physical characteristics and adsorption mechanisms of diatomaceous earth." *Journal of Environmental Management* 69 (3):229-238.

Al-Raoush, Riyadh, Karsten Thompson, and Clinton S Willson. 2003. "Comparison of network generation techniques for unconsolidated porous media." *Soil Science Society of America Journal* 67 (6):1687-1700.

Andersen, Hans C. 1980. "Molecular dynamics simulations at constant pressure and/or temperature." *The Journal of chemical physics* 72 (4):2384-2393.

Aparicio, M, MO Prado, and A Durán. 2006. "Infiltration under isostatic pressure of porous silica glasses with silica sols." *Journal of non-crystalline solids* 352 (32-35):3478-3483.

Aurenhammer, F. 1991. "Voronoi diagrams—a survey of a fundamental geometric data structure. ACM Comput." *Acm Computing Surveys* 23 (3):345-405.

Bedrikovetsky, P, P Tran, WMGT Van den Broek, D Marchesin, E Rezende, A Siqueira, Al L Serra, and F Shecaira. 2002. "Damage characterization of deep bed filtration from pressure measurements." International Symposium and Exhibition on Formation Damage Control.

Biot, Maurice A. 1941. "General Theory of Three-Dimensional Consolidation." *Journal of Applied Physics* 12 (2):155-164.

Bowen, WR, JI Calvo, and A Hernandez. 1995. "Steps of membrane blocking in flux decline during protein microfiltration." *Journal of Membrane Science* 101 (1-2):153-165.

Bryant, Steven L, Peter R King, and David W Mellor. 1993. "Network model evaluation of permeability and spatial correlation in a real random sphere packing." *Transport in porous media* 11 (1):53-70.

Burganos, VN, CA Paraskeva, and AC Payatakes. 1992. "Three-dimensional trajectory analysis and network simulation of deep bed filtration." *Journal of colloid and interface science* 148 (1):167-181.

Busch, Jan, Andreas Cruse, and Wolfgang Marquardt. 2007. "Modeling submerged hollow-fiber membrane filtration for wastewater treatment." *Journal of Membrane Science* 288 (1-2):94-111.

Caravajal, G Stephen, Donald E Leyden, Gregory R Quinting, and Gary E Maciel. 1988. "Structural characterization of (3-aminopropyl) triethoxysilane-modified silicas by silicon-29 and carbon-13 nuclear magnetic resonance." *Analytical Chemistry* 60 (17):1776-1786.

Carman, PC. 1938. "The action of filter aids." *Industrial & Engineering Chemistry* 30 (10):1163-1167.

Carman, Philip Crosbie. 1956. "Flow of gases through porous media."

Chen, Shiyi, and Gary D Doolen. 1998. "Lattice Boltzmann method for fluid flows." *Annual review of fluid mechanics* 30 (1):329-364.

Chi, Tien, and Alkiviades C. Payatakes. 1979. "Advances in Deep Bed Filtration." *Aiche Journal* 25 (5):737–759.

Chiang, Chwan-Hwa, Hatsuo Ishida, and Jack L Koenig. 1980. "The structure of γ-aminopropyltriethoxysilane on glass surfaces." *Journal of Colloid and Interface Science* 74 (2):396-404.

Chiang, Hsu-Wen, and Chi Tien. 1985. "Dynamics of deep-bed filtration. Part I: Analysis of two limiting situations." *AIChE journal* 31 (8):1349-1359.

CHU, W K., YU, and B A. 2008. "Numerical simulation of complex particle-fluid flows." *Powder Technology* 179 (3):104-114.

Chu, KW, and AB Yu. 2008. "Numerical simulation of complex particle–fluid flows." *Powder Technology* 179 (3):104-114.

Chudacek, Michael W, and Anthony G Fane. 1984. "The dynamics of polarisation in unstirred and stirred ultrafiltration." *Journal of membrane science* 21 (2):145-160.

Cundall, Peter A, and Otto DL Strack. 1979. "A discrete numerical model for granular assemblies." *geotechnique* 29 (1):47-65.

Cundall, Peter, R. Hart, and Y. Shimizu. 2004. "Numerical Modeling in Micromechanics via Particle Methods - 2004."

Desmond, Kenneth W, and Eric R Weeks. 2014. "Influence of particle size distribution on random close packing of spheres." *Physical Review E* 90 (2):022204.

Dharmappa, H. B., J. Verink, O. Fujiwara, and S. Vigneswaran. 1992. "Optimization of granular bed filtration treating polydispersed suspension." *Water Research* 26 (10):1307-1318.

Di Carlo, Dino, Jon F Edd, Katherine J Humphry, Howard A Stone, and Mehmet Toner. 2009. "Particle segregation and dynamics in confined flows." *Physical review letters* 102 (9):094503.

Dong, K. J., R.P. Zou, R.Y. Yang, A.B. Yu, and G. Roach. 2009a. "DEM simulation of cake formation in sedimentation and filtration." *Minerals Engineering* 22 (11):921-930.

Dong, KJ, RP Zou, RY Yang, AB Yu, and G Roach. 2009b. "DEM simulation of cake formation in sedimentation and filtration." *Minerals Engineering* 22 (11):921-930.

Eichholz, Christian, Hermann Nirschl, Fei Chen, and T Alan Hatton. 2012. "DEM-simulation of the magnetic field enhanced cake filtration." *AIChE Journal* 58 (12):3633-3644.

Elimelech, Menachem, John Gregory, and Xiadong Jia. 2013. *Particle deposition and aggregation: measurement, modelling and simulation*: Butterworth-Heinemann.

Farr, Robert S. 2013. "Random close packing fractions of lognormal distributions of hard spheres." *Powder technology* 245:28-34.

Fatt, I. 1956. "The network model of porous media III. Dynamic properties of networks with tube radius distribution." *Trans. AIME* 207:164-181.

Flickinger, Michael C. 2013. *Downstream industrial biotechnology: recovery and purification*: John Wiley & Sons.

Furnas, CC. 1931. "Grading aggregates-I.-Mathematical relations for beds of broken solids of maximum density." *Industrial & Engineering Chemistry* 23 (9):1052-1058.

Gitis, Vitaly, Isaak Rubinstein, Maya Livshits, and Gennady Ziskind. 2010. "Deep-bed filtration model with multistage deposition kinetics." *Chemical Engineering Journal* 163 (1-2):78-85.

Green, David J, and Paolo Colombo. 2003. "Cellular ceramics: intriguing structures, novel properties, and innovative applications." *MRS bulletin* 28 (4):296-300.

Grunau, Daryl, Shiyi Chen, and Kenneth Egger. 1993. "A Lattice Boltzmann Model for Multi-phase Fluid Flows." *Phys Fluids A* 5 (10):2557-2562.

Gunstensen, Andrew K., and Daniel H. Rothman. 1993. "Lattice-Boltzmann Studies of Immiscible Two-Phase Flow Through Porous Media." *Journal of Geophysical Research* 98 (B4):6431-6441.

Haiss, Wolfgang, Nguyen TK Thanh, Jenny Aveyard, and David G Fernig. 2007. "Determination of size and concentration of gold nanoparticles from UV− Vis spectra." *Analytical chemistry* 79 (11):4215-4221.

Halama, Stefan, and Hartmut Spliethoff. 2016. "Reaction Kinetics of Pressurized Entrained Flow Coal Gasification: Computational Fluid Dynamics Simulation of a 5 MW Siemens Test Gasifier." *Journal of Energy Resources Technology* 138 (4):042204.

Halbfoster, Christopher J. 1980. Purification of liquids with treated filter aid material and active particulate material. Google Patents.

Harvey, Ronald W, and Stephen P Garabedian. 1991. "Use of colloid filtration theory in modeling movement of bacteria through a contaminated sandy aquifer." *Environmental science & technology* 25 (1):178-185.

Heertjes, PM, and PL Zuideveld. 1978. "Clarification of liquids using filter aids Part I. Mechanisms of filtration." *Powder Technology* 19 (1):17-30.

Hermia, Jacques. 1982. "Constant pressure blocking filtration laws-application to power-law non-Newtonian fluids." *Journal Article* 60:183-187.

Herzig, J. P., D. M. Leclerc, and P. Le. Goff. 1970a. "Flow of Suspensions through Porous Media—Application to Deep Filtration." *Industrial & Engineering Chemistry* 62 (5):8.

Herzig, JP, DM Leclerc, and P Le Goff. 1970b. "Flow of suspensions through porous media—application to deep filtration." *Industrial & Engineering Chemistry* 62 (5):8-35.

Hodgson, PH, GL Leslie, AG Fane, RP Schneider, CJD Fell, and KC Marshall. 1993. "Cake resistance and solute rejection in bacterial microfiltration: the role of the extracellular matrix." *Journal of Membrane Science* 79 (1):35-53.

Höflinger, Wilhelm. 2000. "Symposium "Filtration and separation of fine particle suspensions"." *Umweltwissenschaften und Schadstoff-Forschung* 12 (3):181-181.

Hong, Jung Hwa, Mu Seong Mum, and Tae Hong Lim. 2001. "Strain Rate Dependent Poroelastic Behavior of Bovine Vertebral Trabecular Bone." *Ksme International Journal* 15 (7):1032-1040.

Hou, Shuling, Xiaowen Shan, Qisu Zou, Gary D. Doolen, and Wendy E. Soll. 1997. "Evaluation of Two Lattice Boltzmann Models for Multiphase Flows." *Journal of Computational Physics* 138 (2):695-713.

Hulmes, DJ, Tim J Wess, Darwin J Prockop, and Peter Fratzl. 1995. "Radial packing, order, and disorder in collagen fibrils." *Biophysical journal* 68 (5):1661-1670.

Ison, CR, and KJ Ives. 1969. "Removal mechanisms in deep bed filtration." *Chemical Engineering Science* 24 (4):717-729.

Iwasaki, Tomihisa. 1937. "Some notes on sand filtration." *Journal-American Water Works Association* 29 (10):1591-1597.

Jegatheesan, V, and S Vigneswaran. 2005. "Deep bed filtration: mathematical models and observations." *Critical Reviews in Environmental Science and Technology* 35 (6):515-569.

Joekar-Niasar, V, and SM Hassanizadeh. 2012. "Analysis of fundamentals of two-phase flow in porous media using dynamic pore-network models: A review." *Critical reviews in environmental science and technology* 42 (18):1895-1976.

Johnson, Kenneth Langstreth, and Kenneth Langstreth Johnson. 1987. *Contact mechanics*: Cambridge university press.

Kavoosi, Azad. 2014. "Investigating the Fundamental Parameters of Cake Filtration using a Gravity Column Device."

Koch, Donald L, and Reghan J Hill. 2001. "Inertial effects in suspension and porous-media flows." *Annual Review of Fluid Mechanics* 33 (1):619-647.

Koponen, A, M Kataja, and J Timonen. 1997. "Permeability and effective porosity of porous media." *Physical Review E* 56 (3):3319.

Kuhn, Michael, and Heiko Briesen. 2016. "Dynamic Modeling of Filter-Aid Filtration Including Surface- and Depth-Filtration Effects." *Chemical Engineering & Technology* 39 (3):425-434.

Ladd, Anthony J. C. 2015. "Numerical Simulations of Particulate Suspensions via a Discretized Boltzmann Equation Part II. Numerical Results." *Physics of Fluids* 271 (03):285-310.

Lamb, Horace. 1993. *Hydrodynamics*: Cambridge university press.

Lash, Melissa H, Jahnelle C Jordan, Laura C Blevins, Morgan V Fedorchak, Steven R Little, and Joseph J Mccarthy. 2015. "Frontispiece: non-brownian particle-based materials with microscale and nanoscale hierarchy." *Angewandte Chemie* 54 (20):5854-5858.

Liu, Xinghui, and Faruk Civan. 1996. "Formation damage and filter cake buildup in laboratory core tests: modeling and model-assisted analysis." *SPE Formation Evaluation* 11 (01):26-30.

Luo, Guo-Feng, Wei-Hai Chen, Yun Liu, Jing Zhang, Si-Xue Cheng, Ren-Xi Zhuo, and Xian-Zheng Zhang. 2013. "Charge-reversal plug gate nanovalves on peptide-functionalized mesoporous silica nanoparticles for targeted drug delivery." *Journal of Materials Chemistry B* 1 (41):5723-5732.

Luo, L. S., D. Qi, and L. P. Wang. 2002. *Applications of the Lattice Boltzmann Method to Complex and Turbulent Flows*.

Ma, Jingsen, Assad A Oberai, Donald A Drew, and Richard T Lahey. 2012. "A two-way coupled polydispersed two-fluid model for the simulation of air entrainment beneath a plunging liquid jet." *Journal of fluids engineering* 134 (10):101304.

Mackie, RI, and Renbi Bai. 1992. "Suspended particle size distribution and the performance of deep bed filters." *Water research* 26 (12):1571-1575.

Martel, Joseph M, and Mehmet Toner. 2014. "Inertial focusing in microfluidics." *Annual review of biomedical engineering* 16:371-396.

Martin, Robert E, Edward J Bouwer, and Linda M Hanna. 1992. "Application of clean-bed filtration theory to bacterial deposition in porous media." *Environmental science & technology* 26 (5):1053-1058.

Mauran, S, L Rigaud, and O Coudevylle. 2001. "Application of the Carman–Kozeny correlation to a high-porosity and anisotropic consolidated medium: the compressed expanded natural graphite." *Transport in Porous Media* 43 (2):355-376.

Mcnamara, Guy R., and Gianluigi Zanetti. 1988. "Use of the Boltzmann Equation to Simulate Lattice-Gas Automata." *Physical Review Letters* 61 (20):2332.

Mei, Renwei, Li Shi Luo, and Shyy Wei. 2006. *An Accurate Curved Boundary Treatment in the Lattice Boltzmann Method*.

Mei, Renwei, Wei Shyy, Dazhi Yu, and Li-Shi Luo. 2000. "Lattice Boltzmann Method for 3-D Flows with Curved Boundary." *Journal of Computational Physics* 161 (2):680-699.

Mirabolghasemi, Maryam, Maša Prodanović, David DiCarlo, and Hongyu Ji. 2015. "Prediction of empirical properties using direct pore-scale simulation of straining through 3D microtomography images of porous media." *Journal of Hydrology* 529:768-778.

Mohamad, AA. 2011. *Lattice Boltzmann Method*. Vol. 70: Springer.

Mookiah, Muthu Rama Krishnan, U Rajendra Acharya, Vinod Chandran, Roshan Joy Martis, Jen Hong Tan, Joel EW Koh, Chua Kuang Chua, Louis Tong, and Augustinus Laude. 2015. "Application of higher-order spectra for automated grading of diabetic maculopathy." *Medical & biological engineering & computing* 53 (12):1319-1331.

Mortensen, Niels Asger, Fridolin Okkels, and Henrik Bruus. 2005. "Reexamination of Hagen-Poiseuille flow: Shape dependence of the hydraulic resistance in microchannels." *Physical Review E* 71 (5):057301.

Munjiza, A, T Bangash, and NWM John. 2004. "The combined finite–discrete element method for structural failure and collapse." *Engineering fracture mechanics* 71 (4-6):469-483.

Overton, J Ray. 1973. "Filtration of cigarette smoke: Relative contributions of inertial impaction, diffusional deposition, and direct interception." *Beiträge zur Tabakforschung/Contributions to Tobacco Research* 7 (3):117-120.

Parfitt, GD. 1976. "Surface chemistry of oxides." *Pure and applied chemistry* 48 (4):415-418.

Prieve, Dennis C, and Eli Ruckenstein. 1974. "Effect of London forces upon the rate of deposition of Brownian particles." *AIChE Journal* 20 (6):1178-1187.

Qian, Y. H., D. D'Humières, and P. Lallemand. 2007. "Lattice BGK Models for Navier-Stokes Equation." *Epl* 17 (6BIS):479.

Rajagopalan, Rajamani, and Chi Tien. 1976. "Trajectory analysis of deep-bed filtration with the sphere-in-cell porous media model." *AIChE Journal* 22 (3):523-533.

Reboul, Nadège, Eric Vincens, and Bernard Cambou. 2008. "A statistical analysis of void size distribution in a simulated narrowly graded packing of spheres." *Granular Matter* 10 (6):457-468.

Rege, SD, and H Scott Fogler. 1988. "A network model for deep bed filtration of solid particles and emulsion drops." *AIChE Journal* 34 (11):1761-1772.

Reneau Jr, James T. 1992. Nutsche process filter drive unit. Google Patents.

Rong, LW, KJ Dong, and AB Yu. 2014. "Lattice-Boltzmann simulation of fluid flow through packed beds of spheres: Effect of particle size distribution." *Chemical Engineering Science* 116:508-523.

Rubenstein, Daniel I, and MAR Koehl. 1977. "The mechanisms of filter feeding: some theoretical considerations." *The American Naturalist* 111 (981):981-994.

Rubinstein, R, and L. S. Luo. 2008. "Theory of the lattice Boltzmann equation: symmetry properties of discrete velocity sets." *Physical Review E Statistical Nonlinear & Soft Matter Physics* 77 (3):036709.

Rushton, Albert, Anthony S Ward, and Richard G Holdich. 2008. *Solid-liquid filtration and separation technology*: John Wiley & Sons.

Ruth, BF. 1946. "Correlating filtration theory with industrial practice." *Industrial & Engineering Chemistry* 38 (6):564-571.

Ryan, Joseph N, Menachem Elimelech, Jenny L Baeseman, and Robin D Magelky. 2000. "Silica-coated titania and zirconia colloids for subsurface transport field experiments." *Environmental science & technology* 34 (10):2000-2005.

Sambaer, Wannes, Martin Zatloukal, and Dusan Kimmer. 2011. "3D modeling of filtration process via polyurethane nanofiber based nonwoven filters prepared by electrospinning process." *Chemical Engineering Science* 66 (4):613-623.

Sampath, Muthukumar, Anupam Shukla, and Anurag Rathore. 2014. "Modeling of filtration processes—microfiltration and depth filtration for harvest of a therapeutic protein expressed in Pichia pastoris at constant pressure." *Bioengineering* 1 (4):260-277.

Scheffler, Michael, and Paolo Colombo. 2006. *Cellular ceramics: structure, manufacturing, properties and applications*: John Wiley & Sons.

Schmid, Peter J, and Dan S Henningson. 1994. "Optimal energy density growth in Hagen–Poiseuille flow." *Journal of Fluid Mechanics* 277:197-225.

Shaw, David T. 1978. *Fundamentals of aerosol science*: Wiley New York.

Spielman, Lloyd, and Simon L Goren. 1968. "Model for predicting pressure drop and filtration efficiency in fibrous media." *Environmental Science & Technology* 2 (4):279-287.

Srisutthiyakorn, Nattavadee, and Gerald M Mavko. 2017. "What is the role of tortuosity in the Kozeny-Carman equation?" *Interpretation* 5 (1):SB57-SB67.

Succi, Sauro. 2001. *The Lattice Boltzmann Equation – For Fluid Dynamics and Beyond*.

Succi, Sauro, Roberto Benzi, and Francisco Higuera. 1991. "The lattice Boltzmann equation: A new tool for computational fluid-dynamics." Nato Advanced Research Workshop on Lattice Gas Methods for Pdes: Theory.

Sulpizio, Thomas E. 1999. "Advances in filter aid and precoat filtration technology." *ADVANCES IN FILTRATION AND SEPARATION TECHNOLOGY* 13 (A):371-371.

Sutherland, DN, and P Hidi. 1966. "An investigation of filter-aid behaviour." *TRANSACTIONS OF THE INSTITUTION OF CHEMICAL ENGINEERS AND THE CHEMICAL ENGINEER* 44 (4):T122-+.

Svarovsky, Ladislav. 2000. *Solid-liquid separation*: Elsevier.

Thornton, Ronald K, and David R Sokoloff. 1998. "Assessing student learning of Newton's laws: The force and motion conceptual evaluation and the evaluation of active learning laboratory and lecture curricula." *american Journal of Physics* 66 (4):338-352.

Tien, Chi. 2006. *Introduction to cake filtration: analyses, experiments and applications*: Elsevier.

Tien, Chi. 2013. *Granular filtration of aerosols and hydrosols: Butterworths series in chemical engineering*: Butterworth-Heinemann.

Tiller, Fo M. 1953. "The role of porosity in filtration: numerical methods for constant rate and constant pressure filtration based on Kozeny's law." *Chem. Eng. Progr.* 49:467-479.

Tobiason, John E, and Charles R O'melia. 1988. "Physicochemical aspects of particle removal in depth filtration." *Journal-American Water Works Association* 80 (12):54-64.

Todd, Adrian C, JE Somerville, and Graham Scott. 1984. "The application of depth of formation damage measurements in predicting water injectivity decline." SPE Formation Damage Control Symposium.

Tufenkji, Nathalie, and Menachem Elimelech. 2004. "Correlation equation for predicting single-collector efficiency in physicochemical filtration in saturated porous media." *Environmental science & technology* 38 (2):529-536.

van der Hoef, Martin Anton, R Beetstra, and JAM Kuipers. 2005. "Lattice-Boltzmann simulations of low-Reynolds-number flow past mono-and bidisperse arrays of spheres: results for the permeability and drag force." *Journal of fluid mechanics* 528:233-254.

van Oort, Eric, JFG Van Velzen, and Klaas Leerlooijer. 1993. "Impairment by suspended solids invasion: testing and prediction." *SPE Production & Facilities* 8 (03):178-184.

Velamakanni, Bhaskar V, and Fred F Lange. 1991. "Effect of interparticle potentials and sedimentation on particle packing density of bimodal particle distributions during pressure filtration." *Journal of the American Ceramic Society* 74 (1):166-172.

Whitaker, Stephen. 1986. "Flow in porous media I: A theoretical derivation of Darcy's law." *Transport in porous media* 1 (1):3-25.

Willis, MS, I Tosun, W Choo, GG Chase, and F Desai. 1991. "A dispersed multiphase theory and its application to filtration." *Advances in porous media* 1:179-294.

Wong, R. C. K., and D. C. A. Mettananda. 2010. "Permeability Reduction in Qishn Sandstone Specimens due to Particle Suspension Injection." *Transport in Porous Media* 81 (1):105.

Wyllie, MRJ, and GHF Gardner. 1958. "The generalized Kozeny-Carman equation." *World oil* 146 (4):121-128.

Yao, Kuan-Mu, Mohammad T Habibian, and Charles R O'Melia. 1971. "Water and waste water filtration. Concepts and applications." *Environmental science & technology* 5 (11):1105-1112.

Yeon, Ye-Rim, Young Jun Park, Ji-Sung Lee, Jung-Woo Park, Sin-Gun Kang, and Chul-Ho Jun. 2008. "Sc (OTf) 3-Mediated Silylation of Hydroxy Functional Groups on a Solid Surface: A Catalytic Grafting Method Operating at Room Temperature." *Angewandte Chemie International Edition* 47 (1):109-112.

Yim, Sung Sam, and Young Du Kwon. 1997. "A unified theory on solid-liquid separation: Filtration, expression, sedimentation, filtration by centrifugal force, and cross flow filtration." *Korean Journal of Chemical Engineering* 14 (5):354-358.

Yin, Xiaolong, and Sankaran Sundaresan. 2009. "Fluid-particle drag in low-Reynolds-number polydisperse gas–solid suspensions." *AIChE journal* 55 (6):1352-1368.

You, Zhenjiang, Alexander Badalyan, and Pavel Bedrikovetsky. 2013. "Size-exclusion colloidal transport in porous media--stochastic modeling and experimental study." *SPE Journal* 18 (04):620-633.

Yu, Dazhi, Renwei Mei, Li Shi Luo, and Shyy Wei. 2003. "Viscous flow computations with the method of lattice Boltzmann equation." *Progress in Aerospace Sciences* 39 (5):329-367.

Yuan, Hao, and Alexander A Shapiro. 2010. "Modeling non-Fickian transport and hyperexponential deposition for deep bed filtration." *Chemical Engineering Journal* 162 (3):974-988.

Zhang, Jitao, Yan Li, Xuejian Wu, and Liqiong Zhang. 2010. "Evaluating uncertainty of the mean diameter of silicon sphere by Spherical Harmonics." Precision Electromagnetic Measurements.

Zhang, Siying, and Joseph J McCarthy. 2019. "Modeling of the pressure drop across polydisperse packed beds in cake filtration." *AIChE Journal* 65 (5).

Zhu, HP, ZY Zhou, RY Yang, and AB Yu. 2007. "Discrete particle simulation of particulate systems: theoretical developments." *Chemical Engineering Science* 62 (13):3378-3396.

Zularisam, AW, AF Ismail, and Razman Salim. 2006. "Behaviours of natural organic matter in membrane filtration for surface water treatment—a review." *Desalination* 194 (1-3):211-231.